

Higgs Boson Production in Gluon Fusion through the Next-to-Next-to-Leading Power in Quark Mass



Author: Sneh Modi

Supervisor: Prof. Alexander A. Penin

A thesis submitted to the Faculty of Graduate Studies and Research in partial fulfillment of the requirements for the degree of Doctor of Philosophy

University of Alberta
Department of Physics
Edmonton, AB, Canada
May 10, 2023

© Sneh Modi, 2023

Abstract

The asymptotic behavior of the elementary particle scattering amplitudes at high-energy is a fundamental problem of quantum field theory. In the leading order of the expansion in inverse powers of the characteristic energy scale, the problem has been solved decades ago in the classical works of Sudakov and others [1–9]. Beyond this approximation, however, the problem becomes far more challenging and requires the development of principally new theoretical techniques. Only recently the solution has been found for the leading mass-suppressed amplitudes revealing a number of amazing new effects in quantum field theory [10–14]. In this thesis, we make further advances in the analysis and consider for the first time a high-energy process at the next-to-next-to-leading power.

The main focus of the thesis is the analysis of the QCD effects in the light quark mediated Higgs boson production via gluon fusion. We study the dominant “double-logarithmic” radiative corrections enhanced by the second power of the logarithm of the light quark to Higgs boson mass ratio per each power of strong coupling constant α_s . The analytic result is obtained for the three-loop α_s^3 contribution through the third power in the quark mass. The all-order double-logarithmic asymptotic result is then obtained in two complementary approximations: (i) the large number of colors limit which is supposed to catch the qualitative behavior of real QCD, and (ii) in the Abelian limit which fully reveals the structure of the double-logarithmic result at the next-to-next-to-leading power.

The second problem considered in the thesis is the asymptotic behavior of the massive quark scattering amplitudes by an external color singlet field. The all-order result at next-to-leading power in quark mass for which was first obtained in [13, 14]. We com-

plete this previous analysis and obtain for the first time the fully analytic asymptotic result for the leading mass-suppressed term in the double-logarithmic approximation.

Preface

This thesis serves as a detailed extension of the work the author and his collaborators published in reference [15]. This work in many ways builds upon and is an extension of the previously published work of my collaborators; the most relevant past publications are the references [12–14]. Other previous publications that are partially related or contain certain relevant calculations and/or techniques can be found in references [10, 11].

It is also important to note that the algorithm QGRAF [16–19] was used for diagram generation. The output of the symbolic diagrams generated by QGRAF was converted into the graphs used in this thesis manually. After writing the amplitudes of the relevant diagrams, the algorithm FORM [20] was used to compute the traces and simplify the numerators; with some of the earlier results verified by direct evaluation for cross-checking. The integration in the double-logarithmic region within the Sudakov method [1, 21] is straightforward to compute and was done explicitly for all the cases with the help of Mathematica; along with all other integrals and sums that appear during the calculations presented here. Lastly, all the Feynman diagrams featured in this thesis were drawn with the help of online Feynman diagram maker [22].

भां पप्पा, आ तभारा भाटे.
(Mom dad, this one is for you.)

Acknowledgement

First, I would like to thank my mentor and supervisor **Prof. Alexander A. Penin** from the bottom of my heart for giving me the opportunity to embark upon this journey. I am grateful for the guidance he has provided over the years and the tremendous patience he showed during that time.

I'm also grateful to **Dr. Tao Liu**, our other collaborator on this project, for taking me under his wings when I was just starting out and he was a Postdoctoral Fellow of Prof. Penin. Depending on him and his expertise allowed me to learn the necessary tools required to perform many of the calculations that are presented in this thesis.

I am also thankful to my sister Sonam Modi Handa, her husband Aakash Handa, and my friends Ameir Shaa Bin Akber Ali, Krystal Delver, Luara Gonzalez Rendon, Samiur R. Mir, Dr. Shruti Naik, Ngoné Dior Ngom, Sagar Patel, Smit Patel, Pramodh Viduranga Senarath Yapa Arachchige, Rajvi Shah Patel, and Shivani Sharma for the support they have provided over the years whenever I needed it the most. Counselling and Clinical Services and Dr. Jason Murray also played a very important role and provided necessary counselling to help me through some of the toughest times I've had to weather.

I would also like to take this moment to thank Ameir Shaa Bin Akber Ali, Prof. Jamil Aslam, Dr. Jens Boos, Samiur R. Mir, Muhammad Mubasher, Mason Protter, Dr. Abdur Rehman, and Pramodh Viduranga Senarath Yapa Arachchige for the useful discussions on various research topics, the general subject matter, and all the other arenas related to the academia. Thank you Kishnudaran Krishna Moorthy (Shan) and Dr. Shruti Naik for volunteering to read the first draft of this thesis and providing constructive feedback.

At last, I thank the Campus and Community Recreation Services and all the programs and clubs I participated in during my time at the University of Alberta, as well as all the instructors I had the pleasure to work with during that time as they too played a pivotal role in my mental and physical well-being, and gave me the opportunities to explore my non-academic interests in the most convenient way possible.

Territorial Acknowledgement

The University of Alberta, its campus, all the buildings, and research facilities as well as the place I continue to call home in Edmonton, are all located on traditional territories of the Indigenous people of Canada. These lands are known as part of Alberta Treaties 6, 7, and 8, and are the homeland to the Indigenous communities such as Blackfoot, Cree, Dene, Inuit, Iroquios, Métis, Nakota Sioux and Ojibway/Saulteaux/Anishinaabe Nations. All of us at the University respectfully acknowledge these lands and the sovereignty, histories, languages, and cultures of all the First Nations who have thrived here for centuries and continue to be a vital part of the modern multicultural community.

Contents

Abstract	ii
Preface	iv
Dedication	v
Acknowledgement	vi
Territorial Acknowledgement	vii
Contents	x
List of Figures	xiv
List of Tables	xv
List of Symbols	xvi
List of Abbreviations	xviii
1 Introduction	1
1.1 Amplitudes in the high-energy limit	1
1.2 Outline	3
2 Theoretical background	5
2.1 Quantum Chromodynamics	5
2.2 Origin of the double-logarithms	8
2.3 Factorization of power-suppressed logarithms in QCD	9
2.3.1 Direct evaluation of the LO amplitude	10
2.3.2 Direct evaluation of the NLO amplitude	11
2.3.3 Factorization at the NLO amplitude	16

2.3.4	All-order resummation	21
2.3.5	Large z asymptotic for $g(z)$	21
3	The quark scattering	24
3.1	The 1-loop diagram	25
3.2	The 2-loop diagrams	26
3.3	The 3-loop diagrams	27
3.4	All-order resummation	29
3.5	Large z asymptotic of $f(z)$	31
3.6	Off-shell scalar FF	34
4	Higgs production via light quark mediated gluon fusion	35
4.1	Factorizable contribution with single soft quark exchange	36
4.2	Contribution from triple soft quark exchange	39
4.3	Non-factorizable contribution with single soft quark exchange	41
4.4	Higgs production FF at NNLP	44
4.4.1	The large- N_c limit	45
4.4.2	The Abelian limit	45
4.4.3	Discussion	49
5	Summary	51
5.1	Massive quark FF	51
5.2	Higgs production via gluon fusion	51
	Bibliography	59
A	Gamma matrix identities	60
B	Evaluation of quark scalar FF	62
B.1	The 1-loop diagram	62
B.2	The 2-loop diagrams	63
C	Evaluation of Higgs production FF	71
C.1	Factorizable contribution with single soft quark exchange	72
C.1.1	Diagram generation with QGRAF	72
C.1.2	Trace evaluation in FORM	74
C.1.3	Sudakov method for large double-logarithms	78
C.1.4	Single quark exchange effective diagram	80

C.2	Contribution from triple soft quark exchange	81
C.2.1	The 3-loop diagrams	81
C.2.2	Effective diagrams	84
C.3	Non-factorizable contribution with single soft quark exchange	87

List of Figures

2.1	Examples of diagrams generating the (a) Sudakov, and (b) the power-suppressed non-Sudakov logarithms. The dark vertex connects to the rest of the diagrams via current or an external source.	9
2.2	(a) The LO 1-loop diagram contributing to the quark scattering by the gauge field operator, $(G_{\mu\nu}^a)^2$, denoted by the dark vertex; and (b) the effective 2-loop diagram with soft gluon exchange between the eikonal lines; the hollow vertices denote eikonal color charge non-conservation explained in the text.	10
2.3	The 2-loop diagrams contributing to the NLO of quark scattering by $(G_{\mu\nu}^a)^2$. Symmetric diagrams are not included.	11
2.4	The two configurations for fig. 2.3(b) in which quark propagator (a) above and (b) below the soft gluon emission vertex is soft, and goes on-shell.	13
2.5	Diagrammatic representation of eq. (2.57). The diagram on the left represents $iq_\mu M^\mu$	16
2.6	Diagrammatic representation of the sequence of identities that move the soft gluon vertex from the soft quark to the upper eikonal gluon line. The crossed circle in (b) and (c) are defined in the text. The hollow vertex on the upper eikonal line in (d) represents effective coupling as explained in the text.	18
2.7	Diagrammatic representation of the eikonal factorization. From top left to bottom right they represent fig. 2.3(a), fig. 2.6(d), symmetric counterpart of fig. 2.6(d), fig. 2.3(d), fig. 2.2(a), and the 1-loop vertex correction for quark scattering.	20
3.1	Quark scattering by Higgs boson at 1-loop. The convention shown here are used for all the diagrams and calculations of the scalar FF.	25

3.2	Diagrams for quark scattering by Higgs Boson at 2-loops. Symmetric diagrams and diagrams with opposite particle flow for closed quark loop are not shown. The dark vertex represents the Higgs boson with momentum $q = p_2 - p_1$ coming into the vertex.	26
3.3	Diagrams contributing to the double-logarithmic approximation for the quark scalar FF at 3-loops; symmetric diagrams to (d)-(h), and diagrams with opposite particle flow for the closed quark loop are not included. The dark vertex represents the Higgs boson with momentum $q = p_2 - p_1$ coming into the vertex. All diagrams are obtained by dressing fig. 3.2(b) with leading soft gluon exchange.	27
3.4	(a) The leading 2-loop Feynman diagram for the NLP double-logarithmic correction to the quark scalar FF. (b), (c) The diagrams with effective soft gluon exchange incorporating the all-order non-Sudakov corrections to the scalar FF at NLP. The dark circle represents mass insertion.	29
3.5	The diagrammatic representation of the Ward-Takahashi identities and momentum shift for fig. 3.3(g) and (h). The shift from (c) to (d) is identical to that of fig. 2.3(b), diagrammatically shown in fig. 2.6. The shift from (a) to (b) is almost identical, with the difference explained in the text.	31
4.1	(a) $\mathcal{O}(m_q)$ and (b), (c) $\mathcal{O}(m_q^3)$ double-logarithmic contribution to the ggH amplitude. The dark (empty) circle represents mass (loop momentum) insertion. The blob corresponds to the off-shell scalar FF at $\mathcal{O}(m_q^0)$ and $\mathcal{O}(m_q^2)$	36
4.2	Higgs production via quark mediated gluon fusion at (a) 1-loop, and (b) 2-loop diagram with effective soft gluon exchange. Diagrams with opposite particle flow for the closed quark loop are not shown.	37
4.3	Higgs production via triple soft quark exchange. Diagrams with opposite particle flow for the closed quark loops are not included. Only (a) contributes to double-logarithmic approximation at NNLP. The dark circle represents mass insertion; additional mass factors can come via the on-shell soft quark momentum.	39
4.4	Effective diagrams with triple soft quark exchange for the Higgs production with vertex correction by effective gluon exchange on the topology of fig. 4.3(a). Each diagram corresponds to an exponential in eq. (4.20). The dark circle represents mass insertion.	40

4.5	The non-factorizable Higgs production diagrams with an additional eikonal gluon (represented by the wavy line) being emitted by the soft quark (a) at 2-loops, and (b) effective diagram at 3-loops that gives the total 3-loop QCD contribution from this source; it does not represent the all-order contribution in this case. Symmetric diagrams and diagrams with opposite particle flow for the closed quark loop are not included. The dark circle represents mass insertion.	42
4.6	The 3-loop non-factorizable Higgs production diagrams with an additional eikonal gluon (represented by the wavy line) being emitted by the soft quark where (a) and (b) are Abelian, while (c) and (d) are non-Abelian. Symmetric diagrams and diagrams with opposite particle flow for the closed quark loop are not included. The dark (empty) circle represents mass (loop momentum) insertion.	44
4.7	An example of a higher order Abelian diagram with multiple soft gluon exchanges on the fig. 4.5(a) topology. In this scenario $m' = 5$, and $m = 4$. As outlined in the text, the momenta k_i for $i = 1, 2, \dots, m$ are labelled from the eikonal gluon vertex (eikonal gluon represented by the wavy line) to the Higgs vertex and are labelled at the vertices of the second group on the lower eikonal line. Here, $f_1 = 4, f_2 = 3, f_3 = 6$, and $f_4 = 1$. The numbers from 1 to 9 enumerate the vertices on the upper eikonal quark line, resulting in $j' = 4$ for the vertices 1, 2, 3, 4, and $j = 3$ due to the vertices 1, 3, 4.	46
B.1	The 1-loop diagram. The momentum conventions are shown in fig. 3.1. The Greek letters represent the vector indices, while color indices are denoted by the Latin letters.	63
B.2	The momentum configurations for fig. 3.2(a) and (c). The dark vertex represents the Higgs boson with momentum $q = p_2 - p_1$ coming into the vertex.	64
B.3	The momentum configurations for fig. 3.2(d) and (e). The dark vertex represents the Higgs boson with momentum $q = p_2 - p_1$ coming into the vertex.	65
B.4	The momentum configurations for fig. 3.2(b) and its symmetric counterpart. The dark vertex represents the Higgs boson with momentum $q = p_2 - p_1$ coming into the vertex.	66
C.1	Generic diagram for Higgs production via massive particle loop mediated gluon fusion. This diagram can also describe the Higgs boson to two photon decay.	72

C.2	The QGRAF model file that was used to generate all the Higgs production diagrams. It defines a simplified QCD theory involving quark, antiquark, gluon, Higgs boson, and their possible interaction vertices.	73
C.3	Partial QGRAF output showing the symbolic version of fig. 4.2(a), and the initial code to generate all potential 1-loop diagrams for the theory defined by the model shown in fig. C.2.	74
C.4	Graphical representation of the symbolic Feynman diagram generated by QGRAF corresponding to fig. 4.2(a) in (a) the form of the symbolic output of fig. C.3, and (b) the momentum configuration used for the calculation. The Greek letters represent the vector indices, while color indices are denoted by the Latin letters “i”, “j” and “k”.	75
C.5	Sample FORM code for fig. C.4(b) to reduce the numerator with the help of the projector from eq. (C.5) to get the Higgs FF.	76
C.6	Output of the sample FORM code shown in fig. C.5. The result labelled “loop1” is the trace over the closed quark loop in fig. C.4(b). The variable “pro” gives the product of the projector and the 1-loop result.	77
C.7	The final diagram required for the eikonal factorization of the soft gluon for the 3-loop diagrams fig. 4.6(c) and (d). The wavy line represents the exchange of eikonal gluon between the soft and eikonal quark lines.	94

List of Tables

2.1	The reduced color factors c_λ and the weights w_λ for the 2-loop diagrams in fig. 2.3. Contributions of the symmetric diagrams can be obtained by $\eta \longleftrightarrow \xi$ in the rows b and c.	15
3.1	The reduced color factors c_λ , weights w_λ and the integrals d_λ for 3-loop diagrams in fig. 3.3. Contribution of the symmetric diagrams can be obtained via $\eta_1 \longleftrightarrow \xi_1$ and $\xi_2 \longleftrightarrow \eta_2$ for rows d-h.	28
4.1	The normalized coefficients in the Taylor expansion of the function $h(z)$ and $j^{ab}(z)$ from $n = 1$ to 6.	41

List of Symbols

This is the list of frequently used symbols in this thesis.

d	dimension of spacetime, $d = 4 - 2\varepsilon$ in dimensional regularization
ε	dimensional regulator
$g_{\mu\nu}$	the metric tensor
$\bar{q}(p), q(p)$	quark spinors with momentum p
l_i, k_i, k'_i	loop momenta
p_i	incoming particle momenta
q	momentum transfer/outgoing momentum
$m_q \equiv m$	mass of the (<i>i</i>) scattering quark or (<i>ii</i>) quark in the loop
m_H	mass of the Higgs boson
ρ	the expansion parameter in the high-energy limit, $\rho = m^2/q^2$
u_i, v_i	Sudakov parameters
$S(l)$	Feynman propagator for a fermion carrying momentum l
$D_{\mu\nu}(l)$	gauge boson propagator with momentum l
α, β, \dots	greek letters designating the vector indices at a vertex
a, b, \dots	latin alphabets indicating color indices
F_i	Dirac and Pauli FF for $i = 1, 2$ respectively
F_S	scalar FF for quark scattering
M_{ggH}^q	Higgs production FF

y_q	quark Yukawa coupling
$SU(N_c)$	Special Unitary group, $N_c = 3$ for QCD
T_F	index of the fundamental representation
C_F	quadratic Casimir of the fundamental representation
C_A	quadratic Casimir of the adjoint representation
g_s	the strong coupling appearing in the QCD Lagrangian and vertices
α_s	the strong coupling constant, $\alpha_s = g_s^2/(4\pi)$
$p_i p_j$	scalar product of the 4-momentum p_i and p_j
$x = \frac{\alpha}{4\pi} \ln^2 \rho$	double-logarithmic variable
$z = (C_A - C_F)x$	double-logarithmic variable with standard eikonal color charge

List of Abbreviations

This is the list of all the abbreviations from this thesis.

LHC	Large Hadron Collider
QFT	Quantum Field Theory
QED	Quantum Electrodynamics
QCD	Quantum Chromodynamics
SM	Standard Model
IR	Infrared
LO	Leading Order
NLO	Next-to-Leading Order
NNLO	Next-to-Next-to-Leading Order
LP	Leading Power in quark mass
NLP	Next-to-Leading Power in quark mass
NNLP	Next-to-Next-to-Leading Power in quark mass
FF	Form Factor(s)
LL	Leading Logarithm, referring to the double-logarithmic contribution
NLL	Next-to-Leading Logarithm
nL	n-Loop diagram(s)
nq	Diagram(s) with n-quark exchanges
NF	Non-Factorizable
<i>tr</i>	Trace

Chapter 1

Introduction

The start of the Large Hadron Collider (LHC) era opened up the previously inaccessible energy domain resulting in the experimental verification of the spontaneous electroweak symmetry breaking and mass generation mechanism through the discovery of the Higgs boson in 2012 [23]. Over the last few years, however, the LHC has transformed from a raw discovery into a high-precision machine. Despite many expectations, no direct signal of new phenomena such as extra space dimensions, supersymmetry, low-scale gravity, etc. has been detected so far. Thus the “new physics” is likely to show up only as a tiny deviation of the experimental data from the theoretical predictions based on the Standard Model (SM) of particle interactions. At the same time, the increasing accuracy of the high-energy experiments allows for a very accurate determination of the fundamental parameters of particle physics and becomes competitive in probing physics beyond the SM. Hence, the theoretical analysis which is able to provide the required precision becomes ultimately important. Such an analysis is essentially based on the perturbative quantum field theory and during the last two decades the related computational methods reached an unprecedented level. However, many of the pending problems are still beyond the reach of available techniques and require development of new computational tools as well as a deeper understanding of the dynamics of quantum fields. One such problem is of particle scattering in the high-energy region, to which we turn our attention now.

1.1 Amplitudes in the high-energy limit

For the high-energy processes the fixed order results of perturbative expansion are often insufficient for an accurate description of the strong interaction effects due to the presence of the large logarithms of the ratio of a characteristic infrared scale to the process energy. Such logarithms in the perturbative coefficients result in slow convergence of the series in strong coupling constant and have to be resummed to

all-orders. This program has been completed for the amplitudes which are not suppressed at high-energy by the scale ratio. The asymptotic behavior of such amplitudes is governed by the ‘‘Sudakov’’ radiative corrections enhanced by the second power of the large logarithm of the scale ratio per each power of the coupling constant i.e., $\propto \alpha^n \ln^{2n}(\Lambda^2/q^2)$ with Λ and q denoting the infrared and the high-energy scale of the problem, respectively. Sudakov logarithms exponentiate and result in a strong universal suppression of the scattering amplitudes in the limit when all the kinematic invariants of the process are large [1–9]. The structure of the power-suppressed logarithmically enhanced contributions is by far more complex and the corresponding renormalization group analysis poses a serious challenge to the modern effective field theory. One of the important problems in this category is the analysis of the scattering amplitudes involving massive particle(s) in the limit of small mass or high-energy. The mass effects on the leading power (LP) contributions have been extensively studied in the context of the high-order electroweak and QED radiative corrections [24–34]. The next-to-leading power (NLP) contributions for several key processes in QED and QCD have been analyzed in the leading (double) logarithmic (LL) [10–14, 35–39] and the next-to-leading logarithmic (NLL, $\propto \alpha^n \ln^{2n-1}(\Lambda^2/q^2)$) approximation [40–42]. Many highly nontrivial results for the power corrections in threshold and event shape variables, jettiness, rapidity, scattering angle, etc. have been obtained in various contexts [43–56].

In the processes with massive fermions already at the NLP the origin of the logarithmic corrections and the asymptotic behavior of the amplitudes drastically differ from the LP Sudakov case. The double-logarithmic terms, in this case, are related to the effect of the eikonal (color) charge non-conservation in the process with soft fermion exchange and result in asymptotic exponential enhancement for a wide class of amplitudes and in a breakdown of a formal power counting [10, 13, 14]. Thus, it is of primary theoretical interest to get insight into the asymptotic behavior of the next-to-next-to-leading power (NNLP) contributions and determine whether any qualitatively new phenomenon appears in this order. The renormalization group analysis has not been extended beyond the NLP for any kind of power corrections to the high-energy processes. In this thesis, we present the first NNLP analysis of the simplest but fundamental and phenomenologically important amplitude of the light quark-mediated Higgs boson production in gluon fusion.

The Higgs boson sector remains to be one of the least known and most intriguing parts of the SM, and the study of the Higgs boson properties is currently one of the most important and pursued parts of the physics program at LHC [57]. Matching the increasing precision of the experimental measurements requires the analysis of the high-order effects of the strong interaction, and is one of the biggest challenges for perturbative QCD. For the gluon fusion channel, the amplitude is dominated by the

loop with virtual top quark, as it is directly proportional to the Higgs mass ($\propto m_H^2$); while one of the main sources of theoretical uncertainty is due to the contribution mediated by the bottom quark loop. Though this contribution is suppressed by the bottom quark to Higgs boson mass ratio (m_b^2/m_H^2), it includes the corrections enhanced by the second power of the large logarithm of the mass ratio m_H/m_b . The effective expansion parameter in this case is $\sim 40\alpha_s$ rather than the strong coupling constant α_s and the logarithmically enhanced terms clearly have to be resummed to all-orders.

In this thesis, we obtain the analytic result for the three-loop α_s^3 contribution to the bottom quark mediated amplitude of the Higgs boson production in gluon fusion through the third power in the quark mass. The all-order double-logarithmic asymptotic result for the amplitude is then obtained in two complementary approximations: the limit of large number of colors and the Abelian limit. The results of the analysis are used to get a quantitative estimate of the accuracy of the fixed order calculations [58, 59] and the calculations based on the small mass expansion [60, 61] of the light quark contribution to the Higgs boson production and decays.

In this thesis, we also complete the previous analysis of another fundamental quantity in QCD, the massive quark scattering amplitudes by an external color singlet field. As it has been shown in [13, 14], the double-logarithmic asymptotic behavior of the leading mass-suppressed contribution to the corresponding FF is described by a universal function independent of the Lorentz properties of the external field. We derive the closed form fully analytic result for the high-energy asymptotic behavior of this function.

1.2 Outline

The thesis is organized as follows:

The focus of chapter 2 is the review of background theory and computational techniques. We start with a review of QCD as it pertains to our calculation. This is followed by an overview of the two types of double-logarithms; the so-called ‘‘Sudakov’’ and ‘‘non-Sudakov’’ logarithms. We go over how they are generated and outline their key differences. Then we outline the technique developed in refs [13, 14] for the factorization of power-suppressed QCD amplitudes utilizing an artificial quark scattering amplitude.

In chapter 3, we consider the quark scattering by an external color singlet field. There we summarize the results obtained in [13, 14] for the scalar FF by the direct evaluation of the relevant two and three-loop diagrams for the non-Sudakov logarithms, as well as the all-order result. This is followed by the calculation of the asymptotic

form for the function that encapsulates the resummation result. We generalize the result to the off-shell FF which is a crucial ingredient for the analysis of the Higgs boson production in the following chapter.

The Higgs production FF is discussed in chapter 4. Contribution to the NNLP coefficient is generated via three sources: the factorizable contribution with a single soft quark exchange, the triple soft quark exchange contribution, and the non-factorizable contribution of the single soft quark with an emission of an eikonal gluon. After providing the exact three-loop result in the double-logarithmic approximation we consider two limits for the all-order result: the large number of colors limit of QCD, and the Abelian approximation. We end this chapter with a comparison of our results with other known results and apply them to the phenomenology of the Higgs boson production.

Chapter 5 is our Conclusion. We summarize the major results and discuss their implications.

Chapter 2

Theoretical background

2.1 Quantum Chromodynamics

QCD is the non-Abelian gauge theory describing the interactions of quarks and gluons, which transform in the fundamental and adjoint representation of the gauge group $SU(3)$ respectively. The QCD Lagrangian is

$$\mathcal{L}_{QCD} = -\frac{1}{4}(G_{\mu\nu}^a)^2 + \bar{\psi}_j (i\delta_{jk}\not{\partial} + g_s A^a T_{jk}^a - m\delta_{jk}) \psi_k, \quad (2.1)$$

with the gluon field strength tensor $G_{\mu\nu}^a$ defined as

$$G_{\mu\nu}^a = \partial_\mu A_\nu^a - \partial_\nu A_\mu^a + gf^{abc} A_\mu^b A_\nu^c. \quad (2.2)$$

We have excluded the gauge-fixing, and Faddeev-Popov ghost and anti-ghost terms from the Lagrangian as they do not contribute to the double-logarithmic approximation. The resulting Feynman rules are listed below. The gluon propagator is

$$\begin{array}{c} \mu, m \\ \text{~~~~~} \\ \text{~~~~~} \\ \text{~~~~~} \\ \text{~~~~~} \\ \text{~~~~~} \\ \text{~~~~~} \\ \text{~~~~~} \\ \text{~~~~~} \\ \text{~~~~~} \\ \text{~~~~~} \\ \nu, n \\ \text{~~~~~} \\ p \end{array} \equiv D_{\mu\nu}^{mn}(p) = -i \frac{g_{\mu\nu} - (1-\xi) \frac{p_\mu p_\nu}{p^2}}{p^2 + i\epsilon} \delta^{mn} \xrightarrow{\xi=1} \frac{-ig_{\mu\nu} \delta^{mn}}{p^2 + i\epsilon}; \quad (2.3)$$

we always work in the Feynman gauge for which $\xi = 1$. The propagator of colored fermions with mass m_f is

$$j \xrightarrow[l]{\hspace{1.5cm}} i \equiv S(l) = \frac{i(\not{l} + m_f)}{l^2 - m_f^2 + i\epsilon} \delta^{ij}; \quad (2.4)$$

The fermion gluon interaction vertex is

$$\begin{array}{c} \mu, m \\ \text{wavy line} \\ \swarrow \quad \searrow \\ j \quad \quad i \end{array} = ig_s \gamma^\mu T_{ij}^a. \quad (2.5)$$

The three gluon self-interaction vertex is

$$\begin{array}{c} \mu, m \\ \text{wavy line} \\ \swarrow \quad \searrow \\ \text{wavy line} \quad \text{wavy line} \\ p \quad \quad q \quad \quad k, \rho, r \end{array} = g_s f^{mnr} [g^{\mu\nu} (k-p)^\rho + g^{\nu\rho} (p-q)^\mu + g^{\rho\mu} (q-k)^\nu]. \quad (2.6)$$

The four gluon self-interaction vertex is omitted as it cannot generate contribution in the double-logarithmic approximation. External fermion lines get the factor of spinor u ,

$$\longrightarrow \bigcirc = u(p), \quad (2.7)$$

$$\bigcirc \longrightarrow = \bar{u}(p). \quad (2.8)$$

Similarly, external gluon lines give polarization vector,

$$\mu \text{ wavy line} \bigcirc = \epsilon_\mu(p), \quad (2.9)$$

$$\bigcirc \text{ wavy line} \mu = \epsilon_\mu^*(p). \quad (2.10)$$

For our analysis, we also need the Higgs boson and fermions interaction, $\mathcal{L}_{int} = \frac{g_w m_f}{2m_w} \bar{\psi} \phi \psi$, which generates the vertex

$$\begin{array}{c} \text{fermion line} \\ \swarrow \quad \searrow \\ \text{fermion line} \quad \text{dashed line} \end{array} = \frac{ig_w m_f}{2m_w} \equiv y_f, \quad (2.11)$$

where y_f is the fermion Yukawa coupling. The external scalar particle lines only get a factor of 1. Finally, the equations of motion for on-shell external fermions are

$$\bar{u}(p)(\not{p} - m_f) = (\not{p} - m_f)u(p) = 0. \quad (2.12)$$

Other important rules are that each closed fermion loop in a Feynman diagram gets a factor of (-1) , and the momentum is conserved at each vertex. Note from the Lagrangian of eq. (2.1) that in the massless fermion limit, the left-handed and right-

handed representations of the Dirac fermions completely decouple. More generally, terms with an even number of gamma matrices couple the opposite handedness, while the terms with an odd number of gamma matrices couple the same handedness. Since scalar FF is defined without gamma matrices (eq. (3.1)), it must vanish in the massless fermion limit, similar to the Pauli FF which is defined with two gamma matrices. While the Dirac FF is defined with a single gamma matrix and does not vanish in the massless limit.

The $SU(3)$ generators denoted by T^a , which are 8 traceless Hermitian matrices, also play a vital role in the evaluation of QCD amplitudes. Frequently utilized identities are

$$\text{tr} (T^a T^b) = T_{ij}^a T_{ji}^b = T_F \delta^{ab}, \quad (2.13)$$

$$(T^a T^a)_{ij} = T_{ik}^a T_{kj}^a = C_F \delta_{ij}, \quad (2.14)$$

$$\text{tr} [T^a T^b T^c] = \frac{1}{4} (d^{abc} + i f^{abc}), \quad (2.15)$$

and

$$f^{abc} f^{dbc} = C_A \delta^{ad}. \quad (2.16)$$

The final equation follows from the fact that the elements of the generating matrices in the adjoint representation are defined in terms of the structure constants. T_F is called the index of the fundamental representation, while $C_F(C_A)$ is the quadratic Casimir of the fundamental (adjoint) representation. Another handy relation known as Fierz identity is

$$T_{ij}^a T_{kl}^a = \frac{1}{2} \left(\delta_{il} \delta_{jk} - \frac{1}{N_c} \delta_{ij} \delta_{kl} \right), \quad (2.17)$$

which reduces to eq. (2.14) for $j = k$. For the fundamental representation of $SU(3)$,

$$C_F = \frac{N_c^2 - 1}{2N_c} = \frac{4}{3}, \quad (2.18)$$

$$T_F = \frac{1}{2}; \quad (2.19)$$

and for the adjoint representation

$$C_A = T_A = N_c = 3. \quad (2.20)$$

The Dirac or gamma matrix identities used throughout the calculations are listed in appendix A.

2.2 Origin of the double-logarithms

The double-logarithmic radiative corrections are a distinct feature of the gauge field theories and can be universally associated with the soft and collinear virtual or real particle emission. We focus on two types of double-logarithms: ‘‘Sudakov’’ and ‘‘non-Sudakov’’ logarithms. The Sudakov logarithms are characteristic of the LP of high-energy or small mass expansion; while the non-Sudakov logarithms are power-suppressed. The difference in their origin is the most crucial aspect for our analysis.

The Sudakov logarithms are generated by the exchange of soft virtual gauge boson(s) by highly energetic on-shell charged particles. The momenta of the soft gauge bosons can be ignored in the numerator of the propagators as the integrals involving additional powers of the soft momentum do not develop the necessary singularity needed to get the double-logarithms. In the soft gauge boson limit, the fermion propagator becomes eikonal,

$$S(p_i \pm l) \sim \frac{\not{p}_i \pm \not{l} + m_f}{(p_i \pm l)^2 - m_f^2} \approx \pm \frac{\not{p}_i + m_f}{2p_i l}; \quad (2.21)$$

where m_f is the fermion mass, p_i are the external particle momenta, and l is loop momentum. The soft gauge boson propagator reads

$$D_{\mu\nu}(l) \sim \frac{g_{\mu\nu}}{l^2}. \quad (2.22)$$

Thus, the soft gauge bosons provide the LP double-logarithmic contribution. In general, the massless soft gauge bosons do not generate double-logarithmic corrections at $\mathcal{O}(m_f^2)$ as it has been shown in [11] by using the expansion by regions method [62]. The double-logarithmic contributions from the strongly ordered momenta regions at LP can be obtained by the method outlined in [1, 11, 63]. These Sudakov logarithms exponentiate to provide universal suppression of the amplitude at the LP of the high-energy expansion.

Contrary to the Sudakov logarithms, the non-Sudakov logarithms are generated by an exchange of soft virtual fermions. To account for this crucial change, the momentum configuration from eqs. (2.21) and (2.22) can be modified such that the soft fermion propagators become scalar while the gauge boson propagators become eikonal,

$$S(p_i \pm l) \equiv S(l') \sim \frac{l' + m_f}{l'^2 - m_f^2} \approx \frac{m_f}{l'^2 - m_f^2}, \quad (2.23)$$

$$D_{\mu\nu}(l) \equiv D_{\mu\nu}(\mp(p_i - l')) \sim \frac{g_{\mu\nu}}{(p_i - l')^2} \approx \frac{g_{\mu\nu}}{m_f^2 - 2p_i l'}. \quad (2.24)$$

Therefore, the roles of the fermions and gauge bosons are reversed. From eq. (2.23), it

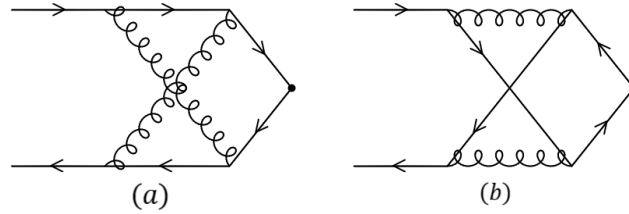


Figure 2.1: Examples of diagrams generating the (a) Sudakov, and (b) the power-suppressed non-Sudakov logarithms. The dark vertex connects to the rest of the diagrams via current or an external source.

is clear that each soft fermion propagator, which is now scalar, explicitly contributes a factor of the fermion mass, leading only to power-suppressed contribution. The double-logarithms can be obtained by following the standard Sudakov parametrization of the soft momenta. The original method of Sudakov [1, 21] can still be utilized to obtain the double-logarithms as the power suppression is explicit [11]. The complex structure of the non-Sudakov logarithms requires systematic treatment of the factorization in both Abelian and non-Abelian theories; making their all-order resummation a much more challenging problem, in turn resulting in limited knowledge of the all-order structure. Further details on the origin of these double-logarithms can be found in ref. [11]. A detailed sample calculation of producing the double-logarithms with Sudakov parametrization and the original method of Sudakov is given in appendix C.1.3.

2.3 Factorization of power-suppressed logarithms in QCD

To study the factorization process in QCD, we focus on a somewhat artificial process that retains the main features of the general problem despite being minimally complex. A massive quark (m_q) is being scattered by a local gauge field operator $(G_{\mu\nu}^a)^2$. The incoming and outgoing momentum of the quark is p_1 and p_2 respectively. The origin of this interaction is not relevant to our discussion but it provides an ideal toy model to derive the factorization in QCD. In fact, this model is the perfect example and precursor for the gauge boson scattering by a scalar field via a massive quark loop i.e., the Higgs production process. Let us first derive the LO and NLO amplitudes for this artificial process by direct evaluation of all the contributing diagrams.

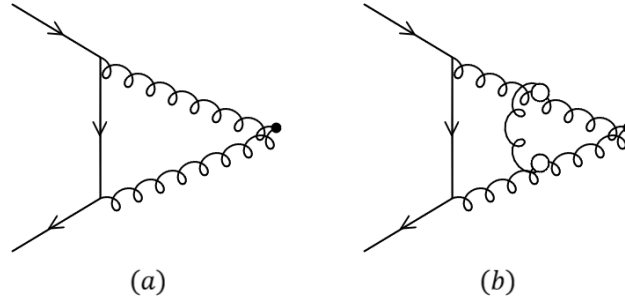


Figure 2.2: (a) The LO 1-loop diagram contributing to the quark scattering by the gauge field operator, $(G_{\mu\nu}^a)^2$, denoted by the dark vertex; and (b) the effective 2-loop diagram with soft gluon exchange between the eikonal lines; the hollow vertices denote eikonal color charge non-conservation explained in the text.

2.3.1 Direct evaluation of the LO amplitude

The LO contribution comes from the one-loop diagram fig. 2.2(a). In the high-energy limit, we have on-shell quarks $p_1^2 = p_2^2 = m_q^2$, and large momentum transfer for scattering $q^2 = -(p_2 - p_1)^2 \approx 2p_2p_1$; this makes the high-energy approximation parameter, $\rho = m_q^2/q^2$, small and positive. A required chirality flip on the virtual quark line in the high-energy limit results in the propagator becoming soft and provides mass suppression for the amplitude. Thus, the one-loop integral reduces to

$$\frac{2iq^2}{\pi^2} \int \frac{d^4l}{(l^2 - m_q^2)(p_1 - l)^2(p_2 - l)^2} \quad (2.25)$$

where the prefactor is kept for convenience. For the $m_q \ll l \ll q$ soft quark limit, the gluon propagators become eikonal, and the quark propagator becomes scalar as explained in section 2.2. By introducing the standard Sudakov parameterization for the loop momentum, $l = up_1 + vp_2 + l_\perp$, the propagators can be approximated as follows:

$$(l^2 - m_q^2) \approx [-2i\pi\delta(q^2uv + l_\perp^2 - m_q^2)]^{-1}, \quad (2.26)$$

$$(p_1 - l)^2 \approx -2p_1l \approx -q^2v, \quad (2.27)$$

$$(p_2 - l)^2 \approx -2p_2l \approx -q^2u. \quad (2.28)$$

The eikonal approximation for the propagators is only valid and thus requires that $|u|, |v| < 1$ along with an additional condition $uv > \rho$ that allows the quark propagator to go on-shell. The integration over the transverse component of the momentum, l_\perp , can now be performed by taking the residue of the soft quark propagator, reducing eq. (2.25) to

$$2 \int_\rho^1 \frac{dv}{v} \int_{\rho/v}^1 \frac{du}{u} = 2 \ln^2 \rho \int_0^1 d\eta \int_0^{1-\eta} d\xi = \ln^2 \rho, \quad (2.29)$$

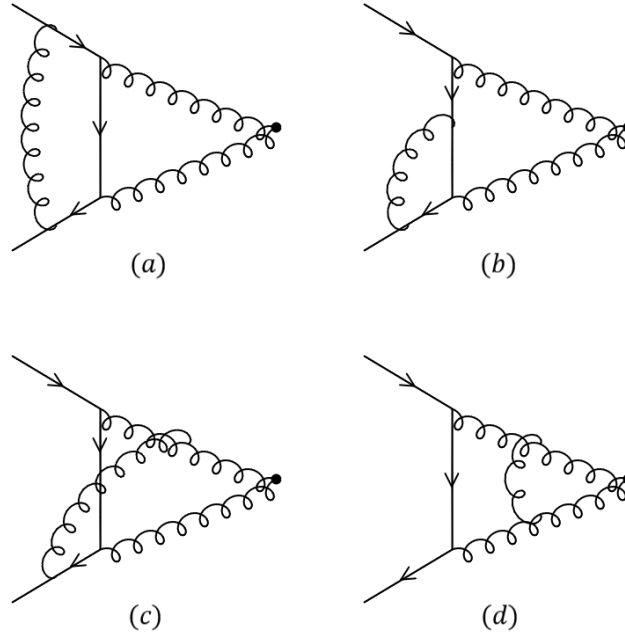


Figure 2.3: The 2-loop diagrams contributing to the NLO of quark scattering by $(G_{\mu\nu}^a)^2$. Symmetric diagrams are not included.

where $\eta = \ln v / \ln \rho$, and $\xi = \ln u / \ln \rho$ are the normalized logarithmic variables. The LO amplitude now reads

$$\mathcal{G}^0 = 2C_F x m_q \bar{q}(p_2) q(p_1), \quad (2.30)$$

with $x = \frac{\alpha_s}{4\pi} \ln^2 \rho$ incorporating the double-logarithmic factors, and α_s being the strong coupling constant. This is a typical example of a massive soft quark exchange generating the power-suppressed non-Sudakov logarithms. The peculiar thing is that the emission of the soft quark also results in the change of the color group representation for the particle propagating along the eikonal lines, known as the *eikonal color charge non-conservation*. This crucial feature plays an important role in further analysis.

2.3.2 Direct evaluation of the NLO amplitude

At the NLO, the contributing diagrams are shown in fig. 2.3. Only the analysis of fig. 2.3(a) poses an additional challenge due to the IR divergence that is present in the final result as it is not regulated by the quark mass. Soft and eikonal approximations of eqs. (2.26) to (2.28) for the soft quark momentum l are still valid. Starting with fig. 2.3(a), the color factor is

$$c_{2.3a} = T_{jk}^m T_{kd}^a T_{dc}^b T_{ci}^n \delta^{ab} \delta^{mn} = T_{jk}^m T_{kd}^a T_{dc}^a T_{ci}^m = T_{jk}^m T_{ci}^m C_F \delta_{kc} = C_F^2 \delta_{ij}; \quad (2.31)$$

resulting in the reduced color $c_a = C_F$ after the one-loop color C_F is factored out. The integral over the soft gluon momentum, l_g , gets the double-logarithmic scaling if

$l_g p_i < l p_i$, making l_g negligible in the eikonal quark propagators with the soft quark momentum l , leading to the condition $u_g < u$ and $v_g < v$ for the corresponding Sudakov parameters. Thus, retaining l_g only in the propagators without the soft quark momentum l , integral over soft gluon momentum reduces to

$$\frac{2iq^2}{\pi^2} \int \frac{d^4 l_g}{l_g^2 \{(p_1 - l_g)^2 - m^2\} \{(p_2 - l_g)^2 - m^2\}}. \quad (2.32)$$

With Sudakov parameterization of $l_g = u_g p_1 + v_g p_2 + l_{g\perp}$, the propagators can be approximated as

$$l_g^2 \approx [-i\pi\delta(q^2 u_g v_g + l_{g\perp}^2)]^{-1}, \quad (2.33)$$

$$(p_1 - l_g)^2 - m^2 \approx -2p_1 l_g \approx -q^2(v_g + 2\rho u_g), \quad (2.34)$$

$$(p_2 - l_g)^2 - m^2 \approx -2p_2 l_g \approx -q^2(u_g + 2\rho v_g). \quad (2.35)$$

After integral over the Dirac delta function and $\rho_\perp = -l_{g\perp}^2$, eq. (2.33) in the double-logarithmic region reduces to

$$2 \int_{\rho u_g}^v \frac{dv_g}{v_g} \int_{\rho v_g}^u \frac{du_g}{u_g}. \quad (2.36)$$

This integral has the aforementioned soft IR divergence when both u_g and v_g become small simultaneously. This divergence can be removed by subtracting ‘‘the factorized expression’’

$$2 \int_{\rho u_g}^1 \frac{dv_g}{v_g} \int_{\rho v_g}^1 \frac{du_g}{u_g}. \quad (2.37)$$

This subtraction term is independent of soft quark momentum and is equivalent to the factorized one-loop Sudakov FF given by

$$\frac{C_F \alpha_s}{4\pi} \frac{2iq^2}{\pi^2} \int \frac{d^4 l_g}{l_g^2 \{(p_1 - l_g)^2 - m_q^2\} \{(p_2 - l_g)^2 - m_q^2\}} = \frac{C_F \alpha_s}{4\pi} \left(2 \frac{\ln \rho}{\varepsilon} + \ln^2 \rho \right). \quad (2.38)$$

This integral is evaluated in dimensional regularization with $d = 4 - 2\varepsilon$, where $\varepsilon \neq 0$ regulates the (soft) IR divergence. This result coincides with the one-loop on-shell Sudakov FF, which includes all the universal Sudakov double-logarithm for the amplitudes with quark-antiquark external lines. The full term is of course given by

$$\int \frac{d^4 l}{(2\pi)^4} \frac{1}{(l^2 - m^2)(p_1 - l)^2(p_2 - l)^2} \times \int \frac{d^4 l_g}{(2\pi)^4} \frac{1}{l_g^2 \{(p_1 - l_g)^2 - m^2\} \{(p_2 - l_g)^2 - m^2\}}; \quad (2.39)$$

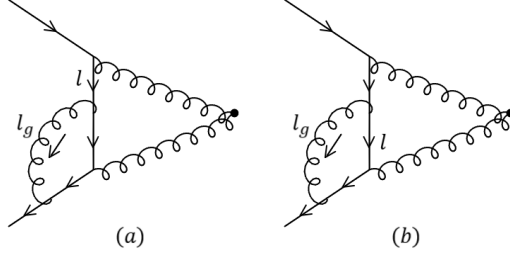


Figure 2.4: The two configurations for fig. 2.3(b) in which quark propagator (a) above and (b) below the soft gluon emission vertex is soft, and goes on-shell.

with the integral over l_g resulting in the Sudakov factor, while the integral over soft quark momentum l is equivalent to the one-loop factor of eq. (2.25). Subtracting the factorized expression eq. (2.37) from eq. (2.36) gives

$$\begin{aligned}
 & 2 \int_{\rho u_g}^v \frac{dv_g}{v_g} \int_{\rho v_g}^u \frac{du_g}{u_g} - 2 \int_{\rho u_g}^1 \frac{dv_g}{v_g} \int_{\rho v_g}^1 \frac{du_g}{u_g} \\
 &= -2 \left(\int_v^1 \frac{dv_g}{v_g} \int_{\rho v_g}^u \frac{du_g}{u_g} + \int_{\rho u_g}^1 \frac{dv_g}{v_g} \int_u^{\rho v_g} \frac{du_g}{u_g} + \int_{\rho u_g}^1 \frac{dv_g}{v_g} \int_{\rho v_g}^1 \frac{du_g}{u_g} \right) \\
 &= -2 \left(\int_v^1 \frac{dv_g}{v_g} \int_{\rho v_g}^u \frac{du_g}{u_g} + \int_{\rho u_g}^1 \frac{dv_g}{v_g} \int_u^1 \frac{du_g}{u_g} \right) \\
 &= -2 \left(\int_v^1 \frac{dv_g}{v_g} \int_{\rho v_g}^u \frac{du_g}{u_g} + \int_u^1 \frac{du_g}{u_g} \int_{\rho u_g}^v \frac{dv_g}{v_g} + \int_v^1 \frac{dv_g}{v_g} \int_u^1 \frac{du_g}{u_g} \right) \\
 &= -2 \ln^2 \rho \left(\int_0^\eta d\eta_g \int_\xi^{1+\eta_g} d\xi_g + \int_0^\xi d\xi_g \int_\eta^{1+\xi_g} d\eta_g + \int_0^\eta d\eta_g \int_0^\xi d\xi_g \right) \\
 &\quad \sim \ln^2 \rho [(\eta - \xi)^2 + 2(\eta + \xi)], \tag{2.40}
 \end{aligned}$$

where we have introduced the standard normalized logarithmic variables $\eta_g = \ln v_g / \ln \rho$ and $\xi_g = \ln u_g / \ln \rho$. In eq. (2.40), the expression obtained after the integral over the soft gluon momentum is called the weight and denoted by $w_\lambda(\eta, \xi) \equiv w_\lambda$.

Next, fig. 2.3(b) too has soft IR divergence which cancels when both configurations of this diagram shown in fig. 2.4 are included. They correspond to the soft quark propagator above and below the soft gluon emission vertex going on-shell. Integral over l_g in these cases is

$$\frac{4i(p_2 l)}{\pi^2} \int \frac{d^4 l_g}{l_g^2 \{(p_2 - l_g)^2 - m^2\} \{(l \pm l_g)^2 - m^2\}}; \tag{2.41}$$

with $l_g = u_g l + v_g p_2 + l_{g\perp}$. Momentum p_1 is replaced by l as it acts as the external momentum for the soft gluon emitted by the soft quark line. The propagators are

approximated as

$$l_g^2 \approx [-i\pi\delta(2p_2 l u_g v_g + l_{g\perp}^2)]^{-1}, \quad (2.42)$$

$$(p_2 - l_g)^2 - m^2 \approx -2p_2 l_g \approx -2p_2 l u_g - m^2 v_g \approx -q^2(u_g u + 2\rho v_g), \quad (2.43)$$

$$(l \pm l_g)^2 - m^2 \approx \pm 2l_g l \approx \pm 2p_2 l v_g \pm m^2 u_g \approx \pm q^2(v_g u + 2\rho u_g). \quad (2.44)$$

When the propagator above and below the soft gluon emission vertex is on-shell, integral of eq. (2.41) reduces to

$$2 \int_{\rho u_g/u}^1 \frac{dv_g}{v_g} \int_{\rho v_g/u}^1 \frac{du_g}{u_g}, \quad (2.45)$$

and

$$-2 \int_{\rho u_g/u}^v \frac{dv_g}{v_g} \int_{\rho v_g/u}^1 \frac{du_g}{u_g} \quad (2.46)$$

respectively. Adding the two, we obtain

$$\begin{aligned} 2 \left[\int_{\rho u_g/u}^1 \frac{dv_g}{v_g} - \int_{\rho u_g/u}^v \frac{dv_g}{v_g} \right] \int_{\rho v_g/u}^1 \frac{du_g}{u_g} &= 2 \int_v^1 \frac{dv_g}{v_g} \int_{\rho v_g/u}^1 \frac{du_g}{u_g} \\ &= 2 \ln^2 \rho \int_0^\eta d\eta_g \int_0^{1-\xi+\eta_g} d\xi_g \sim \ln^2 \rho (\eta^2 - 2\eta\xi + 2\eta). \end{aligned} \quad (2.47)$$

The color of this diagram is

$$\begin{aligned} c_{2.3b} &= T_{jk}^m T_{kd}^a T_{dc}^m T_{ci}^a \\ c_{2.3b} &= \frac{1}{4} \left(\delta_{jc} \delta_{kd} - \frac{1}{N_c} \delta_{jk} \delta_{dc} \right) \left(\delta_{ki} \delta_{cd} - \frac{1}{N_c} \delta_{dk} \delta_{ic} \right) \\ c_{2.3b} &= \frac{\delta_{ij}}{4} \left(-1 + \frac{1}{N_c^2} \right) \sim \delta_{ij} C_F \left(C_F - \frac{C_A}{2} \right) \end{aligned} \quad (2.48)$$

with reduced color of $c_b = (C_A/2) - C_F$.

Moving on to fig. 2.3(c), the color of which is

$$\begin{aligned} c_{2.3c} &= T_{jk}^m T_{kd}^b T_{di}^a f^{amb} \\ c_{2.3c} &= \frac{1}{2} T_{jk}^m [T^b, T^a]_{ki} f^{amb} \\ c_{2.3c} &= \frac{1}{2} T_{jk}^m T_{ki}^n f^{ban} f^{amb} \\ c_{2.3c} &= \frac{C_A}{2} T_{jk}^m T_{ki}^n \delta^{mn} \sim \frac{C_A}{2} C_F \delta_{ij} \end{aligned} \quad (2.49)$$

resulting in the reduced factor of $c_c = -C_A/2$. Eikonal approximation for the new

λ	c_λ	w_λ
a	C_F	$(\eta - \xi)^2 + 2(\xi + \eta)$
b	$-C_F + C_A/2$	$\eta^2 - 2\xi\eta + 2\eta$
c	$-C_A/2$	$\eta^2 - 2\xi\eta + 2\eta$
d	$-C_A$	$2\xi\eta$

Table 2.1: The reduced color factors c_λ and the weights w_λ for the 2-loop diagrams in fig. 2.3. Contributions of the symmetric diagrams can be obtained by $\eta \longleftrightarrow \xi$ in the rows b and c.

propagators are

$$(p_1 - l - l_g)^2 \approx -2p_1(l + l_g) \approx -2p_1p_2(v + v_g) \quad (2.50)$$

$$(p_2 - l - l_g)^2 \approx -2p_2(l + l_g) \approx -2p_2p_1(u + u_g) \quad (2.51)$$

with eqs. (2.26), (2.27), (2.33) and (2.35) still valid. These results in double-logarithm over l_g when $p_1l < p_1l_g$ and $p_2l_g < p_2l$ corresponding to $v < v_g$ and $u_g < u$; integral gives

$$\begin{aligned} & \frac{2iq^2}{\pi^2} \int \frac{d^4l_g}{l_g^2(p_1 - l - l_g)^2\{(p_2 - l_g)^2 - m^2\}} \\ &= 2 \int_v^1 \frac{dv_g}{v_g} \int_{\rho v_g}^u \frac{du_g}{u_g} = 2 \ln^2 \rho \int_0^\eta d\eta_g \int_\xi^{1+\eta_g} d\xi_g \sim \ln^2 \rho (\eta^2 - 2\eta\xi + 2\eta). \end{aligned} \quad (2.52)$$

For the final diagram, fig. 2.3(d), color factor of

$$c_{2.3d} = T_{jk}^b T_{ki}^a f^{amn} f^{bmn} = T_{jk}^a T_{ki}^a C_A \sim C_F C_A \delta_{ij}, \quad (2.53)$$

results in $c_d = -C_A$. With soft and eikonal approximations of eqs. (2.26) to (2.28), (2.33), (2.50) and (2.51), double-logarithmic condition over l_g requires that $p_2l < p_2l_g$ and $p_1l < p_1l_g$ or $u < u_g$ and $v < v_g$. The integral over l_g ,

$$\begin{aligned} & \frac{2iq^2}{\pi^2} \int \frac{d^4l_g}{l_g^2(p_1 - l - l_g)^2(p_2 - l - l_g)^2} \\ &= 2 \int_v^1 \frac{dv_g}{v_g} \int_u^1 \frac{du_g}{u_g} = 2 \ln^2 \rho \int_0^\eta d\eta_g \int_0^\xi d\xi_g \sim \ln^2 \rho (2\eta\xi); \end{aligned} \quad (2.54)$$

results in $w_d = 2\eta\xi$.

Final IR finite results for all the two-loop diagrams are collected in table 2.1. The

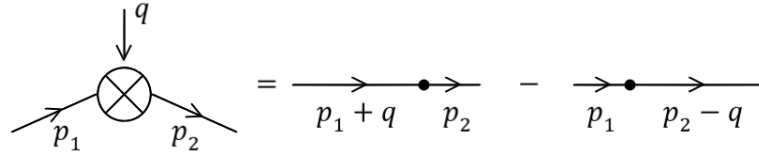


Figure 2.5: Diagrammatic representation of eq. (2.57). The diagram on the left represents $iq_\mu M^\mu$.

total contribution at NLO can be written as the sum,

$$2x \left[\sum_\lambda c_\lambda \int_0^1 d\eta \int_0^{1-\eta} d\xi \omega_\lambda \right] \mathcal{G}^0, \quad (2.55)$$

with the reduced color factor c_λ , and the weight w_λ of table 2.1. This sum must include the contribution from the symmetric diagrams that are not included in fig. 2.3; which can be obtained by interchanging η and ξ in the rows b and c of table 2.1 for their symmetric counterparts. We observe that the sum of eq. (2.55) reduces to

$$-2z \left[\int_0^1 d\eta \int_0^{1-\eta} d\xi (2\eta\xi) \right] \mathcal{G}^0 = -\frac{z}{6} \mathcal{G}^0, \quad (2.56)$$

with $z = (C_A - C_F)x$. An important thing to note in table 2.1 is that the non-Abelian part between rows b and c cancels exactly.

2.3.3 Factorization at the NLO amplitude

Let us see how the same result is obtained by the method of factorization at the NLO. The key to this method is in moving the soft gluon vertex from the virtual quark line in fig. 2.3(b) to the upper eikonal gluon line, obtaining a diagram of the form of fig. 2.3(c). This is done by applying a sequence of identities, graphically represented by fig. 2.6. The lower eikonal quark line in the fig. 2.6(a) can only emit the A^- light-cone component of the gluon field in covariant gauges, with the emission of the other components being suppressed. The interaction of the A^- component is completely determined by the gauge invariance as it does not correspond to a physical polarization of the gluon field. Now we utilize the Ward-Takahashi identity at the interaction vertex on the soft quark line. Standard Ward-Takahashi identity is given by

$$iq_\mu M^\mu(q, p_1, p_2) = M_0(p_1 + q, p_2) - M_0(p_1, p_2 - q), \quad (2.57)$$

diagrammatic representation of which is given in fig. 2.5 [64]. This can be written in terms of the associated vertex with $q^\mu = (p_1 - p_2)^\mu$ as

$$q_\mu S(p_1) \Gamma^\mu(q) S(p_2) = iS(p_1) - iS(p_2); \quad (2.58)$$

where Γ^μ can be replaced with γ^μ to the leading order with no loops present in fig. 2.5. Thus from the Ward-Takahashi identity, with $p_1 = l$ and $p_2 = l + l_g$ in eq. (2.58) we can write

$$S(l) \gamma^\mu S(l + l_g) \approx S(l) \gamma^- S(l + l_g^+) = \frac{1}{l_g^+} [S(l) - S(l + l_g^+)]. \quad (2.59)$$

at the interaction vertex on the soft quark line in fig. 2.3(b). The standard form of the Ward identity can be obtained by multiplying eq. (2.59) with $l_{g\mu} \approx l_{g-} = l_g^+$. Starting with the amplitude of fig. 2.6(a),

$$\mathcal{M} \propto \gamma^\beta S(l) \gamma^\mu S(l + l_g) \gamma^\alpha S(p_2 + l_g) \gamma^\nu D_{\mu\nu}(l_g) D(p_1 - l) D(p_2 - l); \quad (2.60)$$

applying the Ward identity of eq. (2.59) gives

$$\sim \gamma^\beta \frac{1}{l_g^+} [S(l) - S(l + l_g^+)] \gamma^\alpha S(p_2 + l_g) \gamma^\nu D_{\mu\nu}(l_g) D(p_1 - l) D(p_2 - l). \quad (2.61)$$

This is equivalent to fig. 2.6(b) with the crossed circle representing the $S(l) \rightarrow S(l) - S(l + l_g^+)$ replacement, while the upper eikonal quark line absorbs the $1/l_g^+$ factor in the eikonal approximation since $S(p_1 + l_g) \approx 1/(2l_g^+)$. It is important to note that the integral over l_g gives logarithmic scaling when $l_{g+} = l_g^-$ component is ignored in the $S(l + l_g)$, making the propagator proportional to $1/l_{g-}$.

To go from fig. 2.6(b) to (c), i.e., move the crossed circle from the soft quark line to the upper eikonal gluon line, a momentum shift $l \rightarrow l - l_g^+$ must be applied to the second term of the expression in eq. (2.59). For the amplitude in eq. (2.61) this results in

$$\begin{aligned} &\sim \gamma^\beta \frac{1}{l_g^+} S(l) \gamma^\alpha S(p_2 + l_g) \gamma^\nu D_{\mu\nu}(l_g) D(p_1 - l) D(p_2 - l) - \\ &\quad \gamma^\beta \frac{1}{l_g^+} S(l) \gamma^\alpha S(p_2 + l_g) \gamma^\nu D_{\mu\nu}(l_g) D(p_1 - l + l_g^+) D(p_2 - l + l_g^+). \end{aligned} \quad (2.62)$$

Since $p_2^- \approx 0$, the opposite eikonal line with momentum p_2 is insensitive to this shift and remains unaffected; and as long as $l_g \ll l$, we can make the substitution

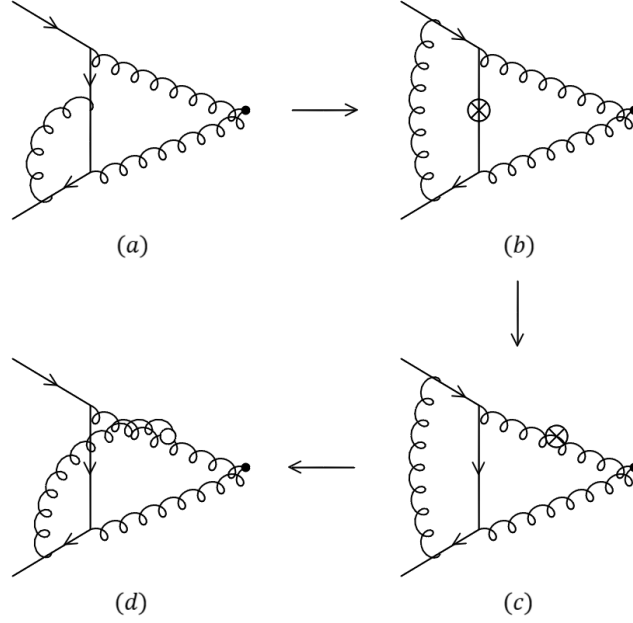


Figure 2.6: Diagrammatic representation of the sequence of identities that move the soft gluon vertex from the soft quark to the upper eikonal gluon line. The crossed circle in (b) and (c) are defined in the text. The hollow vertex on the upper eikonal line in (d) represents effective coupling as explained in the text.

$D(p_2 - l) \approx D(p_2 - l + l_g^+)$, reducing eq. (2.62) to

$$\sim \gamma^\beta \frac{1}{l_g^+} S(l) \gamma^\alpha S(p_2 + l_g) \gamma^\nu D_{\mu\nu}(l_g) [D(p_1 - l) - D(p_1 - l + l_g^+)] D(p_2 - l + l_g^+). \quad (2.63)$$

This is now equivalent to fig. 2.6(c).

Applying the “inverted Ward identity” on the upper gluon eikonal line results in

$$\frac{1}{l_g^+} \left[\frac{1}{-2p_1 l} - \frac{1}{2p_1(-l + l_g^+)} \right] = \frac{1}{-2p_1 l} 2p_1^- \frac{1}{2p_1(-l + l_g^+)} \approx \frac{1}{(p_1 - l)^2} 2p_1^\mu \frac{1}{(p_1 - l + l_g^+)^2}. \quad (2.64)$$

In terms of the amplitude of eq. (2.63), this reads

$$\sim \gamma^\beta S(l) \gamma^\alpha S(p_2 + l_g) \gamma^\nu D_{\mu\nu}(l_g) D(p_1 - l) (2p_1^\mu) D(p_1 - l + l_g^+) D(p_2 - l + l_g^+); \quad (2.65)$$

which corresponds to the final diagram fig. 2.6(d). For $p_1^+ \approx 0$, the $2p_1(-l + l_g^+) \rightarrow (p_1 - l + l_g^+)^2$ replacement works only if $l_g \ll q$. The effective coupling for this diagram is $C_F \alpha_s$, making it equivalent to the sum of the lines *b* and *c* from table 2.1.

Eikonal factorization is then achieved by summing over all the diagrams to get the “ladder” structure. Diagrams required for this summation are fig. 2.6(d), its symmetric counterpart, fig. 2.3(a) and (d). But the reduced color for fig. 2.3(d) is C_A , while the same for the rest in the sum is C_F , thus we must manually add the

contribution of the fig. 2.3(d) with the color factor C_F . The denominators of these diagrams are

$$D_{2.3a} = \{(p_2 - l_g)^2 - m^2\}(l^2 - m^2)\{(p_1 - l_g)^2 - m^2\}(p_1 - l - l_g)^2(p_2 - l - l_g)^2 l_g^2, \quad (2.66)$$

$$D_{2.6d} = \{(p_2 - l_g)^2 - m^2\}(l^2 - m^2)(p_1 - l)^2(p_1 - l - l_g)^2(p_2 - l - l_g)^2 l_g^2, \quad (2.67)$$

$$D_{2.6d_S} = \{(p_1 - l_g)^2 - m^2\}(l^2 - m^2)(p_2 - l)^2(p_1 - l - l_g)^2(p_2 - l - l_g)^2 l_g^2, \quad (2.68)$$

$$D_{2.3d} = (p_2 - l)^2(l^2 - m^2)(p_1 - l)^2(p_1 - l - l_g)^2(p_2 - l - l_g)^2 l_g^2; \quad (2.69)$$

where eq. (2.68) is for the symmetric diagram to fig. 2.6(d), obtained by a similar sequence of Ward identities and momentum shifts from the symmetric counterpart of fig. 2.3(b).

$$\begin{aligned} I_{tot} &\approx \int \frac{d^4 l d^4 l_g}{(2\pi)^8} \left(\frac{1}{D_{2.3a}} + \frac{1}{D_{2.6d}} + \frac{1}{D_{2.6d_S}} + \frac{1}{D_{2.3d}} \right) \\ I_{tot} &= \int \frac{d^4 l d^4 l_g}{(2\pi)^8} \frac{1}{(l^2 - m^2) l_g^2 (p_1 - l - l_g)^2 (p_2 - l - l_g)^2} \\ &\left[\frac{1}{(p_2 - l_g)^2 - m^2} \left\{ \frac{1}{(p_1 - l_g)^2 - m^2} + \frac{1}{(p_1 - l)^2} \right\} + \frac{1}{(p_2 - l)^2} \left\{ \frac{1}{(p_1 - l_g)^2 - m^2} + \frac{1}{(p_1 - l)^2} \right\} \right] \\ I_{tot} &\approx \int \frac{d^4 l d^4 l_g}{(2\pi)^8} \frac{1}{(l^2 - m^2) l_g^2 \{-2p_1(l + l_g)\} \{-2p_2(l + l_g)\}} \\ &\left[\frac{-2p_1(l + l_g)}{(-2p_1 l_g)(-2p_1 l)} \right] \left[\frac{-2p_2(l + l_g)}{(-2p_2 l_g)(-2p_2 l)} \right] \\ I_{tot} &\approx \int \frac{d^4 l}{(2\pi)^4} \frac{1}{(l^2 - m^2)(p_1 - l)^2(p_2 - l)^2} \times \\ &\int \frac{d^4 l_g}{(2\pi)^4} \frac{1}{l_g^2 \{(p_1 - l_g)^2 - m^2\} \{(p_2 - l_g)^2 - m^2\}}; \quad (2.70) \end{aligned}$$

where we have rewritten the full propagators in the last line to emphasize the factorization of the soft gluon contribution. This sum is diagrammatically represented by fig. 2.7. The integral is identical to the full factorized expression of eq. (2.39). Integral over l_g in eq. (2.70) is exactly the same as eq. (2.38) and factors out into the universal Sudakov exponent Z_q^2 ; while the integral over l is identical to the one-loop contribution of eq. (2.25) and factors out into the non-Sudakov exponent i.e., $g(z)$. The function $g(z)$ is discussed in the next section.

The remaining contribution is given by the ‘‘effective diagram’’ fig. 2.2(b) with effective coupling proportional to $(C_A - C_F)\alpha_s$. Apart from the effective coupling

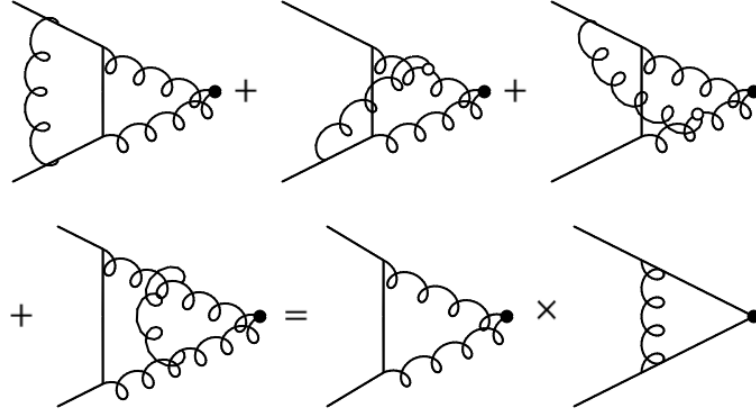


Figure 2.7: Diagrammatic representation of the eikonal factorization. From top left to bottom right they represent fig. 2.3(a), fig. 2.6(d), symmetric counterpart of fig. 2.6(d), fig. 2.3(d), fig. 2.2(a), and the 1-loop vertex correction for quark scattering.

with modified color along the eikonal line, it is obvious that fig. 2.2(b) and fig. 2.3(d) are identical; this change in the color due to the emission of the soft quark is exactly the previously mentioned *eikonal color charge non-conservation*. The corresponding integral is proportional to

$$\left(\frac{2iq^2}{\pi^2}\right)^2 (C_A - C_F) \int \int \frac{d^4l}{(l^2 - m_q^2)(p_1 - l)^2(p_2 - l)^2} \frac{d^4l_g}{l_g^2(p_1 - l - l_g)^2(p_2 - l - l_g)^2}. \quad (2.71)$$

The integrals over both l and l_g produce double-logarithms when $lp_i < l_gp_i$ and thus the soft quark momentum l can be ignored in the eikonal propagators with the gluon momentum l_g . For the Sudakov parameter ordering along the eikonal lines, this reduces to $u < u_g$ and $v < v_g$, identically to fig. 2.3(d) as expected. Soft and eikonal approximations of eqs. (2.26) to (2.28), (2.33), (2.50) and (2.51) are also still valid. By introducing the normalized logarithmic variables after performing the integrals over the transverse components of the momenta, eq. (2.71) reduces to

$$\begin{aligned} & \frac{\alpha_s}{\pi} (C_A - C_F) \ln^4 \rho \int_0^1 d\eta \int_0^{1-\eta} d\xi \int_0^\eta d\eta_g \int_0^\xi d\xi_g \\ & = 2z \left[\int_0^1 d\eta \int_0^{1-\eta} d\xi (2\eta\xi) \right] \mathcal{G}^0 = \frac{z}{6} \mathcal{G}^0 \end{aligned} \quad (2.72)$$

This agrees with the exact result, eq. (2.56), obtained by the direct evaluation of the NLO diagrams. Thus, we have shown the factorization of the amplitude at the NLO in QCD.

2.3.4 All-order resummation

The resummation of the double-logarithms at all-orders in the perturbation theory can now be performed. The procedure can be applied to an arbitrary number of gluons being emitted from the soft quark line as the soft gluons from the eikonal line factorize and exponentiate. These exponentiated one-loop Sudakov logarithms result in a universal suppression factor

$$Z_q^2 = \exp \left[-C_F \left(\frac{\alpha_s \ln \rho}{2\pi \varepsilon} + x \right) \right], \quad (2.73)$$

where ε is the dimensional regulator for the IR divergences. The same statement applies to the soft gluon exchange of the effective diagram fig. 2.2(b). Thus, the all-order non-Sudakov contribution can be obtained similarly by exponentiating the one-loop result, $-2z\eta\xi$, from eq. (2.56), within the integrals over the normalized double-logarithmic variables and reads

$$\mathcal{G} = Z_q^2 g(-z) \mathcal{G}^0. \quad (2.74)$$

The non-Sudakov contribution of an arbitrary number of soft exchanges between the eikonal lines is completely encapsulated within the function $g(z)$. This function is normalized to $z = 0$ as $g(0) = 1$, and can be written explicitly as two-fold integral

$$g(z) = 2 \int_0^1 d\eta \int_0^{1-\eta} d\xi (e^{2z\eta\xi}). \quad (2.75)$$

The exact solution for this function is found in terms of generalized hypergeometric function and can be Taylor expanded as

$$g(z) = {}_2F_2(1, 1; 3/2, 2; z/2) = 2 \sum_0^{\infty} \frac{n!(2z)^n}{(2n+2)!}. \quad (2.76)$$

For a comprehensive review of this technique, including further verification by direct evaluation of the NNLO diagrams for the artificial amplitude considered in this section, readers are encouraged to check ref. [14].

2.3.5 Large z asymptotic for $g(z)$

In the previous section, we showed that the function $g(z)$ encapsulates the all-order contribution to the artificial process we investigated to obtain the factorization. We will encounter this function again in the Higgs production FF. Thus, it is important to find out how this function may behave in different theories and at large values of

z . To calculate the analytical asymptotic form for $g(z)$ as $z \rightarrow \pm\infty$, let us rewrite the function with an explicit sign in front of the variable z ,

$$g(\pm z) = 2 \int_0^1 d\eta_1 \int_0^{1-\eta_1} d\xi_1 (e^{\pm 2z\eta_1\xi_1}). \quad (2.77)$$

To proceed, we must first apply a change of variables $\xi_1 = y\sqrt{\lambda}$ and $\eta_1 = \sqrt{\lambda}/y$ with the Jacobian $|J| = y^{-1}$. The integration limits for the new variables are

$$0 < \lambda < 1/4, \quad \frac{1 - \sqrt{1 - 4\lambda}}{2\sqrt{\lambda}} (\equiv y_L) < y < \frac{1 + \sqrt{1 - 4\lambda}}{2\sqrt{\lambda}} (\equiv y_H); \quad (2.78)$$

obtained by solving the quadratic equation resulting from plugging the original integration limit $\xi_1 = 1 - \eta_1$, in $\eta_1\xi_1 = \lambda$ and $\xi_1/\eta_1 = y^2$. The limits for the y integration enforce the λ integration limits as all the original variables are positive. This gives

$$g(\pm z) = 2 \int_0^{1/4} d\lambda \int_{y_L}^{y_H} dy \frac{e^{2z\lambda}}{y},$$

$$g(\pm z) = 2 \int_0^{1/4} d\lambda e^{\pm 2z\lambda} \ln \left(\frac{1 + \sqrt{1 - 4\lambda}}{1 - \sqrt{1 - 4\lambda}} \right). \quad (2.79)$$

Further evaluation depends on the sign in front of the variable z . For positive z , the integral is enhanced due to the exponential factor and is saturated in the proximity of the maximal value of $\lambda = 1/4$. Expansion of the logarithm around $x = \sqrt{1 - 4\lambda} = 0$ is $\ln \left(\frac{1+x}{1-x} \right) \approx (2x)$, and eq. (2.79) reduces to

$$g(z) = 2 \int_0^{1/4} d\lambda e^{2z\lambda} (2\sqrt{1 - 4\lambda}),$$

$$g(z) = \frac{\sqrt{2}}{z^{3/2}} e^{z/2} \left[\sqrt{\pi} - 2\Gamma \left(\frac{3}{2}, \frac{z}{2} \right) \right]. \quad (2.80)$$

As $z \rightarrow \infty$, the gamma function vanishes and eq. (2.80) reduces to

$$g(z) \approx \left(\frac{2\pi e^z}{z^3} \right)^{1/2}. \quad (2.81)$$

For the opposite limit, we must instead expand the logarithm in eq. (2.79) near $\lambda = 0$; $\frac{1+\sqrt{1-4\lambda}}{1-\sqrt{1-4\lambda}} \approx \frac{1+1}{1-1+2\lambda} \approx \frac{1}{\lambda}$ gives,

$$g(-z) = 2 \int_0^{1/4} d\lambda e^{-2z\lambda} (-\ln \lambda),$$

$$g(-z) = \frac{\gamma_E + E_1 \left(\frac{z}{2} \right) - e^{-z/2} \ln 4 + \ln(2z)}{z}; \quad (2.82)$$

where $E_1(z/2)$ is the exponential integral function. As $z \rightarrow \infty$ limit is applied, eq. (2.82) reduces to

$$g(-z) \approx \frac{\gamma_E + \ln(2z)}{z}. \quad (2.83)$$

The positive z limit is applicable in QCD, and the negative z limit in QED as $C_A = 0 \Rightarrow z = -C_F x$. In general, we can conclude that if a generic QCD amplitude gets exponentially enhanced at high energies, then an amplitude with inverted color charge flow from the eikonal lines defined by the scattering particles, or the same amplitude in QED have logarithmic scaling, and vice versa.

Chapter 3

The quark scattering

Quark scattering by a color singlet external field is one of the simplest fundamental processes in QCD. In the high-energy limit the corresponding FF for the massive quarks have been studied at NLP in [13, 14] where the all-order double-logarithmic result has been derived in the form of the four-fold integral representation. This representation, however, is not suitable for an analytic evaluation of the asymptotic result. Moreover, the analysis of [13, 14] applies to the on-shell FF only, while in many applications the result for slightly off-shell FF is mandatory. In particular, such an off-shell result is necessary for the analysis of the Higgs boson production at the NNLP presented in the next chapter. In this section, we derive an alternative integral representation of the double-logarithmic result and use it to get the fully analytic asymptotic result as well as the all-order result for the off-shell FF. We focus on the case of the scalar external field which is relevant for the application to the Higgs boson production.

Let us start with reproducing the result of [13, 14] for the scalar FF. The amplitude \mathcal{F} for a quark scattering by an external scalar field can be parameterized as

$$\mathcal{F} = \bar{q}(p_2)\Gamma q(p_1) = y_q \bar{q}(p_2) F_S q(p_1), \quad (3.1)$$

where Γ is the vertex function, F_S is known as the scalar FF, and y_q is the Yukawa coupling of the scalar particle with a massive quark of mass m_q . We have used the projection method for our calculations. After projection, the scalar FF is given by

$$F_S = \frac{1}{2N_c y_q (s + 4m_q^2)} \text{tr} [(\not{p}_2 + m_q)\Gamma(\not{p}_1 + m_q)], \quad (3.2)$$

with $s = -(p_2 - p_1)^2$, N_c being the total number of colors in QCD, and the vertex function Γ obtained for the diagram of interest by writing the amplitude in the form of eq. (3.1). We have taken this projector from ref. [65], where it was used to calculate

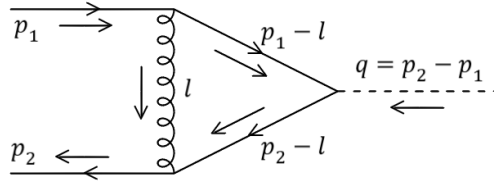


Figure 3.1: Quark scattering by Higgs boson at 1-loop. The convention shown here are used for all the diagrams and calculations of the scalar FF.

the full heavy quark FF at two-loops in QCD.

Starting at one-loop, fig. 3.1 highlights the conventions used for all the diagrams and throughout the calculations of the massive quark scattering problem. For all fermionic lines, the momentum flows in the same direction as the particle flow; while for the external Higgs, the momentum $q = (p_2 - p_1)$ is incoming. External fermions are also taken on-shell i.e., $p_1^2 = p_2^2 = m_q^2$, with m_q being the mass of the quark. And in the high-energy or small mass limit with $m_q \ll l_i \ll q$, for large Euclidean momentum transfer $q^2 = -(p_2 - p_1)^2 = m_H^2$, the ratio $\rho = m_q^2/q^2$ is small and positive. For the remainder of this problem, $m_q \equiv m$. Thus, the scalar FF can be expanded as an asymptotic series in ρ ,

$$F_S = Z_q^2 \sum_{n=0}^{\infty} \rho^n F_S^{(n)} \quad (3.3)$$

with $F_S^{(n)}$ given by power series in α_s . The only remaining ρ dependence for these coefficients can come through the logarithmic enhancement. While the pre-factor Z_q^2 in eq. (3.3) is the LP universal Sudakov correction incorporating all the IR divergence; which is of course same as eq. (2.73) and can be obtained to the LO by evaluating fig. 3.1. With the Sudakov corrections completely factored out, the coefficients $F_S^{(n)}$ can only depend on the non-Sudakov logarithms; implying that the scalar FF is normalized such that the leading coefficient of the series $F_S^{(0)} = 1$.

3.1 The 1-loop diagram

The amplitude for the only non-trivial one-loop diagram contributing to the scalar FF can be written as

$$i\mathcal{M}_{ij} = -ig_s^2 y_q C_F \delta_{ij} \int \frac{d^4 l}{(2\pi)^4} \frac{\bar{q}(p_2) N_{1L} q(p_1)}{l^2 \{(p_1 - l)^2 - m^2\} \{(p_2 - l)^2 - m^2\}}, \quad (3.4)$$

with $N_{1L} = \gamma^\alpha (\not{p}_2 - \not{l} + m)(\not{p}_1 - \not{l} + m)\gamma_\alpha$. This reduces to $4p_2 p_1$ in the double-logarithmic limit; proving that this diagram can only contribute to the leading coefficient $F_S^{(0)}$ as power suppression factors are absent. Then the remaining integral

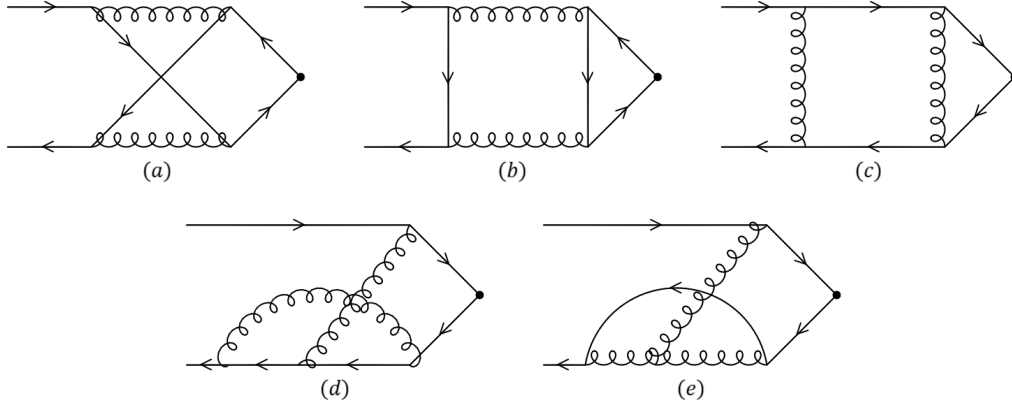


Figure 3.2: Diagrams for quark scattering by Higgs Boson at 2-loops. Symmetric diagrams and diagrams with opposite particle flow for closed quark loop are not shown. The dark vertex represents the Higgs boson with momentum $q = p_2 - p_1$ coming into the vertex.

over the gluon momentum l is identical to the integral in eq. (2.38), resulting in the Sudakov logarithms that have been factored out into Z_q^2 , and $F_S^{(0)} = 1$. The details of this evaluation are given in appendix B.1. For the next coefficient in the series, let us turn our attention to the two-loop diagrams, fig. 3.2, which does generate the power-suppressed contribution.

3.2 The 2-loop diagrams

All two-loop diagrams generated by QGRAF are shown in fig. 3.2. QGRAF was restricted to output only the diagrams that were one particle irreducible, had no self-energy insertions, and had no scalar particle(s) as intermediate states. In fig. 3.2(d) and (e), one of the soft particles is emitted and absorbed by the same eikonal line, i.e., there is no exchange. This configuration cannot produce large double-logarithms and does not contribute to the approximation in consideration. The topology of fig. 3.2(c) is the same as of the one-loop diagram fig. 3.1 with an additional gluon exchange, which does have a double-logarithmic region but can only generate the Sudakov logarithms at the LP of high-energy or small mass expansion as explained in section 2.2. Thus, the contribution of this diagram is already accounted for in terms of the factored out universal Sudakov exponent, Z_q^2 ; resulting in no contribution to the coefficient $F_S^{(1)}$. It was found in [13, 14] that while fig. 3.2(b) and the diagram with opposite particle flow for the closed quark loop, cancel each other for vector scattering due to Furry's theorem; they contribute to the scalar FF due to the additional chirality flip at the vertex. The remaining diagram, fig. 3.2(a), while having the correct topology with soft quark exchanges, cannot generate the power-suppressed large double-logarithmic

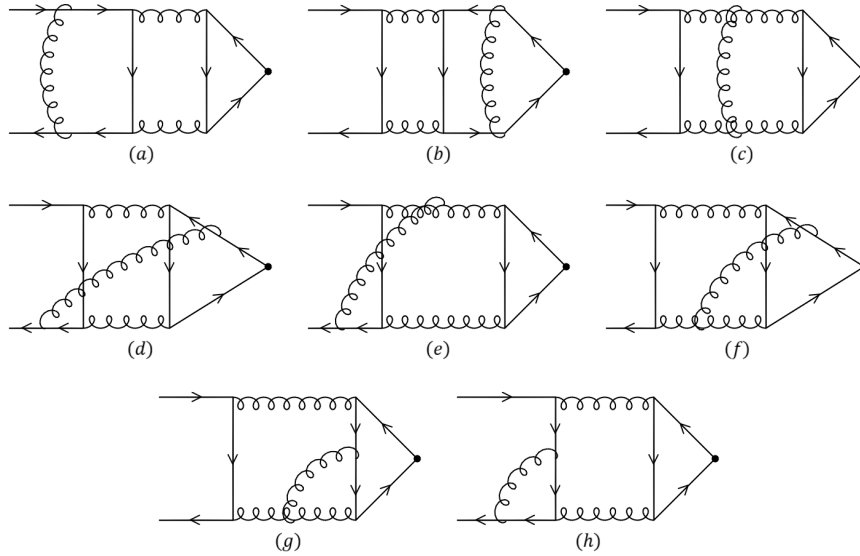


Figure 3.3: Diagrams contributing to the double-logarithmic approximation for the quark scalar FF at 3-loops; symmetric diagrams to (d)-(h), and diagrams with opposite particle flow for the closed quark loop are not included. The dark vertex represents the Higgs boson with momentum $q = p_2 - p_1$ coming into the vertex. All diagrams are obtained by dressing fig. 3.2(b) with leading soft gluon exchange.

contribution to the scalar FF at $\mathcal{O}(\rho)$ due to the chirality flip at the scalar vertex. This is again opposite to the vector FF case where only fig. 3.2(a) generated non-Sudakov double-logarithmic contribution to the Dirac FF at $\mathcal{O}(\rho)$ [13, 14]. In both cases, the chirality flip associated with the soft quark propagator becoming scalar provides the mass suppression factors. The details of the evaluation for the two-loop diagrams are included in appendix B.2. The result obtained at two-loops for the scalar FF at $\mathcal{O}(\rho)$ is

$$F_S^{(1,2L)} = -\frac{\alpha_s^2}{48\pi^2} C_F T_F \ln^4(\rho) = -x^2 \frac{C_F T_F}{3}. \quad (3.5)$$

This agrees with the expansion of the exact two-loop result obtained in ref. [65] along with the result obtained in the high-energy region for the scalar FF at two-loop in [13, 14]. A necessary first step to obtain the all-order result for the FF is to dress the only contributing two-loop diagram with soft gluon exchange to obtain three-loop diagrams; to which we turn our attention.

3.3 The 3-loop diagrams

At three-loops, QGRAF generates a total of 108 diagrams for the same conditions that were used to generate two-loop diagrams; of which only 13 contribute to the double-logarithmic approximation. The rest of the diagrams do not contribute as they either have incorrect topology or simply did not have valid double-logarithmic

λ	c_λ	w_λ	d_λ
a	C_F	$\eta_2(\eta_2 + 2) + \xi_2(\xi_2 - 2\eta_2 + 2)$	$\frac{26}{15}$
b	C_F	$-2\xi_1\eta_1$	$-\frac{1}{15}$
c	$-C_A$	$2(\xi_1 - \xi_2)(\eta_1 - \eta_2)$	$\frac{1}{15}$
d	$-\frac{1}{2}C_A$	$\eta_1(\eta_1 - 2\xi_2 + 2)$	$\frac{1}{3}$
e	$-\frac{1}{2}C_A$	$(\eta_2 - \eta_1)(2 - 2\xi_2 + \eta_1 + \eta_2)$	$\frac{2}{5}$
f	$\frac{1}{2}C_A$	$2\eta_1(\xi_1 - \xi_2)$	$-\frac{1}{15}$
g	$\frac{1}{2}C_A$	$2\eta_1(\xi_1 - \xi_2)$	$-\frac{1}{15}$
h	$\frac{1}{2}C_A - C_F$	$\eta_2(\eta_2 - 2\xi_2 + 2)$	$\frac{11}{15}$

Table 3.1: The reduced color factors c_λ , weights w_λ and the integrals d_λ for 3-loop diagrams in fig. 3.3. Contribution of the symmetric diagrams can be obtained via $\eta_1 \longleftrightarrow \xi_1$ and $\xi_2 \longleftrightarrow \eta_2$ for rows d-h.

regions. The diagrams of fig. 3.3 can be obtained by adding a leading soft gluon exchange on the topology of fig. 3.2(b). Their numerators for the amplitudes of the FF are simplified with the help of FORM [20]. After performing the integrals in the double-logarithmic region over the soft gluon momentum, the result can be written as

$$F_S^{(1,3L)} = -x^3 \frac{C_F T_F}{3} \sum_\lambda c_\lambda d_\lambda. \quad (3.6)$$

The sum in eq. (3.6) must include the contribution from the diagrams symmetric to fig. 3.3(d)-(h). The four-fold integral over the Sudakov parameters for the soft quark momenta is given by,

$$d_\lambda = 4! \int_0^1 d\eta_1 \int_0^{1-\eta_1} d\xi_1 \int_{\eta_1}^{1-\xi_1} d\eta_2 \int_{\xi_1}^{1-\eta_2} d\xi_2 w_\lambda. \quad (3.7)$$

The reduced color factor c_λ , the weight factor w_λ , and the result of the integral d_λ are collected in table 3.1. The weight is obtained after performing the integrals in the double-logarithmic region over the soft gluon momentum l_3 . Symmetric diagrams have the same color, while w_λ can be obtained by $\eta_1 \longleftrightarrow \xi_1$ and $\eta_2 \longleftrightarrow \xi_2$. By adding all the contributions to the scalar FF at three-loops, eq. (3.6) can be reduced to

$$F_S^{(1,3L)} = \frac{1}{15} x^3 (C_A - C_F) T_F C_F. \quad (3.8)$$

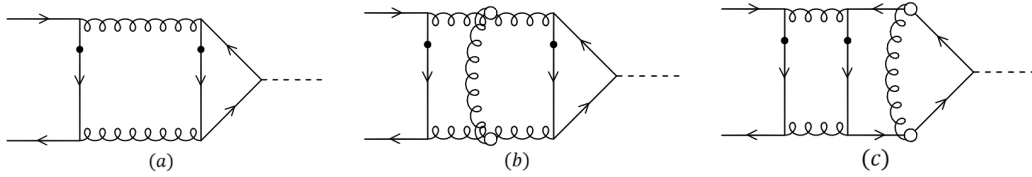


Figure 3.4: (a) The leading 2-loop Feynman diagram for the NLP double-logarithmic correction to the quark scalar FF. (b), (c) The diagrams with effective soft gluon exchange incorporating the all-order non-Sudakov corrections to the scalar FF at NLP. The dark circle represents mass insertion.

Adding this with the two-loop contribution at $\mathcal{O}(\rho)$ gives

$$F_S^{(1)} = -x^2 \frac{T_F C_F}{3} \left[1 - x \frac{C_A - C_F}{5} + \mathcal{O}(x^2) \right] = F_S^{(1,2L)} \left[1 - \frac{z}{5} + \mathcal{O}(z^2) \right], \quad (3.9)$$

with higher order terms corresponding to the diagrams with additional soft gluon exchanges.

3.4 All-order resummation

The results for the scalar FF at two and three-loop at $\mathcal{O}(\rho)$ have been derived for quark scattering via Higgs boson by direct evaluation so far. This allows us to perform the all-order resummation by way of exponentiation as we now show. To do this explicitly, the three-loop result eqs. (3.6) and (3.7) must be slightly modified and written in terms of the two-loop result eq. (3.5) as

$$F_S^{(1,3L)} = 24x \sum_{\lambda} \left[c_{\lambda} \int_0^1 d\eta_1 \int_0^{1-\eta_1} d\xi_1 \int_{\eta_1}^{1-\xi_1} d\eta_2 \int_{\xi_1}^{1-\eta_2} d\xi_2 w_{\lambda} \right] F_S^{(1,2L)}. \quad (3.10)$$

Unlike eq. (3.8), taking the sum in eq. (3.10) before performing the integrals gives

$$F_S^{(1,3L)} = F_S^{(1,2L)}(-24z) \int_0^1 d\eta_1 \int_0^{1-\eta_1} d\xi_1 \int_{\eta_1}^{1-\xi_1} d\eta_2 \int_{\xi_1}^{1-\eta_2} d\xi_2 (2\eta_2 \xi_2 - 2\eta_1 \xi_1). \quad (3.11)$$

Applying the technique of factorization in the non-Abelian amplitudes described in section 2.3 helps write the contribution to the scalar FF as

$$F_S^{(1)} = -x^2 \frac{T_F C_F}{3} f(-z), \quad (3.12)$$

with the function $f(-z)$ incorporating the non-Sudakov double-logarithmic contribution of an arbitrary number of additional soft gluon exchanges on the two-loop topology of fig. 3.2(b). This implies that the function $f(-z)$ is normalized to the

two-loop result with $f(0) = 1$, and is obtained by exponentiating within the integral of eq. (3.11) to give,

$$f(z) = 4! \int_0^1 d\eta_1 \int_0^{1-\eta_1} d\xi_1 \int_{\eta_1}^{1-\xi_1} d\eta_2 \int_{\xi_1}^{1-\eta_2} d\xi_2 (e^{-2z\eta_1\xi_1} e^{2z\xi_2\eta_2}). \quad (3.13)$$

We have obtained the result of the scalar FF that was derived in [13,14]. By comparing the sum in eq. (3.11) with table 3.1, it is clear that the sum of all contributing diagrams reduces to effective diagrams which are identical to fig. 3.4(b) and (c). The only subtlety is related to the fact that for the effective diagram fig. 3.4(b), the integral over the soft gluon momentum factors out of the inner quark loop. We must simply modify the reduced color factor from C_A to $C_A - C_F$ and C_F to $C_F - C_A$ in fig. 3.4(b) and (c) respectively, to account for the color charge non-conservation along the eikonal lines. These effective diagrams can be derived using the sequence of Ward-Takahashi identities and momentum shifts for the soft quarks similar to the process described in section 2.3.3. The result of these transformations for fig. 3.3(g) and (h) are shown in fig. 3.5. The shift in fig. 3.3(h) is identical to that of fig. 2.3(b) with the gluon operator $G_{\mu\nu}^2$ of the artificial amplitude being replaced by the rest of the scattering diagram, the closed quark loop attached to the scalar particle. The transformation of fig. 3.3(g) is almost identical to that of fig. 3.3(h). The main difference is that the roles of the quark and gluon lines on the edge of the diagram are reversed, resulting in the reversal of color flow direction. The set of resulting ladder diagrams fig. 3.5(b) and (d) along with fig. 3.3(a), (b), (c) and (d) complete the eikonal factorization. Adding these diagrams leads to the factorization of the soft gluon contribution to one-loop Sudakov factor of eq. (2.38); and the remaining contribution to $F_S^{(1)}$ is given by fig. 3.4(b) and (c).

Getting back to eq. (3.13), Taylor expansion of $f(z)$,

$$f(z) = 1 + \frac{z}{5} + \frac{11z^2}{420} + \frac{z^3}{378} + \dots, \quad (3.14)$$

gives loop-by-loop approximation for the scalar FF; as clearly visible from the three-loop term in eq. (3.9). In general, the n^{th} term in the expansion of the exponential corresponds to $(n+2)$ -loop diagrams with two soft quark exchanges with the topology of fig. 3.2(b) and n additional soft gluon exchanges. It is challenging to solve the four-fold integral entirely and does not provide any real insights into the result but a closed analytic form for the asymptotic behavior can be obtained. In the next section, we provide the full derivation for the form of $f(\pm z)$ as $z \rightarrow \infty$.

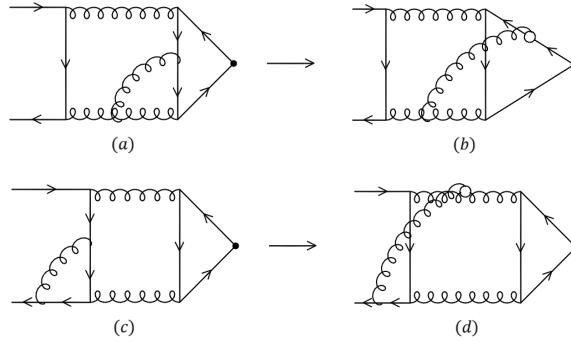


Figure 3.5: The diagrammatic representation of the Ward-Takahashi identities and momentum shift for fig. 3.3(g) and (h). The shift from (c) to (d) is identical to that of fig. 2.3(b), diagrammatically shown in fig. 2.6. The shift from (a) to (b) is almost identical, with the difference explained in the text.

3.5 Large z asymptotic of $f(z)$

In the previous section, we encapsulated the all-order result for the coefficient $F_S^{(1)}$, which corresponds to the $\mathcal{O}(\rho)$ in the series expansion of the scalar FF in the high-energy limit, in terms of the function $f(z)$. To calculate the analytical asymptotic form of $f(z)$ for large z , we introduce an explicit sign in front of the variable z as we did in section 2.3.5 for evaluation of the large- z asymptotic of $g(z)$. Note that the representation of the function $f(z)$ is not unique. An alternative representation was obtained in the analysis of the vector FF and reads [13, 14]

$$f(z) = 12 \int_0^1 d\eta_1 \int_{\eta_1}^1 d\eta_2 \int_0^{1-\eta_2} d\xi_2 \int_{\xi_2}^{1-\eta_1} d\xi_1 [e^{2z\eta_1(\xi_1-\xi_2)} e^{2z\xi_2(\eta_2-\eta_1)}]. \quad (3.15)$$

However, both representations eqs. (3.13) and (3.15) are not suitable for the analytic evaluation of the large z asymptotic behavior of the function $f(z)$ since the integrations over the logarithmic variables are entangled. At the same time, we can rearrange the integration limits in eq. (3.13) preserving the actual integration domain and transforming it into

$$f(\pm z) = 4! \int_0^1 d\eta_1 \int_0^{1-\eta_1} d\xi_1 (e^{\pm 2z\eta_1\xi_1}) \int_0^{\eta_1} d\eta_2 \int_0^{\xi_1} d\xi_2 (e^{\mp 2z\eta_2\xi_2}). \quad (3.16)$$

The equivalence of all three representations can be directly verified by Taylor expansion in z with the explicit integration of the resulting polynomial coefficients. However, in contrast to eq. (3.13) the integration over ξ_2 and η_2 in eq. (3.16) decouples

and can be done explicitly with the result

$$\begin{aligned} 2 \int_0^{\eta_1} d\eta_2 \int_0^{\xi_1} d\xi_2 (e^{\mp 2z\eta_2\xi_2}) &= \pm \int_0^{\eta_1} d\eta_2 \left(\frac{1 - e^{\mp 2z\eta_2\xi_1}}{\eta_2 z} \right) \\ &= \pm \frac{1}{z} [\gamma_E + \ln(2z\eta_1\xi_1) - Ei(\mp 2z\eta_1\xi_1)], \end{aligned} \quad (3.17)$$

where the Euler gamma constant $\gamma_E = 0.57721\dots$, and $Ei(x)$ is the exponential integral function of x . For the remaining integrals, we must apply the change of variables from section 2.3.5, $\xi_1 = y\sqrt{\lambda}$ and $\eta_1 = \sqrt{\lambda}/y$ with the Jacobian $|J| = y^{-1}$. Then eq. (3.16) simplifies to

$$\begin{aligned} f(\pm z) &= \pm 12 \int_0^{1/4} d\lambda \int_{y_L}^{y_H} dy \left[\frac{e^{2z\lambda}}{zy} \{ \gamma_E + \ln(2z\lambda) - Ei(\mp 2z\lambda) \} \right] \\ f(\pm z) &= \pm 12 \int_0^{1/4} d\lambda \left[\frac{e^{\pm 2z\lambda}}{z} \{ \gamma_E + \ln(2z\lambda) - Ei(\mp 2z\lambda) \} \ln \left(\frac{1 + \sqrt{1 - 4\lambda}}{1 - \sqrt{1 - 4\lambda}} \right) \right]. \end{aligned} \quad (3.18)$$

The further evaluation depends on the sign in front of the argument of $f(z)$. Let us first look at the case of $z \rightarrow \infty$. The exponential factor $e^{2z\eta_1\xi_1} = e^{2z\lambda}$ provides enhancement making the integral over λ saturated around the region of maximal value $\lambda = 1/4$. Thus expanding around $\lambda = 1/4$ reduces eq. (3.18) to

$$\begin{aligned} f(z) &\approx 12 \left[\gamma_E + \ln \left(\frac{z}{2} \right) - Ei \left(-\frac{z}{2} \right) \right] \int_0^{1/4} d\lambda \left[\frac{e^{2z\lambda}}{z} (2\sqrt{1 - 4\lambda}) \right] \\ f(z) &= 6 \left(\frac{2e^z}{z^5} \right)^{1/2} \left[\sqrt{\pi} - 2\Gamma \left(\frac{3}{2}, \frac{z}{2} \right) \right] \left[\gamma_E - Ei \left(-\frac{z}{2} \right) + \ln \left(\frac{z}{2} \right) \right]. \end{aligned} \quad (3.19)$$

As $z \rightarrow \infty$, eq. (3.19) reduces to

$$f(z) \sim \left(\frac{72\pi e^z}{z^5} \right)^{1/2} \left[\gamma_E + \ln \left(\frac{z}{2} \right) \right]. \quad (3.20)$$

Thus, there is an exponential enhancement when $z \rightarrow \infty$. Let us turn our attention to the evaluation of $f(-z)$. By applying another change of variable $\lambda \equiv 2z\lambda$, eq. (3.18) is reduced to

$$f(-z) = \frac{6}{z^2} \int_0^{z/2} d\lambda \left[\{ Ei(\lambda) - \gamma_E - \ln \lambda \} e^{-\lambda} \ln \left(\frac{1 + \sqrt{1 - 2\lambda/z}}{1 - \sqrt{1 - 2\lambda/z}} \right) \right]. \quad (3.21)$$

To further evaluate this integral, the asymptotic behavior of the exponential integral function and the logarithm are required. For very large z , $\sqrt{1 - 2\lambda/z} \approx 1 - \lambda/z$, thus the logarithm can be approximated as $\ln \left(\frac{1 + \sqrt{1 - 2\lambda/z}}{1 - \sqrt{1 - 2\lambda/z}} \right) \approx \ln \left(\frac{1 + 1}{1 - 1 + \lambda/z} \right) \approx \ln \left(\frac{2z}{\lambda} \right)$. Sim-

ilarly, $Ei(\lambda) \approx \frac{e^\lambda - 1}{\lambda}$ with $1/\lambda$ dominating around 0 and the exponential dominating at very large λ . With these, we get

$$f(-z) = \frac{6}{z^2} \int_0^{z/2} d\lambda \left[\frac{e^\lambda - 1}{\lambda} + Ei(\lambda) - \frac{e^\lambda - 1}{\lambda} - \gamma_E - \ln \lambda \right] \times e^{-\lambda} \left[\ln \left(\frac{2z}{\lambda} \right) + \ln \left(\frac{1 + \sqrt{1 - 2\lambda/z}}{1 - \sqrt{1 - 2\lambda/z}} \right) - \ln \left(\frac{2z}{\lambda} \right) \right]. \quad (3.22)$$

Expanding the terms into a sum of six integrals gives,

$$I_1 = \int_0^{z/2} d\lambda \left[\frac{e^\lambda - 1}{\lambda} e^{-\lambda} \ln \left(\frac{2z}{\lambda} \right) \right] \\ \implies I_1 \approx \frac{\gamma_E^2}{2} + \frac{\pi^2}{12} + \gamma_E \ln(2z) - \frac{3}{2} \ln^2 2 + \ln 2 \ln z + \frac{1}{2} \ln^2 z, \quad (3.23)$$

$$I_2 = \int_0^{z/2} d\lambda \left[\frac{e^\lambda - 1}{\lambda} e^{-\lambda} \left\{ \ln \left(\frac{1 + \sqrt{1 - 2\lambda/z}}{1 - \sqrt{1 - 2\lambda/z}} \right) - \ln \left(\frac{2z}{\lambda} \right) \right\} \right] \\ \implies I_2 \approx -\frac{\pi^2}{6} + 2 \ln^2 2, \quad (3.24)$$

$$I_3 = \int_0^{z/2} d\lambda \left[\left\{ Ei(\lambda) - \frac{e^\lambda - 1}{\lambda} \right\} e^{-\lambda} \ln \left(\frac{2z}{\lambda} \right) \right] \\ \implies I_3 \approx -\frac{\pi^2}{3}, \quad (3.25)$$

$$I_4 = \int_0^{z/2} d\lambda \left[\left\{ Ei(\lambda) - \frac{e^\lambda - 1}{\lambda} \right\} e^{-\lambda} \left\{ \ln \left(\frac{1 + \sqrt{1 - 2\lambda/z}}{1 - \sqrt{1 - 2\lambda/z}} \right) - \ln \left(\frac{2z}{\lambda} \right) \right\} \right] \\ \implies I_4 \approx 0, \quad (3.26)$$

$$I_5 = \int_0^{z/2} d\lambda \left[\left\{ -\ln \lambda - \gamma_E \right\} e^{-\lambda} \ln \left(\frac{2z}{\lambda} \right) \right] \\ \implies I_5 \approx \frac{\pi^2}{6}, \quad (3.27)$$

and

$$I_6 = \int_0^{z/2} d\lambda \left[\left\{ -\ln \lambda - \gamma_E \right\} e^{-\lambda} \left\{ \ln \left(\frac{1 + \sqrt{1 - 2\lambda/z}}{1 - \sqrt{1 - 2\lambda/z}} \right) - \ln \left(\frac{2z}{\lambda} \right) \right\} \right] \\ \implies I_6 \approx 0. \quad (3.28)$$

Adding these contributions gives the $f(-z)$ asymptotic,

$$f(-z) \sim \frac{3}{z^2} \left[\left\{ \gamma_E + \ln(2z) \right\}^2 - \frac{\pi^2}{2} \right]. \quad (3.29)$$

This implies that the amplitude is logarithmically suppressed when $z \rightarrow -\infty$.

For QCD the parameter $z = (C_A - C_F)x > 0$, and since the FF is proportional to $f(-z)$, in the asymptotic range it scales with the double-logarithmic variable $\ln^2 x$ as the factor of z^2 cancels with x^2 in eq. (3.12). Similarly, in QED $C_A = 0$ makes $z = -C_F x < 0$, and the leading asymptotic behavior of the FF is proportional to $e^{x/2}$.

3.6 Off-shell scalar FF

In the previous sections, we have computed the result for the on-shell scalar FF i.e., the external quark lines were on-shell and satisfied the relation $p_i^2 = m^2$. Before we move on to the Higgs production process, we would like to briefly discuss the off-shell scalar FF; the reason behind will become apparent in the next chapter. The off-shell “external” momenta are $\Delta_i = (p_i - l_1)^2 - m^2$. In the double-logarithmic approximation, we can set $l_1^2 = m^2$ for the soft quark momentum, leading to $\Delta_1 = -2p_1 l_1 = -v_1 q^2$ and $\Delta_2 = -2p_2 l_1 = -u_1 q^2$, and consider the case $|\Delta_i| \gg m^2$. The FF can be expanded in ρ and Δ_i/q^2 as

$$F_S = Z_q^2 \sum_{n=0}^{\infty} \left[\rho^n F_S^{(n)} + \mathcal{O}(\Delta_i/q^2) \right]. \quad (3.30)$$

Since the terms vanishing for $\Delta_i = 0$ cannot generate double-logarithms, we can ignore them. The coefficient

$$Z_q^2 = e^{-2C_F x \eta_1 \xi_1} \quad (3.31)$$

represents the usual Sudakov factor, analog of eq. (2.73), computed for the off-shell external lines. Thus, eq. (3.30) is also normalized such that the leading coefficient $F_S^{(0)} = 1$, and the next coefficient $F_S^{(1)}$ gets power-suppressed double-logarithmic contribution from fig. 3.4(a) i.e., the diagrams with soft quark pair exchange. The analysis can be extended to the off-shell FF by simply replacing the IR cutoff from m^2 to Δ_i . Thus, the lower limit on integration over the parameters u_i and v_i are changed from ρ to Δ_i/q^2 . The off-shell FF differs from the eqs. (3.12) and (3.13) in the on-shell scalar FF case only by these integration limits. Unlike the on-shell FF, the η_i and ξ_i variables are not correlated, and the integration limits are obtained here by simply ordering these variables along the eikonal lines as $\xi_1 > \xi_2 > \xi_3$ and $\eta_1 > \eta_2 > \eta_3$. This leads to a modification of the upper integration limits in eq. (3.16) with the result

$$F_S^{(1)} = 8x^2 C_F T_F \int_0^{\eta_1} d\eta_2 \int_0^{\xi_1} d\xi_2 \int_0^{\eta_2} d\eta_3 \int_0^{\xi_2} d\xi_3 \left(e^{-2z\eta_2\xi_2} e^{2z\eta_3\xi_3} \right), \quad (3.32)$$

with the exponential factors corresponding to the effective diagrams fig. 3.4(b) and (c).

Chapter 4

Higgs production via light quark mediated gluon fusion

We turn our attention to the Higgs production via quark-mediated gluon fusion in this chapter. Since the amplitude for this process can only be loop generated, it can be parameterized as

$$\mathcal{M}_{ggH}^q = T_F \frac{\alpha_s y_q m_q}{\pi m_H^2} (p_1^\nu p_2^\mu - g^{\mu\nu} p_1 p_2) A_\mu^m(p_1) A_\nu^m(p_2) H M_{ggH}^q, \quad (4.1)$$

where y_q is the quark Yukawa coupling to the Higgs field, m_H is the Higgs mass, A_μ^m is the gluon field, H is the Higgs field, $T_F = 1/2$ is known as the index of the fundamental representation of $SU(3)$, and M_{ggH}^q is the Higgs production FF. Note that the amplitude is denoted by \mathcal{M}_{ggH}^q while the FF is denoted by M_{ggH}^q . The quark mass factor comes from the chirality flip on the soft quark line. The Higgs coupling to the quark field also provides another chirality flip, and the associated mass factor is part of the Yukawa coupling (see eq. (2.11)). The on-shell condition for the external particles means that $p_1^2 = p_2^2 = 0$ for the gluons, and $q^2 = (p_1 + p_2)^2 = 2p_2 p_1 = m_H^2$ for the Higgs boson with $\rho = m_q^2/q^2 = m_q^2/m_H^2$. For the remainder of this problem, $m_q \equiv m$. Recall that the amplitude is dominated by the contribution from the top (heavy) quark loop as in the heavy quark limit, the scalar amplitude approaches the value $M_{ggH}^q = -2/3\rho$ i.e., it is directly proportional to the Higgs boson mass. At the same time for the same process with the bottom (light) quark loop, the amplitude is suppressed by a factor of m_b^2/m_H^2 . But as mentioned in chapter 1, in the asymptotic region, with the help of the large double-logarithms the effective coupling goes from α_s to $\alpha_s \ln^2(m_b^2/m_H^2) \approx 40\alpha_s$, necessitating computation of the bottom loop contribution to improve the theoretical accuracy. In this limit, the FF can be expanded in asymptotic series

$$M_{ggH}^q = Z_g^2 \sum_{n=0}^{\infty} \rho^n M_{ggH}^{(n)}, \quad (4.2)$$

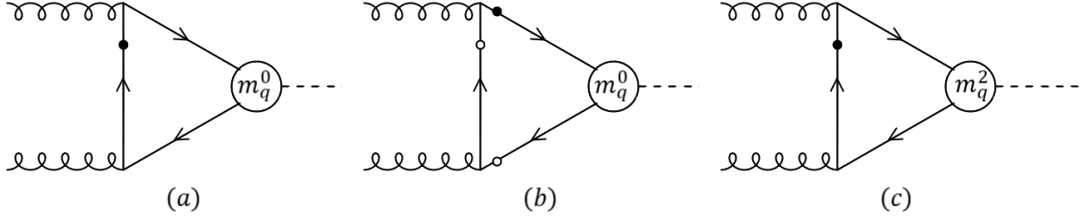


Figure 4.1: (a) $\mathcal{O}(m_q^0)$ and (b), (c) $\mathcal{O}(m_q^2)$ double-logarithmic contribution to the ggH amplitude. The dark (empty) circle represents mass (loop momentum) insertion. The blob corresponds to the off-shell scalar FF at $\mathcal{O}(m_q^0)$ and $\mathcal{O}(m_q^2)$.

where the finite coefficients $M_{ggH}^{(n)}$ depend on ρ only through the power-suppressed non-Sudakov logarithms, and Z_g^2 incorporates the entire IR divergence from the on-shell external gluon lines. This universal Sudakov factor is given by

$$Z_g^2 = \exp\left(-\frac{C_A s^{-\varepsilon}}{\varepsilon^2} \frac{\alpha_s}{2\pi}\right). \quad (4.3)$$

The leading coefficient $M_{ggH}^{(0)}$, that was calculated in refs. [13, 14] will be reproduced during the evaluation of the next coefficient in the series, $M_{ggH}^{(1)}$. Three distinct sources need consideration:

- (i) Factorizable contribution with single soft quark exchange,
- (ii) Contribution from triple soft quark exchange,
- (iii) Non-factorizable contribution with single soft quark exchange.

The general topology of the diagrams generating contributions to the FF is outlined in fig. 4.1. Each of the contributions is discussed in sections 4.1 to 4.3 respectively. Let us now turn our attention to the first group of diagrams and compute their full contribution.

4.1 Factorizable contribution with single soft quark exchange

The one-loop single soft quark exchange Higgs production diagram is shown in fig. 4.2(a). Furry's theorem does not apply to this case as there is no purely QED interaction vertex; the diagram with opposite particle flow in the closed quark loop has exactly equal contribution as fig. 4.2(a). The presence of this quark loop simplifies the problem significantly as the numerator reduces to a trace. The projector for this

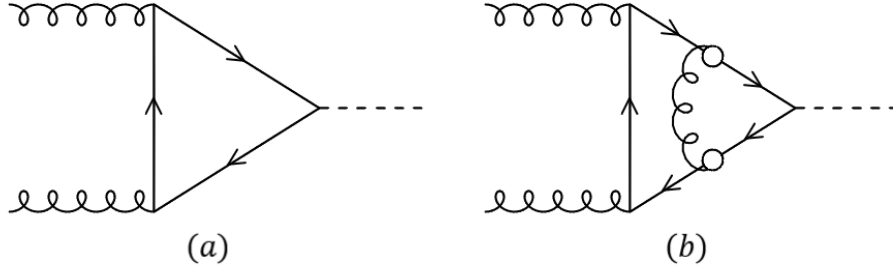


Figure 4.2: Higgs production via quark mediated gluon fusion at (a) 1-loop, and (b) 2-loop diagram with effective soft gluon exchange. Diagrams with opposite particle flow for the closed quark loop are not shown.

process is given by

$$P_{\mu\nu} = \frac{4}{(d-2)} \frac{1}{q^4} [g_{\mu\nu}(p_2 p_1) - p_{1,\mu} p_{2,\nu} - p_{1,\nu} p_{2,\mu}]; \quad (4.4)$$

simple derivation for which is in appendix C. The amplitude for fig. 4.2(a) is

$$\mathcal{M}_{ggH,1L}^{\mu\nu,mn} = -i g_s^2 y_q \int \frac{d^4 l_1}{(2\pi)^4} \frac{N_{4.2a}^{\mu\nu,mn}}{D_{4.2a}} \quad (4.5)$$

with

$$N_{4.2a}^{\mu\nu,mn} = \text{tr} [(\not{p}_1 + \not{l}_1 + m) \gamma^\mu T_{ij}^m (\not{l}_1 + m) \gamma^\nu T_{ji}^n (\not{l}_1 - \not{p}_2 + m)], \quad (4.6)$$

and

$$D_{4.2a} = (l_1^2 - m^2) \{(p_1 + l_1)^2 - m^2\} \{(p_2 - l_1)^2 - m^2\}. \quad (4.7)$$

The trace over the $SU(3)$ generator matrices, and the color indices in eq. (4.6) reads $\text{tr}(T_{ij}^m T_{ji}^n) = T_F \delta^{mn}$ as per eq. (2.13). Appendix C.1 provides full technical details of the calculation of this diagram starting from diagram generation with QGRAF to trace evaluation by FORM and integration in the double-logarithmic region with the Sudakov method. Multiplying the projector, eq. (4.4), after taking the trace over vector indices reduces to

$$N_{4.2a} \sim 4m(1 - 4\rho). \quad (4.8)$$

Only the integral over loop momentum remains; the factors in the numerator correspond to no and double insertion of the soft loop momentum l_1 respectively for the terms proportional to 1 and ρ . These are responsible for the contribution to the $\mathcal{O}(m)$ and $\mathcal{O}(m^3)$ coefficients, $M_{ggH}^{(0)}$ and $M_{ggH}^{(1)}$ respectively. It is important to note we have encountered the first instance of additional mass factors coming from the on-shell condition $l_1^2 = m^2$, for the soft quark loop momentum rather than the chirality flip at the propagator for the $\mathcal{O}(m^3)$ contribution. With no factors of loop momentum remaining in the numerator, we introduce the Sudakov parameterization to obtain

the following soft and eikonal approximations:

$$l_1^2 - m^2 = [-2i\pi\delta(u_1 v_1 q^2 + l_{1\perp}^2 - m^2)]^{-1}, \quad (4.9)$$

$$\frac{1}{(p_i \pm l_1)^2 - m^2} = \pm \frac{1}{2p_i l_1} \left[\frac{1}{1 \pm \frac{l_1^2 - m^2}{2p_i l_1}} \right] \approx \pm \frac{1}{2p_i l_1} \left[1 \mp \frac{l_1^2 - m^2}{2p_i l_1} + \dots \right]. \quad (4.10)$$

Only the leading term can contribute as all the subleading terms in the above equation cancel the soft quark propagator, and cannot generate double-logarithms. Using $2p_1 l_1 = v_1(2p_2 p_1)$ and $2p_2 l_1 = u_1(2p_2 p_1)$, the integral is reduced to,

$$I_{4.2a} \propto \int_\rho^1 \frac{dv_1}{v_1} \int_{\rho/v_1}^1 \frac{du_1}{u_1} = \ln^2 \rho \int_0^1 d\eta_1 \int_0^{1-\eta_1} d\xi_1 = \frac{\ln^2 \rho}{2}. \quad (4.11)$$

Combining all the components for the amplitude, from eq. (4.1), the Higgs production FF for fig. 4.2(a) is

$$[M_{ggH}^q]_{4.2a} = (1 - 4\rho) \ln^2 \rho. \quad (4.12)$$

The coefficients, $M_{ggH}^{(n)}$, for $n = 0$ and 1 can simply be read off from the above equation, and at one-loop we have

$$[M_{ggH}^{(0)}]_{4.2a} = \ln^2 \rho, \quad (4.13)$$

and

$$[M_{ggH}^{(1)}]_{4.2a} = -4 \ln^2 \rho = -4 [M_{ggH}^{(0)}]_{4.2a}. \quad (4.14)$$

To get the all-order result for the diagrams with single soft quark exchange, we must dress fig. 4.2(a) with additional leading soft gluon exchanges similar to the artificial amplitude and the scalar FF. The diagrams at two-loops and higher would be, while not identical but very similar to that of the artificial amplitude from section 2.3.3. External line Sudakov corrections factor out into Z_g^2 , the universal Sudakov factor for external gluons. The remaining non-Sudakov contribution is given by the effective gluon exchange Higgs vertex correction diagram fig. 4.2(b) at two-loops. This is identical to the LP term in eq. (3.31) in the expansion of the off-shell scalar FF, diagrammatically represented by fig. 4.1(a). To account for the non-conservation of the color charge along the eikonal lines due to the soft quark exchange the color factor must be changed from C_F to $C_F - C_A$ [13–15]. The all-order result is then obtained by exponentiating the two-loop result to give

$$M_{ggH}^{(0)} = \ln^2 \rho g(z), \quad (4.15)$$

with $g(z)$ defined by eqs. (2.75) and (2.76). The asymptotic behavior for this function as $\pm z \rightarrow \infty$ also has been calculated in section 2.3.5. The main difference between

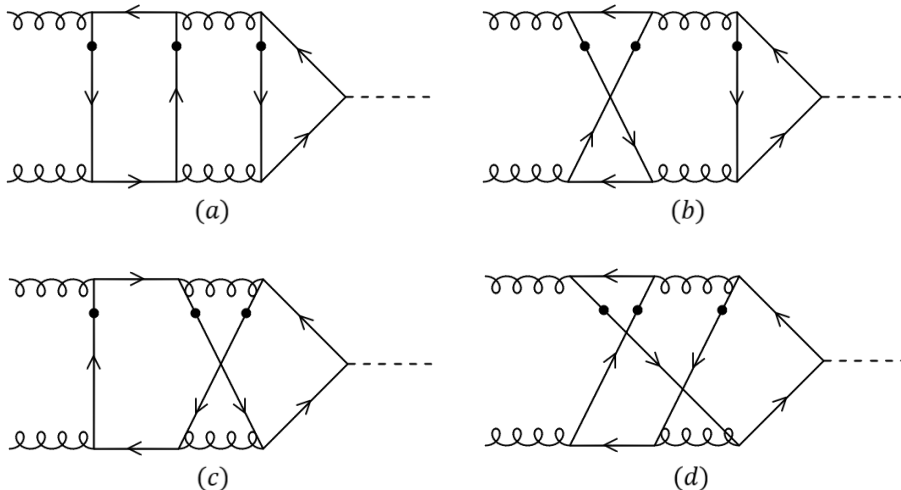


Figure 4.3: Higgs production via triple soft quark exchange. Diagrams with opposite particle flow for the closed quark loops are not included. Only (a) contributes to double-logarithmic approximation at NNLP. The dark circle represents mass insertion; additional mass factors can come via the on-shell soft quark momentum.

the all-order result in this problem and the artificial amplitude of section 2.3 is the sign in front of the parameter z within the function g , which is to say that the color flows in the opposite direction with respect to each other. Bringing our attention back to the Higgs problem, since the same diagram(s) generate part of the contribution to the next order coefficient (see fig. 4.1(b)), the same factorization applies; and we can write

$$\left[M_{ggH}^{(1)} \right]_{1q} = -4 \ln^2 \rho g(z) = -4 M_{ggH}^{(0)}. \quad (4.16)$$

This is only partial contribution to the coefficient $M_{ggH}^{(1)}$. To get the complete result at NNLP, we must investigate the diagrams for the other two sources as well.

4.2 Contribution from triple soft quark exchange

Out of 54 QGRAF generated diagrams at three-loops, only the diagrams shown in fig. 4.3 require consideration. Of these, only fig. 4.3(a) contributes to the $\mathcal{O}(m^3)$ of the approximation with the contribution starting at higher powers for the rest. It is clear that fig. 4.3(a) has two-loop off-shell scalar FF substructure of fig. 3.4(a) present within i.e., it has the structure of fig. 4.1(c). Corresponding correction to the FF is obtained by including the NLP term $Z_q^2 F_S^{(1)}$ from eq. (3.30) into the integral eq. (4.11). This way the result for the triple quark exchange at three-loops can be

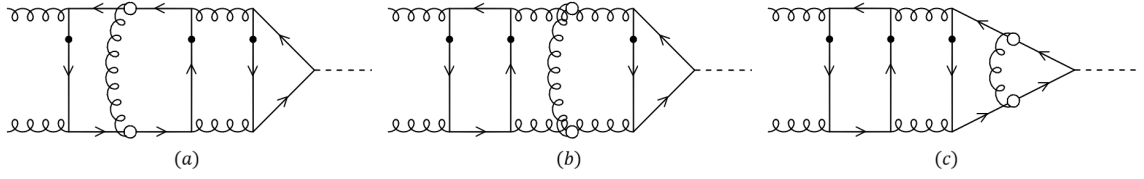


Figure 4.4: Effective diagrams with triple soft quark exchange for the Higgs production with vertex correction by effective gluon exchange on the topology of fig. 4.3(a). Each diagram corresponds to an exponential in eq. (4.20). The dark circle represents mass insertion.

expressed as

$$\begin{aligned} \left[M_{ggH}^{(1)} \right]_{4.3a} &= \frac{\alpha_s^2 T_F C_F}{\pi^2} \ln^6 \rho \int_0^1 d\eta_1 \int_0^{1-\eta_1} d\xi_1 \int_0^{\eta_1} d\eta_2 \int_0^{\xi_1} d\xi_2 \int_0^{\eta_2} d\eta_3 \int_0^{\xi_2} d\xi_3, \\ \left[M_{ggH}^{(1)} \right]_{4.3a} &= \frac{x^2 T_F C_F}{45} \ln^2 \rho = -\frac{x^2 T_F C_F}{180} \left[M_{ggH}^{(1)} \right]_{4.2a}. \end{aligned} \quad (4.17)$$

The integrals over the Sudakov parameters corresponding to the loop momenta $l_{1,2,3}$ in the fig. 4.3(a) are double-logarithmic when $u_1 < u_2 < u_3$ and $v_1 < v_2 < v_3$ with $u_1 v_1 > \rho$ for the “outer” loop. The expression above accounts for the diagrams with opposite particle flow for the closed quark loops. Appendix C.2.1 shows the complete evaluation of all the triple soft quark exchange diagrams. For resummation, we dress fig. 4.3(a) with additional leading soft gluon exchange to obtain the next order of diagrams. All diagrams reduce to three effective diagrams shown in fig. 4.4 with eikonal color non-conservation due to the soft quark exchanges. The full contribution of the effective diagrams to the Higgs production FF can be written as

$$\begin{aligned} \left[M_{ggH}^{(1)} \right]_{4.4} &= 64x^2 T_F C_F \ln^2 \rho \int_0^1 d\eta_1 \int_0^{1-\eta_1} d\xi_1 \int_0^{\eta_1} d\eta_2 \int_0^{\xi_1} d\xi_2 \\ &\quad \int_0^{\eta_2} d\eta_3 \int_0^{\xi_2} d\xi_3 (2z\eta_1\xi_1 - 2z\eta_2\xi_2 + 2z\eta_3\xi_3). \end{aligned} \quad (4.18)$$

Exponentiating the integrand in the above equation results in the all-order contribution from this source, normalized to the three-loop result eq. (4.17) as

$$\left[M_{ggH}^{(1)} \right]_{3q} = \ln^2 \rho \frac{x^2 T_F C_F}{45} h(z) \quad (4.19)$$

n	1	2	3	4	5	6
$n^2 2^n n! h_n$	$\frac{3}{7}$	$\frac{8}{9}$	$\frac{90}{77}$	$\frac{59392}{45045}$	$\frac{5360}{3861}$	$\frac{7559936}{5360355}$
$n! j_n^{ab}$	$\frac{17}{28}$	$\frac{83}{175}$	$\frac{241}{550}$	$\frac{47984}{105105}$	$\frac{3645}{7007}$	$\frac{97228}{153153}$

Table 4.1: The normalized coefficients in the Taylor expansion of the function $h(z)$ and $j^{ab}(z)$ from $n = 1$ to 6.

with the six-fold integral representation of the function $h(z)$ given by

$$h(z) = 6! \int_0^1 d\eta_1 \int_0^{1-\eta_1} d\xi_1 \int_0^{\eta_1} d\eta_2 \int_0^{\xi_1} d\xi_2 \int_0^{\eta_2} d\eta_3 \int_0^{\xi_2} d\xi_3 (e^{2z\eta_1\xi_1} e^{-2z\eta_2\xi_2} e^{2z\eta_3\xi_3}). \quad (4.20)$$

The Taylor expansion $h(z) = 1 + \sum_{n=1}^{\infty} h_n z^n$ can be obtained by expanding the exponents with the n^{th} term corresponding to $(n+3)$ -loop contribution. The first six coefficients for the series are listed in table 4.1. We can now turn our attention to the final group of diagrams, and investigate the non-factorizable contribution.

4.3 Non-factorizable contribution with single soft quark exchange

This group of diagrams corresponds to a new source where an eikonal gluon line connects the soft and eikonal quark lines on the single soft quark exchange topology. We refer to them as non-factorizable because their contribution does not factor out into effective Higgs boson vertex correction. We must first consider the two-loop diagram to understand the origin of the contribution. The double-logarithmic scaling can appear for fig. 4.5(a) when the gluon emitted by the soft quark line is eikonal i.e., the propagator is proportional to $1/(l_1 l_2)$. Since the momenta p_2 and l_1 act as the external momentum for l_2 , the standard double-logarithmic scaling for l_2 appears with the eikonal factor $1/(p_2 l_1)$. For the integral over l_1 to get the double-logarithms, this eikonal factor must be cancelled by the numerator. However, the appropriate tensor structure does not appear in the Dirac chain of the numerator due to the transverse polarization of the external gluons. In other words, upon projecting the numerator of fig. 4.5(a) to the FF, appropriate factors do not appear to generate the double-logarithms at two-loops.

We can turn our attention to three-loops where the appropriate structure does appear in the numerator. The diagrams of fig. 4.6 are divided into Abelian (fig. 4.6(a,b))

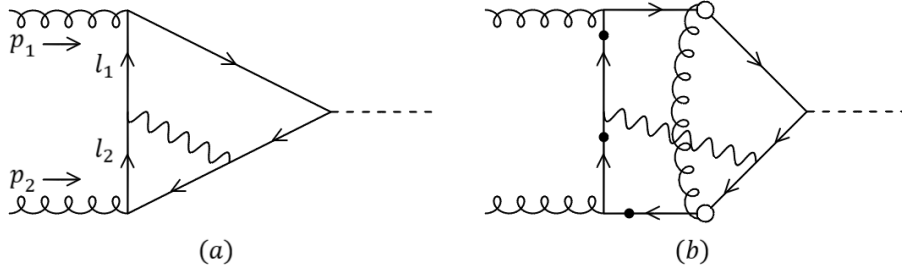


Figure 4.5: The non-factorizable Higgs production diagrams with an additional eikonal gluon (represented by the wavy line) being emitted by the soft quark (a) at 2-loops, and (b) effective diagram at 3-loops that gives the total 3-loop QCD contribution from this source; it does not represent the all-order contribution in this case. Symmetric diagrams and diagrams with opposite particle flow for the closed quark loop are not included. The dark circle represents mass insertion.

and non-Abelian (fig. 4.6(c,d)) subgroup. Let us begin with nonplanar topology fig. 4.6(a), we define the Sudakov parameterization as $l_2 = u_2 l_1 + v_2 p_2 + l_{2\perp}$ and $k'_1 = r'_1 p_1 + w'_1 p_2 + k'_{1\perp}$, and assume that in the light-cone coordinates $p_1 = p_1^-$ and $p_2 = p_2^+$. The double-logarithmic integral over l_2 results in the factor $1/(p_2 l_1) = 1/(p_2^+ l_1^-)$ which has the same structure as the lower eikonal quark propagator

$$S(l_1 - k'_1 - p_2) \approx -\frac{\gamma^-}{2l_1^-} + \dots, \quad (4.21)$$

where we used the relation $k'_1{}^- < l_1^-$ in the double-logarithmic region. This factor of $1/l_1^-$ must be cancelled to obtain double-logarithms. We find that only the upper eikonal quark line has the relevant tensor structure in the numerator

$$S(p_1 + l_1 - k'_1) \approx \frac{\gamma^+}{2k'_1{}^+} \left(1 + \frac{l_1^- - k'_1{}^-}{p_1^-} \right) + \dots, \quad (4.22)$$

as indicated in fig. 4.6(a) as real (virtual) gluons have transversal (light-cone) polarization. The integrals obtain double-logarithmic scaling for $v_1 < w'_1 < 1$ and $u_1 u_2 < r'_1 < u_1$, with on-shell conditions for the soft quark propagators requiring $u_1 v_1 > \rho$ and $u_2 v_2 > \rho/u_1$. Then the contribution of fig. 4.6(a) to $M_{ggH}^{(1)}$ reduces to

$$\begin{aligned} [M_{ggH}^{(1)}]_{4.6a} &= -8z^2 \ln^2 \rho \int_0^1 d\eta_1 \int_0^{1-\eta_1} d\xi_1 \int_0^{1-\xi_1} d\eta_2 \int_0^{1-\xi_1-\eta_2} d\xi_2 \int_0^{\eta_1} d\eta_3 \int_{\xi_1}^{\xi_1+\xi_2} d\xi_3, \\ [M_{ggH}^{(1)}]_{4.6a} &= -8z^2 \ln^2 \rho \int_0^1 d\eta_1 \int_0^{1-\eta_1} d\xi_1 \int_0^{1-\xi_1} d\eta_2 \int_0^{1-\xi_1-\eta_2} d\xi_2 (\eta_1 \xi_2), \\ [M_{ggH}^{(1)}]_{4.6a} &= -\left(\frac{z \ln \rho}{3} \right)^2, \end{aligned} \quad (4.23)$$

for $z = -C_F x$. Note that the integral over Sudakov parameters r'_1 and w'_1 results in the standard one-loop Sudakov correction factor $2z\eta_1\xi_2$. Turning our attention to the planar diagram fig. 4.6(b), integration over soft gluon momentum $k_1 = r_1 u_1 + w_1 v_1 + k_{1\perp}$ generates the factor $2z\eta_1\xi_1$ for $v_1 < w_1 < 1$ and $u_1 < r_1 < 1$ corresponding to $l_1^- < k_1^-$ in the logarithmic region. In contrast to the nonplanar case, the required l_1^- term is generated in two ways. The lower eikonal quark propagator can be expanded as

$$S(l_1 - k_1 - p_2) \approx -\frac{\gamma^-}{2k_1^-} \left(1 + \frac{l_1^-}{k_1^-} \right) + \dots, \quad (4.24)$$

while the upper quark propagator has an expansion similar to eq. (4.22),

$$S(p_1 - k_1 + l_1) \approx -\frac{\gamma^+}{2k_1^+} \left(1 + \frac{l_1^- - k_1^-}{p_1^-} \right) + \dots. \quad (4.25)$$

The relevant structure is generated by product of l_1^-/k_1^- term from eq. (4.24) and k_1^-/p_1^- term from eq. (4.25), which cancels with the product of the leading term from eq. (4.24) and l_1^-/p_1^- term from eq. (4.25). Thus the contribution of the planar diagram to the FF vanishes in the double-logarithmic region. This cancellation is specific to three-loops and does not hold for higher-order diagrams with multiple soft gluon exchanges in the planar topology. Moreover, for the non-Abelian diagrams, the contribution of the soft gluon momentum coming from the three gluon vertex is not included. Though such a term produces a double-logarithmic contribution for the given diagram, it is proportional to the momentum of the on-shell soft gluon and after we cut the corresponding gluon line it vanishes in the sum of the diagrams by the Ward identity. Complete evaluation for these diagrams is given in appendix C.3. After factoring out the IR divergence, the remaining IR finite result reduces to the effective diagram fig. 4.5(b), which is the same as the Abelian diagram fig. 4.6(a) with effective soft gluon exchange. Contribution to $M_{ggH}^{(1)}$ at three-loops reduces to

$$\left[M_{ggH}^{(1)} \right]_{4.5b} = -\frac{(C_A - C_F)(C_A - 2C_F)x^2}{9} \ln^2 \rho, \quad (4.26)$$

with the $(C_A - C_F)$ factor accounting for the eikonal color charge variation due to the soft quark. While emission of the eikonal gluon provides the $(C_A - 2C_F)$ factor, and accounts for the eikonal quark and antiquark changing into color octet.

Resummation requires dressing fig. 4.5(a) with multiple additional soft gluon exchanges to get higher-order diagrams. Obtaining the full result would in turn require systematic treatment of factorization in QCD. This is a rather challenging problem due to the gluon self-interactions; specifically, further soft emissions by the eikonal gluon itself start contributing from four-loops. Thus full QCD analysis to obtain the all-order contribution is beyond the scope of our current work.

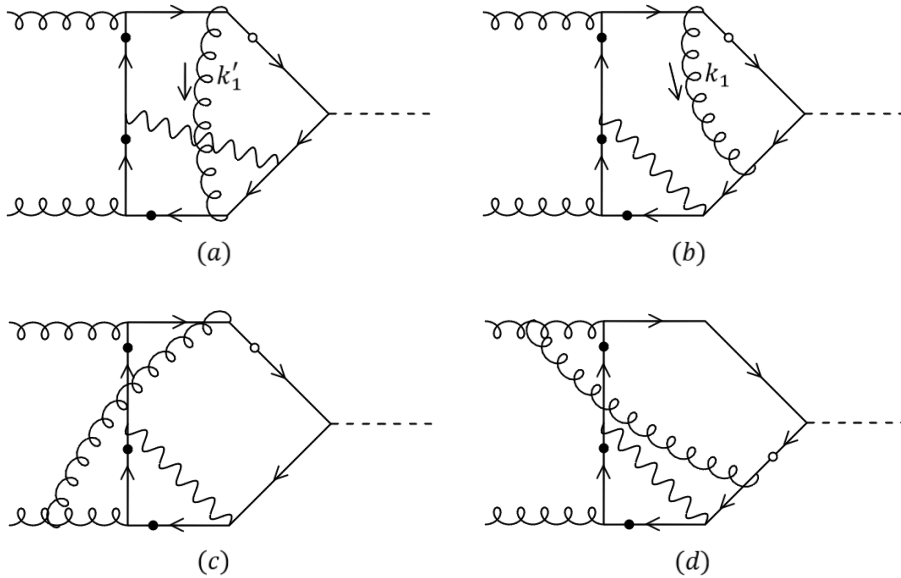


Figure 4.6: The 3-loop non-factorizable Higgs production diagrams with an additional eikonal gluon (represented by the wavy line) being emitted by the soft quark where (a) and (b) are Abelian, while (c) and (d) are non-Abelian. Symmetric diagrams and diagrams with opposite particle flow for the closed quark loop are not included. The dark (empty) circle represents mass (loop momentum) insertion.

4.4 Higgs production FF at>NNLP

So far we have obtained the all-order result for the factorizable contributions to Higgs production from diagrams with single and triple soft quark exchanges. We also obtained the non-factorizable contribution from diagrams with single soft quark exchange at three-loops. Previous resummation results were written in terms of the functions $g(z)$, $f(z)$, and $h(z)$ corresponding to single, double, and triple soft quark exchanges respectively. These functions were also normalized to the base one, two, and three-loop diagrams. Similarly, the non-factorizable contribution can be normalized to the three-loop result of eq. (4.26); we denote this resummation via the function $j(z)$. We can finally write down the>NNLP coefficient in the asymptotic expansion of the Higgs production FF in the high-energy limit as

$$M_{ggH}^{(1)} = \ln^2 \rho \left[-4g(z) + \left\{ \frac{T_F C_F}{45} h(z) - \frac{(C_A - C_F)(C_A - 2C_F)}{9} j(z) \right\} x^2 \right]. \quad (4.27)$$

As mentioned, deriving the all-order full QCD result for the function $j(z)$ is beyond the scope of our current work. Instead, we consider two complementary limits: (i) the large- N_c limit of QCD, and (ii) the Abelian limit. Though this gives only an approximate result, such an analysis is quite instructive. Indeed, the large- N_c limit catches the qualitative behavior of real QCD and very often gives reasonable quan-

titative estimates of the perturbative coefficients. At the same time, the Abelian gauge group includes all-order non-factorizable corrections and therefore represents the general case for the mass-suppressed amplitudes at the NNLP.

4.4.1 The large- N_c limit

The large number of colors limit is defined as $N_c \rightarrow \infty$ with simultaneously $g \rightarrow 0$ such that the product $\lambda \equiv g^2 N_c \approx \alpha_s N_c$ remains constant [66]. The coefficient of the function j in this approximation vanishes since

$$x^2(C_A - 2C_F) \sim \alpha_s^2 \left(N_c - \frac{N_c^2 - 1}{N_c} \right) = \alpha_s^2 \frac{1}{N_c} \rightarrow 0. \quad (4.28)$$

While the same for the function h reads

$$x^2 C_F \sim \alpha_s^2 \left(\frac{N_c^2 - 1}{2N_c} \right) \approx \alpha_s^2 N_c \rightarrow 0. \quad (4.29)$$

Thus, in this limit the dependence of the coefficient $M_{ggH}^{(1)}$ reduces to the function g with $z = (C_A - C_F)x \approx N_c x/2$;

$$M_{ggH}^{(1)} \approx -4 \ln^2 \rho g \left(\frac{N_c x}{2} \right). \quad (4.30)$$

Next, we consider the Abelian limit.

4.4.2 The Abelian limit

In this limit, the self-interactions between the gluons are absent, but the analysis of the function $j(z)$ is still highly non-trivial. We consider the case of n soft gluon exchanges. Contribution from which is generated by a diagram with m' leading soft gluon exchanges with the topology of fig. 4.6(a), and $m = n - m'$ exchanges with the topology of fig. 4.6(b); all possible permutations of the n vertices are along the upper eikonal quark line. We denote the momenta of these gluons by k'_i and k_i respectively. All n gluon exchanges result in a factor of l_1^- from the upper eikonal quark propagator similar to eqs. (4.22) and (4.25). After the sum over all the permutations of the n vertices on the upper eikonal line, the integral over $k_1^{+'}$ and k_1^+ factorizes. Similarly, the sum over $m'! m!$ permutations of vertices on the lower eikonal line, the integrals over $k_1^{-'}$ and k_1^- also factorize within each group. This results in n -loop soft contribution of

$$n \frac{(2z\eta_1\xi_2)^{m'}}{m'!} \frac{(2z\eta_1\xi_1)^m}{m!}, \quad (4.31)$$

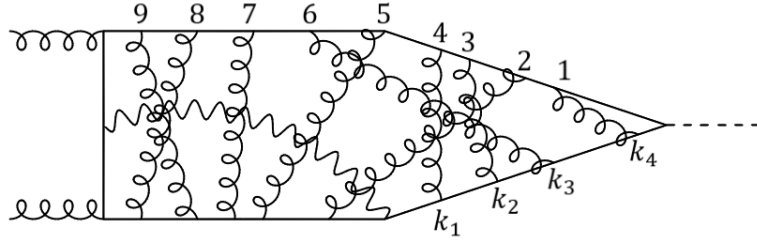


Figure 4.7: An example of a higher order Abelian diagram with multiple soft gluon exchanges on the fig. 4.5(a) topology. In this scenario $m' = 5$, and $m = 4$. As outlined in the text, the momenta k_i for $i = 1, 2, \dots, m$ are labelled from the eikonal gluon vertex (eikonal gluon represented by the wavy line) to the Higgs vertex and are labelled at the vertices of the second group on the lower eikonal line. Here, $f_1 = 4$, $f_2 = 3$, $f_3 = 6$, and $f_4 = 1$. The numbers from 1 to 9 enumerate the vertices on the upper eikonal quark line, resulting in $j' = 4$ for the vertices 1, 2, 3, 4, and $j = 3$ due to the vertices 1, 3, 4.

where $z = -C_F x$ since $C_A = 0$ in the Abelian approximation. When all n exchanges are of type fig. 4.6(a) i.e., $m = 0$ and $n = m'$, eq. (4.31) reduces to

$$\frac{(2z\eta_1\xi_2)^{m'}}{(m' - 1)!}. \quad (4.32)$$

Analysis of the l_1^- terms originating from the denominator of the lower eikonal quark propagators similar to eq. (4.24) is more involved. Only soft gluons from the second group, fig. 4.6(b), can generate this factor from the expansion of the following expression

$$\frac{f_1 k_1^- + \dots + f_m k_m^-}{(k_1^- + l_1^-) \dots (k_m^- + l_1^-)}; \quad (4.33)$$

the gluon momenta are labelled from eikonal gluon to the Higgs boson vertex as shown in fig. 4.7. f_i is the number of the eikonal propagators carrying the momentum k_i on the upper quark line for a given diagram. Rewriting the numerator of eq. (4.33) as

$$\begin{aligned} & f_m(k_1^- + \dots + k_m^- + l_1^-) + \\ & (f_{m-1} - f_m)(k_1^- + \dots + k_{m-1}^- + l_1^-) + \\ & (f_1 - f_2)(k_1^- + l_1^-) - f_1 l_1^-, \end{aligned} \quad (4.34)$$

results in the cancellation of one of the terms in the denominator of eq. (4.33) by each term except for the last one. The cancellation removes the necessary scaling to obtain the double-logarithms; thus we only need to consider the $f_1 l_1^-$ term which corresponds to the soft gluon next to the eikonal gluon vertex. To obtain the total result, the coefficients f_1 must be summed over the diagrams with all possible permutations of the remaining vertices. Let us perform the convenient double-logarithmic integrals

over k'_i and k_i first. Recall that in the logarithmic region, the Sudakov parameters are ordered along the eikonal lines, thus the n -fold integral for each diagram over w'_i and w_i gives $\eta_1^n/n!$; while m and m' -fold integral over r_i and r'_i gives $\xi_1^m/m!$ and $\xi_2^{m'}/m'!$ respectively. The combined n -loop factor is

$$\frac{(2z\eta_1\xi_2)^{m'}(2z\eta_1\xi_1)^m}{n!m'm!}. \quad (4.35)$$

Summation over the permutations of the m' and $(m-1)$ remaining vertices within each group on the lower quark line can be performed as f_1 only depends on the routing of k_1 , and is independent of all other soft gluon momenta; this results in

$$m'!(m-1)! \quad (4.36)$$

for $m > 0$. Now let j' and j be the number of vertex with momentum k_1 in a sequence of all n and m vertices on the upper quark line respectively, counted from the Higgs boson vertex. Then $f_1 = j'$ for a given diagram, and the sum over all gives

$$\sum_{j=1}^m \sum_{j'=j}^{j+m'} \frac{(j'-1)!}{(j-1)!(j'-j)!} \frac{(n-j')!}{(m-j)!(m'+j-j')!} j' = \frac{(-1)^{m'+1}m(m+1)(n+1)\text{Pochhammer}[-n, m'-1]}{2m'!}, \quad (4.37)$$

where the combinatorial factors in eq. (4.37) corresponds to the number of ways m' ordered vertices from the first group, and $m-1$ vertices from the second group for given j' and j can be arranged. The Pochhammer function is defined as

$$\text{Pochhammer}[n, m] = n(n+1)(n+2)\cdots(n+m-1) \quad (4.38)$$

Plugging this definition in eq. (4.37) gives

$$\begin{aligned} \text{Pochhammer}[-n, m'-1] &= (-n)(-n+1)\cdots(-n+m'-2) \\ &= (-1)^{m'-1}n(n-1)\cdots(n-m'+2) \\ &= (-1)^{m'-1}\frac{n!}{(n-m'+1)!} = (-1)^{m'-1}\frac{n!}{(m+1)!}. \end{aligned} \quad (4.39)$$

We have used $n = m' + m$ and the fact that all m , m' , and n are non-negative integers. Substituting eq. (4.39) back into eq. (4.37) gives

$$\sum_{j=1}^m \sum_{j'=j}^{j+m'} \frac{(j'-1)!}{(j-1)!(j'-j)!} \frac{(n-j')!}{(m-j)!(m'+j-j')!} j' = \frac{n!}{m!m'} \frac{m(n+1)}{2}. \quad (4.40)$$

Bringing the factors together from eqs. (4.34) to (4.36) and (4.40) results in

$$-\frac{(2z\eta_1\xi_2)^{m'}(2z\eta_1\xi_1)^m}{n!m'm!}m'(m-1)!\frac{n!}{m!m'}\frac{m(n+1)}{2}=-\frac{n+1}{2m'm!}(2z\eta_1\xi_2)^{m'}(2z\eta_1\xi_1)^m. \quad (4.41)$$

Adding eqs. (4.31) and (4.41) gives

$$\frac{m+m'-1}{2m'm!}(2z\eta_1\xi_2)^{m'}(2z\eta_1\xi_1)^m, \quad (4.42)$$

the total for $m > 0$. The dependence on m and m' factorizes, allowing the direct summation over the number of soft gluons in each group;

$$\sum_{m'=0}^{\infty} \frac{(2z\eta_1\xi_2)^{m'}}{m'} \left[\sum_{m=0}^{\infty} \left\{ \frac{m+m'-1}{2m!} (2z\eta_1\xi_1)^m \right\} + \frac{m'+1}{2} \right] \quad (4.43)$$

where the last term is added to obtain correct $m = 0$ contribution, eq. (4.32). It is simpler to sum over each term in the above equation individually; these sums are

$$\begin{aligned} \sum_{m'=0}^{\infty} \left[\frac{(2z\eta_1\xi_2)^{m'}}{m'} \right] \sum_{m=0}^{\infty} \left[\frac{m}{2m!} (2z\eta_1\xi_1)^m \right] &= e^{2z\eta_1\xi_2} \left[0 + \frac{1}{2} \sum_{m=1}^{\infty} \frac{(2z\eta_1\xi_1)^{m-1}}{(m-1)!} (2z\eta_1\xi_1) \right] \\ &= \frac{e^{2z\eta_1\xi_2} e^{2z\eta_1\xi_1}}{2} (2z\eta_1\xi_1), \end{aligned} \quad (4.44)$$

$$\sum_{m'=0}^{\infty} \left[\frac{(2z\eta_1\xi_2)^{m'}}{m'} \right] \sum_{m=0}^{\infty} \left[\frac{(2z\eta_1\xi_1)^m}{2m!} \right] = \frac{e^{2z\eta_1\xi_2} e^{2z\eta_1\xi_1}}{2} (2z\eta_1\xi_2), \quad (4.45)$$

$$\sum_{m'=0}^{\infty} \left[\frac{(2z\eta_1\xi_2)^{m'}}{m'} \right] \sum_{m=0}^{\infty} \left[-\frac{(2z\eta_1\xi_1)^m}{2m!} \right] = -\frac{e^{2z\eta_1\xi_2} e^{2z\eta_1\xi_1}}{2}, \quad (4.46)$$

$$\sum_{m'=0}^{\infty} \left[\frac{(2z\eta_1\xi_2)^{m'}}{m'} \frac{m'}{2} \right] = \frac{e^{2z\eta_1\xi_2}}{2} (2z\eta_1\xi_2), \quad (4.47)$$

and

$$\sum_{m'=0}^{\infty} \left[\frac{(2z\eta_1\xi_2)^{m'}}{m'} \frac{1}{2} \right] = \frac{e^{2z\eta_1\xi_2}}{2}. \quad (4.48)$$

Putting factors from eqs. (4.44) to (4.48) together, we obtain,

$$\begin{aligned} \text{eq. (4.43)} &= \frac{e^{2z\eta_1(\xi_1+\xi_2)}}{2} \left[(e^{-2z\eta_1\xi_1} - 1 + 2z\eta_1\xi_1) + (2z\eta_1\xi_2) (1 + e^{-2z\eta_1\xi_1}) \right] \\ &= (2z\eta_1\xi_2) e^{2z\eta_1(\xi_1+\xi_2)} \left[1 + \frac{e^{-2z\eta_1\xi_1} - 1}{2} + \frac{e^{-2z\eta_1\xi_1} - 1 + 2z\eta_1\xi_1}{4z\eta_1\xi_2} \right]. \end{aligned} \quad (4.49)$$

It is important to note that the contribution of soft gluon exchanges from both groups factorizes and exponentiates in the final result. After factoring out the leading soft

gluon contribution $2z\eta_1\xi_2$, we obtain following form for the integral representation of $j(z)$ in the absence of gluon self-coupling

$$j^{ab}(z) = 72 \int_0^1 d\eta_1 \int_0^{1-\eta_1} d\xi_1 \int_0^{1-\xi_1} d\eta_2 \int_0^{1-\eta_2-\xi_1} d\xi_2 [\eta_1\xi_2 e^{2z\eta_1(\xi_1+\xi_2)}] \left[1 + \frac{e^{-2z\eta_1\xi_1} - 1}{2} + \frac{e^{-2z\eta_1\xi_1} - 1 + 2z\eta_1\xi_1}{4z\eta_1\xi_2} \right], \quad (4.50)$$

with $z = -C_F x$. First six coefficients of the Taylor expansion $j^{ab}(z) = 1 + \sum_{n=1}^{\infty} j_n^{ab} z^n$ are given in table 4.1.

4.4.3 Discussion

In this section, we compare our analysis to the available results obtained by different methods and discuss the phenomenological applications to the Higgs boson physics at the LHC. Loop by loop perturbative expansion of the full coefficient in eq. (4.27) is

$$M_{ggH}^{(1)} = \ln^2 \rho \left[-4 - \frac{2}{3}(C_A - C_F)x \right] + \ln^2 \rho \left[\frac{x^2}{45} (T_F C_F - 14C_F^2 + 23C_F C_A - 9C_A^2) + c_3 x^3 + \dots \right], \quad (4.51)$$

with the exact result up to three-loops given by terms $\mathcal{O}(x^2)$ in the double-logarithmic region of the high-energy or small mass approximation. The four-loop coefficient $c_3 = -N_c^3/840$ in the large- N_c approximation, and in the Abelian approximation $c_3 = \frac{T_F C_F^2}{210} + \frac{13C_F^3}{90}$. The expansion of the exact analytic result at two-loops from ref. [67] agrees with the two-loop term in eq. (4.51). Numerical result for ggH amplitude in the high-energy approximation was obtained in ref. [58]. 0.0005738811728 is the numeric coefficient of the double-logarithmic term L_s^6/z^2 in eq. (C.1) of [58]; where the authors of [58] define the scale ratio as “ z ”, which is equivalent to $1/(4\rho)$ as per the notations used in our calculation. Extracting the coefficient from eqs. (4.1) and (4.51) for L_s^6/z^2 term results in

$$\frac{1}{23040} (-T_F C_F + 14C_F^2 - 23C_F C_A + 9C_A^2); \quad (4.52)$$

this agrees with the numerical value from [58]. The gluon fusion to Higgs boson result can be transformed into the Higgs boson to two photon decay by changing the color factor of the external lines from C_A to zero. Thus $C_A - C_F \rightarrow -C_F$ replacement is required in eq. (4.26), and in the definition of the variable z in eq. (4.27). Using

similar notations, for the Higgs decay FF we get

$$M_{H\gamma\gamma}^{(1)} = \ln^2 \rho \left[-4 + \frac{2}{3} C_F x + \frac{x^2}{45} (T_F C_F - 14 C_F^2 + 5 C_F C_A) + \dots \right]. \quad (4.53)$$

Numerical result for $H\gamma\gamma$ amplitude obtained in ref. [59] has 0.001099537037 as the coefficient of the L_s^6/z^2 term in eq. (C.1); where z is the same scale ratio as that in [58]. Extracting the coefficient from eqs. (4.1) and (4.53) for L_s^6/z^2 term results in

$$\frac{1}{3840} (-T_F C_F + 14 C_F^2 - 5 C_F C_A), \quad (4.54)$$

and agrees with the numerical value from [59].

Finally, let us consider the asymptotic behavior of the all-order result for the Higgs production FF in the high-energy or small mass approximation. As mentioned earlier, in QCD with large- N_c approximation, eq. (4.27) reduces to

$$M_{ggH}^{(1)} = -4 \ln^2 \rho g \left(\frac{N_c x}{2} \right). \quad (4.55)$$

Since the argument of the function g is positive, the asymptotic behavior is determined by eq. (2.81) i.e., the amplitude is exponentially enhanced. Note that we take the $N_c \rightarrow \infty$ limit first, and in general, this limit may not commute with the kinematical limit of $z \rightarrow \infty$. Similarly, in the Abelian approximation the asymptotic behavior of the functions in eq. (4.27) as $z \rightarrow -\infty$ are

$$g(-z) \sim \frac{\ln 2z + \gamma_E}{z}, \quad h(-z) = \mathcal{O}(1/z^3), \quad j^{ab}(-z) \sim \frac{9}{2z^2}. \quad (4.56)$$

With $C_F = 1$ and $C_A = 0$ in the Abelian approximation, the coefficient, eq. (4.27), asymptotically approaches the value $M_{ggH}^{(1)} = -\ln^2 \rho$. Thus, the double-logarithmic corrections effectively reduce the LO coefficient, eq. (4.14), by factor four.

To estimate the effect of the high order term we have computed, for physical values of the parameter; let us rewrite the coefficient $M_{ggH}^{(1)}$ with respect to $M_{ggH}^{(0)}$,

$$1 + \rho \left[-4 + \left\{ \frac{T_F C_F}{45} h(z) - \frac{(C_A - C_F)(C_A - 2C_F)}{9} j(z) \right\} \frac{x^2}{g(z)} \right]. \quad (4.57)$$

In the large- N_c approximation the above equation reduces to $1-4\rho$ with $\rho \approx 1.6 \times 10^{-3}$ for bottom quark, which amounts to approximately 0.64% negative correction to the $O(m)$ contribution. In this limit, the dependence of eq. (4.57) on x disappears and it becomes valid for both gluon and photon external lines. Thus, we get a universal all-order estimate of the NNLP contribution to the production and decay processes.

Chapter 5

Summary

In this thesis, we have addressed one of the challenging problems of the modern quantum field theory: the high-energy asymptotic behavior of the power-suppressed scattering amplitudes. We focused on the massive quark scattering, and the light quark loop mediated Higgs boson production and decays in the double-logarithmic approximation.

5.1 Massive quark FF

The quark scattering has been studied through the second order of the small quark mass expansion. The asymptotic behavior of the corresponding FF at the NLP is determined by the non-Sudakov double-logarithmic corrections resulting from the eikonal color charge non-conservation in the process with the exchange of the soft virtual quark pair. They are described by a universal function that shows exponential growth for the large values of the double-logarithmic variable in QED and a logarithmic scaling in QCD. We have presented for the first time the complete analytic asymptotic results for this function (eqs. (3.20) and (3.29)). At $\mathcal{O}(\alpha_s^3)$ the result has been recently confirmed through the direct evaluation of the three-loop vector, axial, scalar, and pseudoscalar FF [68].

5.2 Higgs production via gluon fusion

The Higgs boson amplitude has been studied through the third order of the small quark mass expansion. To our knowledge, this is the first example of the renormalization group analysis at the NNLP. The double-logarithmic corrections to the $\mathcal{O}(m^3)$ Higgs boson production and decay amplitudes are induced by single and triple soft quark exchanges. This is the first example where the mass suppression of the

double-logarithmic contribution is not entirely associated with the chirality flip on a fermion line. Starting with three-loops a new source of the double-logarithmic corrections opens up with the emission of an additional virtual eikonal gluon by the soft quark. Our analytic result agrees with the previous numerical evaluation of the three-loop QCD corrections to the Higgs boson production [58] and two photon decay [59]. Beyond three-loops the all-order double-logarithmic asymptotic behavior of the amplitudes has been derived in two complementary approximations. In the large- N_c limit, which is supposed to catch the qualitative behavior of real QCD, the structure of the double-logarithmic corrections significantly simplifies and becomes identical to the one of the leading $\mathcal{O}(m)$ contribution, which is exponentially enhanced for the large values of the double-logarithmic variable. The Abelian limit with $C_A = 0$, though less phenomenologically relevant, reveals a more complex structure of the double-logarithmic contributions and represents the general case for the mass-suppressed amplitudes at the NNLP.

We have also presented a quantitative estimate of the accuracy of the high-order calculations based on the small mass expansion for the Higgs boson production and decays mediated by the bottom quark loop, which may become relevant with the permanently increasing accuracy of the QCD predictions [69]. Based on the double-logarithmic analysis we conclude that neglecting the terms suppressed by the mass ratio m_b^2/m_H^2 in such a calculation introduces a relative error at the scale of one percent in every order of the perturbative expansion. Our result can also be generalized to estimate the high-order subleading top quark mass effects on the double Higgs boson production in the high-energy limit [70, 71], where the role of the NNLP terms could be significant.

Bibliography

- [1] V. Sudakov, “Vertex parts at very high-energies in quantum electrodynamics,” *Sov. Phys. JETP*, vol. 3, pp. 65–71, 1956. [[JETP](#)], [[INSPIRE](#)]. (Cited on pages ii, iv, 2, 8, 9, and 78.)
- [2] J. Frenkel and J. Taylor, “Exponentiation of Leading Infrared Divergences in Massless Yang-Mills Theories,” *Nucl. Phys. B*, vol. 116, pp. 185–194, 1976. [[ScienceDirect](#)], [[INSPIRE](#)]. (Cited on pages ii and 2.)
- [3] A. V. Smilga, “NEXT-TO-LEADING LOGARITHMS IN THE HIGH-ENERGY ASYMPTOTICS OF THE QUARK FORM-FACTOR AND THE JET CROSS-SECTION,” *Nucl. Phys. B*, vol. 161, pp. 449–468, 1979. [[ScienceDirect](#)], [[INSPIRE](#)]. (Cited on pages ii and 2.)
- [4] A. H. Mueller, “On the Asymptotic Behavior of the Sudakov Form-factor,” *Phys. Rev. D*, vol. 20, p. 2037, 1979. [[APS](#)], [[INSPIRE](#)]. (Cited on pages ii and 2.)
- [5] J. C. Collins, “Algorithm to Compute Corrections to the Sudakov Form-factor,” *Phys. Rev. D*, vol. 22, p. 1478, 1980. [[APS](#)], [[INSPIRE](#)]. (Cited on pages ii and 2.)
- [6] A. Sen, “Asymptotic Behavior of the Sudakov Form-Factor in QCD,” *Phys. Rev. D*, vol. 24, p. 3281, 1981. [[APS](#)], [[INSPIRE](#)]. (Cited on pages ii and 2.)
- [7] G. F. Sterman, “Summation of Large Corrections to Short Distance Hadronic Cross-Sections,” *Nucl. Phys. B*, vol. 281, pp. 310–364, 1987. [[ScienceDirect](#)], [[INSPIRE](#)]. (Cited on pages ii and 2.)
- [8] G. P. Korchemsky, “Sudakov Form-factor in QCD,” *Phys. Lett. B*, vol. 220, pp. 629–634, 1989. [[ScienceDirect](#)], [[INSPIRE](#)]. (Cited on pages ii and 2.)
- [9] G. P. Korchemsky, “Double Logarithmic Asymptotics in QCD,” *Phys. Lett. B*, vol. 217, pp. 330–334, 1989. [[ScienceDirect](#)], [[INSPIRE](#)]. (Cited on pages ii and 2.)
- [10] A. A. Penin, “High-energy limit of quantum electrodynamics beyond sudakov approximation,” *Physics Letters B*, vol. 745, p. 69–72, 05 2015. [[ScienceDirect](#)], [[INSPIRE](#)]. (Cited on pages ii, iv, and 2.)

- [11] A. A. Penin and N. Zerf, “Two-loop bhabha scattering at high energy beyond leading power approximation,” *Physics Letters B*, vol. 760, p. 816–822, Sep 2016. [[ScienceDirect](#)], [[INSPIRE](#)]. (Cited on pages ii, iv, 2, 8, and 9.)
- [12] T. Liu, A. A. Penin, and N. Zerf, “Three-loop quark form factor at high energy: The leading mass corrections,” *Physics Letters B*, vol. 771, p. 492–496, 08 2017. [[ScienceDirect](#)], [[arXiv](#)]. (Cited on pages ii, iv, 2, and 70.)
- [13] T. Liu and A. A. Penin, “High-Energy Limit of QCD beyond the Sudakov Approximation,” *Phys. Rev. Lett.*, vol. 119, no. 26, p. 262001, 2017. [[APS](#)], [[arXiv](#)]. (Cited on pages ii, iv, 2, 3, 24, 26, 27, 30, 31, 36, and 38.)
- [14] T. Liu and A. Penin, “High-energy limit of mass-suppressed amplitudes in gauge theories,” *Journal of High Energy Physics*, vol. 2018, Nov 2018. [[JHEP](#)], [[arXiv](#)]. (Cited on pages ii, iv, 2, 3, 21, 24, 26, 27, 30, 31, 36, and 38.)
- [15] T. Liu, S. Modi, and A. A. Penin, “Higgs boson production and quark scattering amplitudes at high energy through the next-to-next-to-leading power in quark mass,” *Journal of High Energy Physics*, vol. 2022, p. 170, Feb 2022. [[JHEP](#)], [[arXiv](#)]. (Cited on pages iv and 38.)
- [16] P. Nogueira, “Qgraf downloads.” <http://cfif.ist.utl.pt/~paulo/qgraf.html>. Accessed: 2023-03-11. (Cited on pages iv, 71, and 72.)
- [17] P. Nogueira, “Automatic feynman graph generation,” *Journal of Computational Physics*, vol. 105, no. 2, pp. 279 – 289, 1993. [[ScienceDirect](#)]. (Cited on pages iv, 71, and 72.)
- [18] P. Nogueira, “Abusing qgraf,” *Nuclear Instruments and Methods in Physics Research Section A: Accelerators, Spectrometers, Detectors and Associated Equipment*, vol. 559, no. 1, pp. 220–223, 2006. Proceedings of the X International Workshop on Advanced Computing and Analysis Techniques in Physics Research, [[ScienceDirect](#)]. (Cited on pages iv, 71, and 72.)
- [19] P. Nogueira, “Feynman graph generation and propagator mixing, i,” *Computer Physics Communications*, vol. 269, p. 108103, 2021. [[ScienceDirect](#)]. (Cited on pages iv and 71.)
- [20] J. A. Vermaseren, “New features of form,” *arXiv preprint math-ph/0010025*, 10 2000. [[arXiv](#)]. (Cited on pages iv, 28, and 71.)
- [21] V. Berestetskii, L. Pitaevskii, and E. Lifshitz, *Quantum Electrodynamics: Volume 4*. No. v. 4 in Course of theoretical physics, Elsevier Science, 2012. [[gBooks](#)]. (Cited on pages iv, 9, and 78.)

- [22] A. Randle-Conde, “Feynman diagram maker.” aidansean.com/feynman/, 2022. Accessed: 2022-07-31. (Cited on page iv.)
- [23] G. Aad *et al.*, “Observation of a new particle in the search for the Standard Model Higgs boson with the ATLAS detector at the LHC,” *Phys. Lett. B*, vol. 716, pp. 1–29, 2012. [[ScienceDirect](#)], [[INSPIRE](#)], [[arXiv](#)]. (Cited on page 1.)
- [24] J. H. Kuhn, A. A. Penin, and V. A. Smirnov, “Summing up subleading Sudakov logarithms,” *Eur. Phys. J. C*, vol. 17, pp. 97–105, 2000. [[JHEP](#)], [[INSPIRE](#)]. (Cited on page 2.)
- [25] J. H. Kuhn, S. Moch, A. A. Penin, and V. A. Smirnov, “Next-to-next-to-leading logarithms in four fermion electroweak processes at high-energy,” *Nucl. Phys. B*, vol. 616, pp. 286–306, 2001. [Erratum: *Nucl.Phys.B* 648, 455–456 (2003)], [[ScienceDirect](#)], [[INSPIRE](#)]. (Cited on page 2.)
- [26] B. Feucht, J. H. Kuhn, A. A. Penin, and V. A. Smirnov, “Two loop Sudakov form-factor in a theory with mass gap,” *Phys. Rev. Lett.*, vol. 93, p. 101802, 2004. [[APS](#)], [[INSPIRE](#)]. (Cited on page 2.)
- [27] B. Jantzen, J. H. Kuhn, A. A. Penin, and V. A. Smirnov, “Two-loop electroweak logarithms in four-fermion processes at high energy,” *Nucl. Phys. B*, vol. 731, pp. 188–212, 2005. [Erratum: *Nucl.Phys.B* 752, 327–328 (2006)], [[ScienceDirect](#)], [[INSPIRE](#)]. (Cited on page 2.)
- [28] A. A. Penin, “Two-loop photonic corrections to massive Bhabha scattering,” *Nucl. Phys. B*, vol. 734, pp. 185–202, 2006. [[ScienceDirect](#)], [[INSPIRE](#)]. (Cited on page 2.)
- [29] A. A. Penin, “Two-loop corrections to Bhabha scattering,” *Phys. Rev. Lett.*, vol. 95, p. 010408, 2005. [[APS](#)], [[INSPIRE](#)], [[arXiv](#)]. (Cited on page 2.)
- [30] R. Bonciani, A. Ferroglia, and A. A. Penin, “Heavy-flavor contribution to Bhabha scattering,” *Phys. Rev. Lett.*, vol. 100, p. 131601, 2008. [[JHEP](#)], [[INSPIRE](#)]. (Cited on page 2.)
- [31] R. Bonciani, A. Ferroglia, and A. A. Penin, “Calculation of the Two-Loop Heavy-Flavor Contribution to Bhabha Scattering,” *JHEP*, vol. 02, p. 080, 2008. [[JHEP](#)], [[INSPIRE](#)], [[arXiv](#)]. (Cited on page 2.)
- [32] J. H. Kühn, F. Metzler, and A. A. Penin, “Next-to-next-to-leading electroweak logarithms in W-pair production at ILC,” *Nucl. Phys. B*, vol. 795, pp. 277–290, 2008. [Erratum: *Nucl.Phys.B* 818, 135–135 (2009)], [[JHEP](#)] [[ScienceDirect](#)]. (Cited on page 2.)

- [33] J. H. Kuhn, F. Metzler, A. A. Penin, and S. Uccirati, “Next-to-Next-to-Leading Electroweak Logarithms for W-Pair Production at LHC,” *JHEP*, vol. 06, p. 143, 2011. [[JHEP](#)], [[iNSPIRE](#)], [[arXiv](#)]. (Cited on page 2.)
- [34] A. A. Penin and G. Ryan, “Two-loop electroweak corrections to high energy large-angle Bhabha scattering,” *JHEP*, vol. 11, p. 081, 2011. [[JHEP](#)], [[iNSPIRE](#)], [[arXiv](#)]. (Cited on page 2.)
- [35] V. G. Gorshkov, V. N. Gribov, L. N. Lipatov, and G. V. Frolov, “Doubly logarithmic asymptotic behavior in quantum electrodynamics,” *Yad. Fiz.*, vol. 6, p. 129, 1967. [[iNSPIRE](#)]. (Cited on page 2.)
- [36] M. I. Kotsky and O. I. Yakovlev, “On the resummation of double logarithms in the process $Higgs \rightarrow \gamma\gamma$,” *Phys. Lett. B*, vol. 418, pp. 335–344, 1998. [[ScienceDirect](#)], [[iNSPIRE](#)], [[arXiv](#)]. (Cited on page 2.)
- [37] K. Melnikov and A. Penin, “On the light quark mass effects in Higgs boson production in gluon fusion,” *JHEP*, vol. 05, p. 172, 2016. [[JHEP](#)], [[iNSPIRE](#)], [[arXiv](#)]. (Cited on page 2.)
- [38] Z. L. Liu and M. Neubert, “Factorization at subleading power and endpoint-divergent convolutions in $h \rightarrow \gamma\gamma$ decay,” *JHEP*, vol. 04, p. 033, 2020. [[JHEP](#)], [[iNSPIRE](#)], [[arXiv](#)]. (Cited on page 2.)
- [39] J. Wang, “Resummation of double logarithms in loop-induced processes with effective field theory,” 12 2019. [[iNSPIRE](#)], [[arXiv](#)]. (Cited on page 2.)
- [40] C. Anastasiou and A. Penin, “Light Quark Mediated Higgs Boson Threshold Production in the Next-to-Leading Logarithmic Approximation,” *JHEP*, vol. 07, p. 195, 2020. [Erratum: *JHEP* 01, 164 (2021)], [[JHEP](#)], [[iNSPIRE](#)], [[arXiv](#)]. (Cited on page 2.)
- [41] Z. L. Liu, B. Mecaj, M. Neubert, and X. Wang, “Factorization at subleading power, Sudakov resummation, and endpoint divergences in soft-collinear effective theory,” *Phys. Rev. D*, vol. 104, no. 1, p. 014004, 2021. [[APS](#)], [[iNSPIRE](#)], [[arXiv](#)]. (Cited on page 2.)
- [42] Z. L. Liu, B. Mecaj, M. Neubert, and X. Wang, “Factorization at subleading power and endpoint divergences in $h \rightarrow \gamma\gamma$ decay. Part II. Renormalization and scale evolution,” *JHEP*, vol. 01, p. 077, 2021. [[JHEP](#)], [[iNSPIRE](#)], [[arXiv](#)]. (Cited on page 2.)

- [43] A. Ferroglia, M. Neubert, B. D. Pecjak, and L. L. Yang, “Two-loop divergences of qcd scattering amplitudes with massive partons,” *Phys. Rev. Lett.*, vol. 103, p. 201601, Nov 2009. [APS], [INSPIRE], [arXiv]. (Cited on page 2.)
- [44] E. Laenen, L. Magnea, G. Stavenga, and C. D. White, “Next-to-Eikonal Corrections to Soft Gluon Radiation: A Diagrammatic Approach,” *JHEP*, vol. 01, p. 141, 2011. [JHEP], [INSPIRE], [arXiv]. (Cited on page 2.)
- [45] T. Becher and G. Bell, “Enhanced nonperturbative effects through the collinear anomaly,” *Phys. Rev. Lett.*, vol. 112, p. 182002, May 2014. [APS], [INSPIRE], [arXiv]. (Cited on page 2.)
- [46] D. de Florian, J. Mazzitelli, S. Moch, and A. Vogt, “Approximate n3lo higgs-boson production cross section using physical-kernel constraints,” *Journal of High Energy Physics*, vol. 2014, p. 176, Oct 2014. [JHEP], [INSPIRE], [arXiv]. (Cited on page 2.)
- [47] C. Anastasiou, C. Duhr, F. Dulat, E. Furlan, T. Gehrmann, F. Herzog, and B. Mistlberger, “Higgs boson gluon-fusion production beyond threshold in n3lo qcd,” 2014. [JHEP], [INSPIRE], [arXiv]. (Cited on page 2.)
- [48] R. Boughezal, A. Isgrò, and F. Petriello, “Next-to-leading-logarithmic power corrections for N -jettiness subtraction in color-singlet production,” *Phys. Rev. D*, vol. 97, no. 7, p. 076006, 2018. [INSPIRE], [APS], [arXiv]. (Cited on page 2.)
- [49] R. Brüser, S. Caron-Huot, and J. M. Henn, “Subleading Regge limit from a soft anomalous dimension,” *JHEP*, vol. 04, p. 047, 2018. [JHEP], [INSPIRE], [arXiv]. (Cited on page 2.)
- [50] I. Moulton, I. W. Stewart, G. Vita, and H. X. Zhu, “First Subleading Power Resummation for Event Shapes,” *JHEP*, vol. 08, p. 013, 2018. [JHEP], [INSPIRE], [arXiv]. (Cited on page 2.)
- [51] M. A. Ebert, I. Moulton, I. W. Stewart, F. J. Tackmann, G. Vita, and H. X. Zhu, “Power Corrections for N-Jettiness Subtractions at $\mathcal{O}(\alpha_s)$,” *JHEP*, vol. 12, p. 084, 2018. [JHEP], [INSPIRE], [arXiv]. (Cited on page 2.)
- [52] M. Beneke, A. Broggio, M. Garry, S. Jaskiewicz, R. Szafron, L. Vernazza, and J. Wang, “Leading-logarithmic threshold resummation of the Drell-Yan process at next-to-leading power,” *JHEP*, vol. 03, p. 043, 2019. [JHEP], [INSPIRE], [arXiv]. (Cited on page 2.)

- [53] T. Engel, C. Gnendiger, A. Signer, and Y. Ulrich, “Small-mass effects in heavy-to-light form factors,” *JHEP*, vol. 02, p. 118, 2019. [[JHEP](#)], [[INSPIRE](#)], [[arXiv](#)]. (Cited on page 2.)
- [54] M. A. Ebert, I. Moulton, I. W. Stewart, F. J. Tackmann, G. Vita, and H. X. Zhu, “Subleading power rapidity divergences and power corrections for q_T ,” *JHEP*, vol. 04, p. 123, 2019. [[JHEP](#)], [[INSPIRE](#)], [[arXiv](#)]. (Cited on page 2.)
- [55] A. A. Penin, “Regge Limit of Gauge Theory Amplitudes beyond Leading Power Approximation,” *JHEP*, vol. 04, p. 156, 2020. [[JHEP](#)], [[INSPIRE](#)], [[arXiv](#)]. (Cited on page 2.)
- [56] M. Beneke, M. Garny, S. Jaskiewicz, R. Szafron, L. Vernazza, and J. Wang, “Leading-logarithmic threshold resummation of Higgs production in gluon fusion at next-to-leading power,” *JHEP*, vol. 01, p. 094, 2020. [[JHEP](#)], [[INSPIRE](#)], [[arXiv](#)]. (Cited on page 2.)
- [57] M. Cepeda *et al.*, “Report from Working Group 2: Higgs Physics at the HL-LHC and HE-LHC,” *CERN Yellow Rep. Monogr.*, vol. 7, pp. 221–584, 2019. [[CERN](#)], [[INSPIRE](#)], [[arXiv](#)]. (Cited on page 2.)
- [58] M. Czakon and M. Niggetiedt, “Exact quark-mass dependence of the higgs-gluon form factor at three loops in qcd,” *Journal of High Energy Physics*, vol. 2020, May 2020. [[JHEP](#)], [[INSPIRE](#)], [[arXiv](#)]. (Cited on pages 3, 49, 50, and 52.)
- [59] M. Niggetiedt, “Exact quark-mass dependence of the higgs-photon form factor at three loops in qcd,” *Journal of High Energy Physics*, vol. 2021, p. 196, Apr 2021. [[JHEP](#)], [[INSPIRE](#)], [[arXiv](#)]. (Cited on pages 3, 50, and 52.)
- [60] K. Melnikov, L. Tancredi, and C. Wever, “Two-loop $gg \rightarrow Hg$ amplitude mediated by a nearly massless quark,” *JHEP*, vol. 11, p. 104, 2016. [[JHEP](#)], [[INSPIRE](#)], [[arXiv](#)]. (Cited on page 3.)
- [61] J. M. Lindert, K. Melnikov, L. Tancredi, and C. Wever, “Top-bottom interference effects in Higgs plus jet production at the LHC,” *Phys. Rev. Lett.*, vol. 118, no. 25, p. 252002, 2017. [[APS](#)], [[INSPIRE](#)], [[arXiv](#)]. (Cited on page 3.)
- [62] V. A. Smirnov, “Applied asymptotic expansions in momenta and masses,” *Springer Tracts Mod. Phys.*, vol. 177, pp. 1–262, 2002. [[INSPIRE](#)]. (Cited on page 8.)
- [63] G. Frolov, V. Gorshkov, V. Gribov, and L. Lipatov, “Double logarithmic asymptotics of quantum electrodynamics,” *Physics Letters*, vol. 22, no. 5, pp. 671 – 673, 1966. [[ScienceDirect](#)]. (Cited on page 8.)

- [64] M. Schwartz, *Quantum Field Theory and the Standard Model*. Quantum Field Theory and the Standard Model, Cambridge University Press, 2014. [[Cambridge](#)], [[gBooks](#)]. (Cited on page 17.)
- [65] W. Bernreuther, R. Bonciani, T. Gehrmann, R. Heinesch, P. Mastrolia, and E. Remiddi, “Decays of scalar and pseudoscalar higgs bosons into fermions: Two-loop qcd corrections to the higgs-quark-antiquark amplitude,” *Phys. Rev. D*, vol. 72, p. 096002, Nov 2005. [[APS](#)]. (Cited on pages 24 and 27.)
- [66] B. Lucini and M. Panero, “Introductory lectures to large-n qcd phenomenology and lattice results,” *Progress in Particle and Nuclear Physics*, vol. 75, pp. 1–40, 2014. [[ScienceDirect](#)], [[arXiv](#)]. (Cited on page 45.)
- [67] U. Aglietti, R. Bonciani, G. Degrossi, and A. Vicini, “Analytic results for virtual QCD corrections to higgs production and decay,” *Journal of High Energy Physics*, vol. 2007, pp. 021–021, jan 2007. [[JHEP](#)], [[iNSPIRE](#)], [[arXiv](#)]. (Cited on page 49.)
- [68] M. Fael, F. Lange, K. Schönwald, and M. Steinhauser, “Singlet and nonsinglet three-loop massive form factors,” *Phys. Rev. D*, vol. 106, no. 3, p. 034029, 2022. [[APS](#)], [[iNSPIRE](#)], [[arXiv](#)]. (Cited on page 51.)
- [69] J. Davies and F. Herren, “Higgs boson decay into photons at four loops,” *Phys. Rev. D*, vol. 104, no. 5, p. 053010, 2021. [[APS](#)], [[iNSPIRE](#)], [[arXiv](#)]. (Cited on page 52.)
- [70] J. Davies, G. Mishima, M. Steinhauser, and D. Wellmann, “Double Higgs boson production at NLO in the high-energy limit: complete analytic results,” *JHEP*, vol. 01, p. 176, 2019. [[JHEP](#)], [[iNSPIRE](#)], [[arXiv](#)]. (Cited on page 52.)
- [71] J. Davies, G. Heinrich, S. P. Jones, M. Kerner, G. Mishima, M. Steinhauser, and D. Wellmann, “Double Higgs boson production at NLO: combining the exact numerical result and high-energy expansion,” *JHEP*, vol. 11, p. 024, 2019. [[JHEP](#)], [[iNSPIRE](#)], [[arXiv](#)]. (Cited on page 52.)
- [72] M. Peskin and D. Schroeder, *An Introduction To Quantum Field Theory*. Frontiers in Physics, Avalon Publishing, 1995. [[gBooks](#)]. (Cited on page 79.)

Appendix A

Gamma matrix identities

Here we list the most useful gamma matrix identities from Dirac algebra, which are used throughout the calculations presented in this thesis.

$$\{\gamma^\mu, \gamma^\nu\} = 2g^{\mu\nu} \quad (\text{A.1})$$

$$\not{a} = a_\mu \gamma^\mu = a^\nu \gamma^\mu g_{\mu\nu} = a^\mu \gamma_\mu = a_\nu \gamma_\mu g^{\mu\nu} \quad (\text{A.2})$$

$$\not{a}\not{b} + \not{b}\not{a} = 2(a \cdot b) \quad (\text{A.3})$$

$$g^{\mu\nu} g_{\mu\nu} = d \quad (\text{A.4})$$

$$\gamma^\mu \gamma_\mu = d \quad (\text{A.5})$$

$$\gamma^\mu \gamma^\nu \gamma_\mu = (2 - d)\gamma^\nu \quad (\text{A.6})$$

$$\gamma^\mu \not{a} \gamma_\mu = (2 - d)\not{a} \quad (\text{A.7})$$

$$\gamma^\mu \gamma^\alpha \gamma^\beta \gamma_\mu = 4g^{\alpha\beta} + (d - 4)\gamma^\alpha \gamma^\beta \quad (\text{A.8})$$

$$\gamma^\mu \not{a}\not{b} \gamma_\mu = 4(a \cdot b) + (d - 4)\not{a}\not{b} \quad (\text{A.9})$$

$$\gamma^\mu \gamma^\alpha \gamma^\beta \gamma^\nu \gamma_\mu = -2\gamma^\nu \gamma^\beta \gamma^\alpha - (d - 4)\gamma^\alpha \gamma^\beta \gamma^\nu \quad (\text{A.10})$$

$$\gamma^\mu \not{a}\not{b}\not{c} \gamma_\mu = -2\not{c}\not{b}\not{a} - (d - 4)\not{a}\not{b}\not{c} \quad (\text{A.11})$$

$$\gamma^\mu \gamma^\alpha \gamma^\beta \gamma^\nu \gamma^\sigma \gamma_\mu = 2\gamma^\alpha \gamma^\sigma \gamma^\nu \gamma^\beta + 2\gamma^\beta \gamma^\nu \gamma^\sigma \gamma^\alpha + (d - 4)\gamma^\alpha \gamma^\beta \gamma^\nu \gamma^\sigma \quad (\text{A.12})$$

$$\gamma^\mu \not{a}\not{b}\not{c}\not{d} \gamma_\mu = 2\not{a}\not{d}\not{c}\not{b} + 2\not{b}\not{c}\not{d}\not{a} + (d - 4)\not{a}\not{b}\not{c}\not{d} \quad (\text{A.13})$$

$$\text{tr} [\text{Odd Number of Gamma Matrices}] = 0 \quad (\text{A.14})$$

$$\text{tr} (\gamma^\mu \gamma^\nu) = 4g^{\mu\nu} \quad (\text{A.15})$$

$$\text{tr} (\not{a}\not{b}) = 4(a \cdot b) \quad (\text{A.16})$$

$$\text{tr} (\gamma^\mu \gamma^\nu \gamma^\alpha \gamma^\beta) = 4(g^{\mu\nu} g^{\alpha\beta} - g^{\mu\alpha} g^{\nu\beta} + g^{\mu\beta} g^{\nu\alpha}) \quad (\text{A.17})$$

$$\text{tr} (\not{a}\not{b}\not{c}\not{d}) = 4[(a \cdot b)(c \cdot d) - (a \cdot c)(b \cdot d) + (a \cdot d)(b \cdot c)] \quad (\text{A.18})$$

$$\begin{aligned} \text{tr} (\gamma^\alpha \gamma^\beta \gamma^\mu \gamma^\nu \gamma^\rho \gamma^\sigma) = & 4[g^{\alpha\beta} (g^{\mu\nu} g^{\rho\sigma} - g^{\mu\rho} g^{\nu\sigma} + g^{\mu\sigma} g^{\nu\rho}) \\ & - g^{\alpha\mu} (g^{\beta\nu} g^{\rho\sigma} - g^{\beta\rho} g^{\nu\sigma} + g^{\beta\sigma} g^{\nu\rho}) \\ & + g^{\alpha\nu} (g^{\mu\beta} g^{\rho\sigma} - g^{\mu\sigma} g^{\beta\rho} + g^{\beta\sigma} g^{\mu\rho}) \\ & - g^{\alpha\rho} (g^{\beta\mu} g^{\nu\sigma} - g^{\nu\beta} g^{\mu\sigma} + g^{\beta\sigma} g^{\mu\nu}) \\ & + g^{\alpha\sigma} (g^{\mu\nu} g^{\rho\beta} - g^{\mu\rho} g^{\nu\beta} + g^{\mu\beta} g^{\nu\rho})] \end{aligned} \quad (\text{A.19})$$

Appendix B

Evaluation of quark scalar FF

In this appendix, we provide the technical details of the evaluation of the scalar FF for the one and two-loop diagrams. While we already know that the one-loop diagram can only contribute to the LP Sudakov logarithms, it is included as it provides a simple and interesting insight into these calculations.

B.1 The 1-loop diagram

For the one-loop diagram shown in fig. 3.1, we can write down the amplitude as

$$\begin{aligned}
 i\mathcal{M} &= \int \frac{d^4l}{(2\pi)^4} \bar{q}(p_2) (ig_s \gamma^\alpha T_{jk}^a) \frac{i(\not{p}_2 - \not{l} + m)}{(p_2 - l)^2 - m^2} y_q \\
 &\quad \frac{i(\not{p}_1 - \not{l} + m)}{(p_1 - l)^2 - m^2} (ig_s \gamma^\beta T_{ki}^b) \frac{(-ig_{\alpha\beta} \delta^{ab})}{l^2} q(p_1) \\
 &= -i(4\pi\alpha_s) C_F \delta_{ij} y_q \int \frac{d^4l}{(2\pi)^4} \frac{\bar{q}(p_2) N_{1L} q(p_1)}{l^2 \{(p_1 - l)^2 - m^2\} \{(p_2 - l)^2 - m^2\}}, \quad (\text{B.1})
 \end{aligned}$$

where we have used eq. (2.14) for the generator matrices, and omitted the trivial Kronecker deltas related to the quark propagators in the numerator. With the help of gamma matrix identities of appendix A, the numerator can be simplified in the following manner:

$$\begin{aligned}
 N_{1L} &= \gamma^\alpha (\not{p}_2 - \not{l} + m) (\not{p}_1 - \not{l} + m) \gamma_\alpha, \\
 N_{1L} &\approx \gamma^\alpha (\not{p}_2 + m) (\not{p}_1 + m) \gamma_\alpha, \quad (\text{B.2}) \\
 N_{1L} &= 4p_2 p_1 + (d-4)\not{p}_2 \not{p}_1 + (2-d)m(\not{p}_2 + \not{p}_1) + m^2 d, \\
 N_{1L} &= 4p_2 p_1 + m^2(d-4+2-d+2-d+d),
 \end{aligned}$$

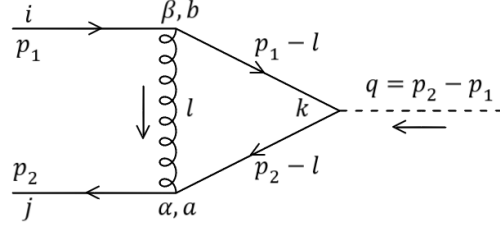


Figure B.1: The 1-loop diagram. The momentum conventions are shown in fig. 3.1. The Greek letters represent the vector indices, while color indices are denoted by the Latin letters.

$$N_{1L} = 4p_2p_1, \quad (\text{B.3})$$

where we have ignored the loop momentum as terms with higher powers of loop momentum in the numerator cannot generate double-logarithms, and utilized the equation of motion, eq. (2.12), once there are no gamma matrices in between the spinor and corresponding external momentum. It is from the Dirac algebra that the terms proportional to the quark mass vanish but one must be careful and work in d -dimensions. As previously mentioned, the remaining integral is the standard Sudakov integral of eq. (2.38) which factors out into the function Z_q^2 of eq. (3.3).

B.2 The 2-loop diagrams

All the non-trivial two-loop diagrams for the quark scattering by Higgs boson are shown in fig. 3.2. To show that fig. 3.2(a), redrawn here with the momentum configuration in fig. B.2(a), does not generate the power-suppressed double-logarithmic contribution to $\mathcal{O}(\rho)$ coefficient of the scalar FF in the high-energy asymptotic series, we focus on the Dirac chain in the numerator

$$N_{3.2a} = \gamma^\alpha (\not{l}_1 + m) \gamma^\rho (\not{l}_1 + \not{l}_2 - \not{p}_1 + m) (\not{l}_1 + \not{l}_2 - \not{p}_2 + m) \gamma_\alpha (\not{l}_2 + m) \gamma_\rho. \quad (\text{B.4})$$

In the double-logarithmic region with negligible loop momenta, this reduces to

$$N_{3.2a} \approx m^2 \gamma^\alpha \gamma^\rho (m - \not{p}_1) (m - \not{p}_2) \gamma_\alpha \gamma_\rho,$$

$$N_{3.2a} = m^2 \gamma^\alpha \gamma^\rho (m^2 - m\not{p}_1 - m\not{p}_2 + \not{p}_1\not{p}_2) \gamma_\alpha \gamma_\rho,$$

$$N_{3.2a} = m^2 \gamma^\alpha \left[(2-d)m^2 \gamma_\alpha - 4mp_{1,\alpha} - (d-4)m\not{p}_1 \gamma_\alpha - 4mp_{2,\alpha} \right. \\ \left. - (d-4)m\not{p}_2 \gamma_\alpha - 2\gamma_\alpha \not{p}_2 \not{p}_1 - (d-4)\not{p}_1 \not{p}_2 \gamma_\alpha \right],$$

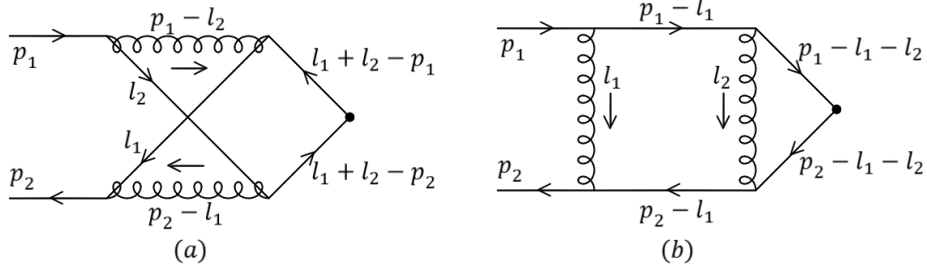


Figure B.2: The momentum configurations for fig. 3.2(a) and (c). The dark vertex represents the Higgs boson with momentum $q = p_2 - p_1$ coming into the vertex.

$$N_{3.2a} = m^2 [d(2-d)m^2 - 4m\cancel{p}_1 - (d-4)(2-d)m\cancel{p}_1 - 4m\cancel{p}_2 - (d-4)(2-d)m\cancel{p}_2 - 2d\cancel{p}_2\cancel{p}_1 - 4(d-4)p_2p_1 - (d-4)^2\cancel{p}_1\cancel{p}_2],$$

$$N_{3.2a} = m^2 [d^2(2m^2 - 2p_2p_1) + d(12p_2p_1 - 20m^2) + 24m^2 - 16p_2p_1]. \quad (\text{B.5})$$

We can now plug in $d = 4 - 2\varepsilon$ with $\varepsilon \rightarrow 0$ to get

$$N_{3.2a} = -24m^4. \quad (\text{B.6})$$

Thus, fig. 3.2(a) cannot generate contribution to $F_S^{(1)}$ in the double-logarithmic region. We leave the calculation of fig. 3.2(b) for last and tackle the remaining diagrams first, starting with fig. 3.2(c), shown with momentum configuration in fig. B.2(b). For this diagram also, it is sufficient to focus on the Dirac chain in the numerator and simplify it for the small loop momenta in the double-logarithmic region:

$$N_{3.2c} = \gamma^\alpha (\cancel{p}_2 - \cancel{l}_1 + m) \gamma^\rho (\cancel{p}_2 - \cancel{l}_1 - \cancel{l}_2 + m) (\cancel{p}_1 - \cancel{l}_1 - \cancel{l}_2 + m) \gamma_\rho (\cancel{p}_1 - \cancel{l}_1 + m) \gamma_\alpha,$$

$$N_{3.2c} = \gamma^\alpha (m + \cancel{p}_2) \gamma^\rho (m + \cancel{p}_2) (m + \cancel{p}_1) \gamma_\rho (m + \cancel{p}_1) \gamma_\alpha. \quad (\text{B.7})$$

Further evaluation is simpler if we focus on parts of the numerator rather than the entire Dirac chain. Let us look at $n_1^\rho \equiv (m + \cancel{p}_2) \gamma^\rho (m + \cancel{p}_2)$:

$$n_1^\rho = m^2 \gamma^\rho + m \gamma^\rho \cancel{p}_2 + m \cancel{p}_2 \gamma^\rho + \cancel{p}_2 \gamma^\rho \cancel{p}_2,$$

$$n_1^\rho = m^2 \gamma^\rho + m p_{2,\sigma} (\gamma^\rho \gamma^\sigma + \gamma^\sigma \gamma^\rho) + \cancel{p}_2 \gamma^\rho \gamma^\sigma p_{2,\sigma},$$

$$n_1^\rho = m^2 \gamma^\rho + m p_{2,\sigma} (2g^{\sigma\rho}) + \cancel{p}_2 (2g^{\sigma\rho} - \gamma^\sigma \gamma^\rho) p_{2,\sigma},$$

$$n_1^\rho = m^2 \gamma^\rho + 2m p_2^\rho + 2\cancel{p}_2 p_2^\rho - \cancel{p}_2 \cancel{p}_2 \gamma^\rho,$$

$$n_1^\rho = 2p_2^\rho (m + \cancel{p}_2), \quad (\text{B.8})$$

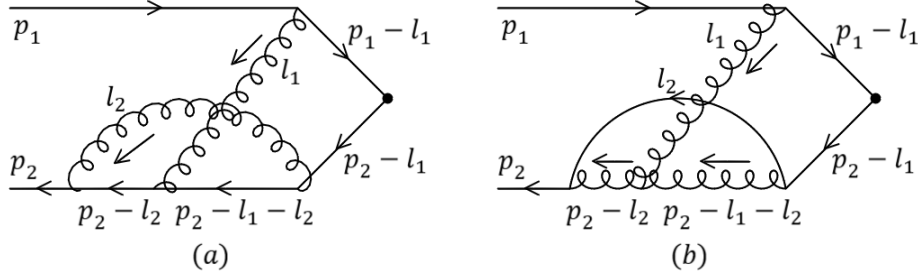


Figure B.3: The momentum configurations for fig. 3.2(d) and (e). The dark vertex represents the Higgs boson with momentum $q = p_2 - p_1$ coming into the vertex.

where we have used the on-shell condition $\not{p}_2^2 = p_2^2 = m^2$ for the external particle. Identically, $n_{2,\rho} = (m + \not{p}_1)\gamma_\rho(m + \not{p}_1)$ reduces to $2p_{1,\rho}(m + \not{p}_1)$. Plugging this and eq. (B.8) back into eq. (B.7) leads to

$$N_{3.2c} = (4p_2p_1)\gamma^\alpha(m + \not{p}_2)(m + \not{p}_1)\gamma_\alpha. \quad (\text{B.9})$$

The remaining part of the Dirac chain is identical to eq. (B.2), the one-loop Dirac chain in the double-logarithmic region, resulting in $N_{3.2c} = (4p_2p_1)^2$. As expected, this cannot generate the power-suppressed logarithms but rather contributes to the next order, $\mathcal{O}(\alpha_s^2)$, at the LP in the mass expansion i.e., to the second term in the expansion of the universal Sudakov function Z_q^2 . For fig. 3.2(d) and (e), we need to inspect the denominators of the propagators to see why double-logarithms are not generated when a soft particle is emitted and absorbed by the same external line and there is no exchange. For convenience, fig. B.3 shows these diagrams with their momentum configuration.

$$D_{3.2d} \propto \{(p_1 - l_1)^2 - m^2\}\{(p_2 - l_1)^2 - m^2\} \\ \{(p_2 - l_1 - l_2)^2 - m^2\}\{(p_2 - l_2)^2 - m^2\}l_2^2l_1^2, \quad (\text{B.10})$$

and

$$D_{3.2e} \propto \{(p_1 - l_1)^2 - m^2\}\{(p_2 - l_1)^2 - m^2\} \\ (p_2 - l_1 - l_2)^2(p_2 - l_2)^2(l_2^2 - m^2)l_1^2 \quad (\text{B.11})$$

are the denominators. The propagators l_1^2 , l_2^2 , and $l_2^2 - m^2$ are soft and go on-shell, and can be replaced by the residue at the pole. With the standard Sudakov parameterization, the remaining propagators in the eikonal approximation reduce to,

$$(p_1 - l_1)^2 - m^2 \approx -v_1(2p_2p_1), \quad (\text{B.12})$$

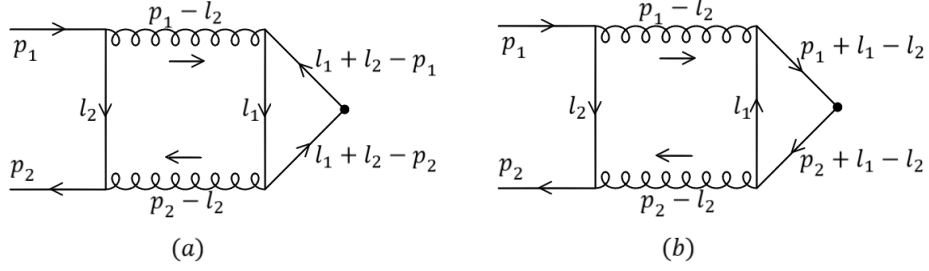


Figure B.4: The momentum configurations for fig. 3.2(b) and its symmetric counterpart. The dark vertex represents the Higgs boson with momentum $q = p_2 - p_1$ coming into the vertex.

$$(p_2 - l_1)^2 - m^2 \approx -u_1(2p_2p_1), \quad (\text{B.13})$$

$$(p_2 - l_1 - l_2)^2 - \chi m^2 \approx -(u_1 + u_2)(2p_2p_1), \quad (\text{B.14})$$

$$(p_2 - l_2)^2 - \chi m^2 \approx -u_2(2p_2p_1); \quad (\text{B.15})$$

where $\chi = 1$ and 0 for fig. B.3(a) and (b) respectively. It is clear that the Sudakov parameter v_2 does not appear in both cases, while u_2 appears twice for $l_1 < l_2$; thus the loop momentum l_2 cannot generate double-logarithm as expected. Only fig. 3.2(b) remains, fig. B.4 shows this diagram along with the diagram with opposite particle flow for the closed loop, with their momentum configuration. The color for these diagrams is

$$c_{3.2b} = T_{jk}^a T_{ki}^r \text{tr} [T^a T^r] = T_F \delta^{ar} T_{jk}^a T_{ki}^r = T_F C_F \delta_{ij}. \quad (\text{B.16})$$

The rest of the numerators are

$$N_{B.4a} = \gamma_\beta (\not{l}_2 + m) \gamma_\sigma \text{tr} [\gamma^\sigma (\not{l}_1 + \not{l}_2 - \not{p}_1 + m) (\not{l}_1 + \not{l}_2 - \not{p}_2 + m) \gamma^\beta (\not{l}_1 + m)], \quad (\text{B.17})$$

and

$$N_{B.4b} = \gamma_\beta (\not{l}_2 + m) \gamma_\sigma \text{tr} [\gamma^\sigma (\not{l}_1 + m) \gamma^\beta (\not{p}_2 + \not{l}_1 - \not{l}_2 + m) (\not{p}_1 + \not{l}_1 - \not{l}_2 + m)]. \quad (\text{B.18})$$

Since the main difference between these two diagrams is only in the particle flow inside the closed loop, we can focus on the trace over the loop. For fig. B.4(a) with the negligible loop momenta in the double-logarithmic approximation, the trace in eq. (B.17) reduces to,

$$n_{B.4a}^{\beta\sigma} = (m) \text{tr} [\gamma^\beta \gamma^\sigma (m - \not{p}_1)(m - \not{p}_2)],$$

$$n_{B.4a}^{\beta\sigma} = (4m) [m^2 g^{\beta\sigma} - 0 - 0 + g^{\beta\sigma} (p_2 p_1) - p_1^\beta p_2^\sigma + p_2^\beta p_1^\sigma]. \quad (\text{B.19})$$

Similarly, for fig. B.4(b) it is

$$n_{B.4b}^{\beta\sigma} = (m) \text{tr} [\gamma^\beta (m + \not{p}_2) (m + \not{p}_1) \gamma^\sigma],$$

$$n_{B.4b}^{\beta\sigma} = (4m) [m^2 g^{\beta\sigma} + 0 + 0 + p_2^\beta p_1^\sigma - p_1^\beta p_2^\sigma + g^{\beta\sigma} (p_2 p_1)]. \quad (\text{B.20})$$

The traces are equal in both cases as seen from eqs. (B.19) and (B.20). Thus, for the remainder, we can focus only on one of the diagrams. The full numerator can now be simplified as

$$N_{B.4a} = \gamma_\beta (\not{l}_2 + m) \gamma_\sigma n_{B.4a}^{\beta\sigma}$$

$$N_{B.4a} \approx (4m^2) [m^2 d + d(p_2 p_1) - \not{p}_1 \not{p}_2 + \not{p}_2 \not{p}_1]$$

$$N_{B.4a} = (4m^2) [m^2 d + d(p_2 p_1) - (2p_2 p_1) + \not{p}_2 \not{p}_1 + m^2]$$

$$N_{B.4a} = (4m^2) [(d+2)m^2 d + (d-2)(p_2 p_1)]$$

$$N_{B.4a} \approx (4m^2) (2p_2 p_1) \quad (\text{B.21})$$

where we have only kept the leading term in the last step after letting $\varepsilon \rightarrow 0$ for $d = 4 - 2\varepsilon$. Only the integrals over loop momenta remain. We now introduce the standard Sudakov parameterization $l_i = u_i p_1 + v_i p_2 + l_{i\perp}^2$. While not necessary, applying $l_1 \rightarrow -l_1$ variable change in fig. B.4(b) makes the denominator for both diagrams identical. In the soft loop momenta region, the denominators reduce to

$$l_i^2 - m^2 \approx [-2\pi i \delta(2u_i v_i p_2 p_1 - m^2 + l_{i\perp}^2)]^{-1}, \quad (\text{B.22})$$

$$(p_1 - l_2)^2 \approx -2p_1 l_2 \approx -q^2 v_2, \quad (\text{B.23})$$

$$(p_2 - l_2)^2 \approx -2p_2 l_2 \approx -q^2 u_2, \quad (\text{B.24})$$

$$(l_1 + l_2 - p_1)^2 - m^2 \approx -2p_1 (l_1 + l_2) \approx -q^2 (v_1 + v_2), \quad (\text{B.25})$$

$$(l_1 + l_2 - p_2)^2 - m^2 \approx -2p_2 (l_1 + l_2) \approx -q^2 (u_1 + u_2). \quad (\text{B.26})$$

This is double-logarithmic for $p_1 l_2 < p_1 l_1$ and $p_2 l_2 < p_2 l_1$, corresponding to Sudakov parameters ordering of $v_2 < v_1$ and $u_2 < u_1$; along with the additional constraint $u_i v_i > \rho$. The integral can be evaluated now:

$$I_{B.4a} = \int \frac{d^4 l_1}{(l_1^2 - m^2) \{(l_1 + l_2 - p_1)^2 - m^2\} \{(l_1 + l_2 - p_2)^2 - m^2\}} \times \frac{d^4 l_2}{(l_2^2 - m^2) (p_1 - l_2)^2 (p_2 - l_2)^2}$$

$$\begin{aligned}
I_{B.4a} &\approx -\frac{\pi^4}{q^4} \int_{\rho}^1 \frac{dv_1}{v_1 + v_2} \int_{\rho/v_1}^1 \frac{du_1}{u_1 + u_2} \int_{\rho/u_1}^{v_1} \frac{dv_2}{v_2} \int_{\rho/v_2}^{u_1} \frac{du_2}{u_2} \\
I_{B.4a} &\approx -\frac{\pi^4}{q^4} \ln^4 \rho \int_0^1 d\eta_1 \int_0^{1-\eta_1} d\xi_1 \int_{\eta_1}^{1-\xi_1} d\eta_2 \int_{\xi_1}^{1-\eta_2} d\xi_2 \\
I_{B.4a} &= -\frac{\pi^4 \ln^4 \rho}{q^4} \frac{1}{24}
\end{aligned} \tag{B.27}$$

Putting all the factors together, for amplitude we get

$$i\mathcal{M} = \frac{4\alpha_s^2}{(2\pi)^6} y_q T_F C_F N_c \bar{q}(p_2) N_{B.4a} I_{B.4a} q(p_1), \tag{B.28}$$

from which we can easily read off the FF.

$$\begin{aligned}
F_{S,B.4a} &= \frac{4\alpha_s^2}{(2\pi)^6} T_F C_F N_{B.4a} I_{B.4a}, \\
F_{S,B.4a} &= \left(\frac{\alpha_s}{4\pi}\right)^2 \frac{T_F C_F}{\pi^4} (4m^2 q^2) \left(-\frac{\pi^4 \ln^4 \rho}{q^4} \frac{1}{24}\right), \\
F_{S,B.4a} &= \left(-x^2 \frac{T_F C_F}{6}\right) \rho,
\end{aligned} \tag{B.29}$$

with $x = \frac{\alpha_s}{4\pi} \ln^2 \rho$. Multiplying eq. (B.29) by 2 for fig. B.4(b) results in the two-loop scalar FF which is equivalent to eq. (3.5) for the $n = 1$ coefficient in the series expansion of the scalar FF.

The three-loop diagrams of fig. 3.3 are obtained by an additional leading gluon exchange on fig. 3.2(b). Thus, in the double-logarithmic approximation, it can be easily shown that the numerators of the three-loop diagrams reduce to that of the two-loop substructure. Since the required factors of m^2 for $F_S^{(1)}$ come directly from the chirality flip on the soft quark lines, the additional parts of the numerator can only contribute a factor of $(p_2 p_1)$. Let us consider fig. 3.3(d) first, the numerator of this diagram in the double-logarithmic region reduces to,

$$\begin{aligned}
N_{3.3d} &= \gamma_\nu(\not{p}_2 - \not{l}_3 + m) \gamma_\beta(\not{l}_2 + m) \gamma_\sigma \text{tr} [\gamma^\sigma(\not{l}_1 + \not{l}_2 - \not{p}_1 + m) \\
&\quad \gamma^\nu(\not{l}_1 + \not{l}_2 + \not{l}_3 - \not{p}_1 + m)(\not{l}_1 + \not{l}_2 + \not{l}_3 - \not{p}_2 + m) \gamma^\beta(\not{l}_1 + m)], \\
N_{3.3d} &\approx \gamma_\nu(\not{p}_2 + m) \gamma_\beta(m) \gamma_\sigma \text{tr} [\gamma^\sigma(m - \not{p}_1) \gamma^\nu(m - \not{p}_1)(m - \not{p}_2) \gamma^\beta(m)].
\end{aligned} \tag{B.30}$$

It helps to focus on the part of the numerator around the soft gluon emission vertices. For the vertex near the external line carrying the momentum p_2 we get,

$$n_\nu = \gamma_\nu(\not{p}_2 + m) = \gamma_\nu(\gamma_\mu p_2^\mu + m),$$

$$\begin{aligned}
n_\nu &= [(2g_{\mu\nu} - \gamma_\mu\gamma_\nu)p_2^\mu + m\gamma_\nu], \\
n_\nu &= [2p_{2,\nu} - \not{p}_2\gamma_\nu + m\gamma_\nu], \\
n_\nu &= (2p_{2,\nu}),
\end{aligned} \tag{B.31}$$

where in the last line we have used eq. (2.12). The factor around soft gluon vertex along the upper eikonal line $(m - \not{p}_1)\gamma^\nu(m - \not{p}_1)$ reduces to $2p_1^\nu(m - \not{p}_1)$ similarly to eqs. (B.7) and (B.8). Plugging these back into eq. (B.30) gives

$$N_{3.3d} \approx m^2(4p_2p_1)\gamma_\beta\gamma_\sigma \text{tr} [\gamma^\sigma(m - \not{p}_1)(m - \not{p}_2)\gamma^\beta], \tag{B.32}$$

which has indeed reduced to the two-loop numerator eq. (B.17) with negligible loop momenta and a factor of $(4p_2p_1)$. Next, we consider fig. 3.3(g), the numerator for which reduces to

$$\begin{aligned}
N_{3.3g} &= \gamma^\alpha(l_2 + m)\gamma_\sigma \text{tr} [\gamma^\sigma(l_1 + l_2 - \not{p}_1 + m)(l_1 + l_2 - \not{p}_2 + m) \\
&\quad \gamma^\beta(l_1 - l_3 + m)\gamma^\mu(l_1 + m)] [g_{\alpha\beta}(l_2 - p_2 - p_2 + l_2 + l_3)_\mu + \\
&\quad g_{\beta\mu}(p_2 - l_2 - l_3 - l_3)_\alpha + g_{\mu\alpha}(l_3 - l_2 + p_2)_\beta], \\
N_{3.3g} &= \gamma^\alpha(m)\gamma_\sigma \text{tr} [\gamma^\sigma(m - \not{p}_1)(m - \not{p}_2)\gamma^\beta(l_1 + m)\gamma^\mu(l_1 + m) \\
&\quad [g_{\alpha\beta}(-2p_{2,\mu}) + g_{\beta\mu}(p_{2,\alpha}) + g_{\mu\alpha}(p_{2,\beta})]. \tag{B.33}
\end{aligned}$$

Again, focusing on the propagators near the soft gluon vertices, $(l_1 + m)\gamma^\mu(l_1 + m)$ reduces to $2l_1^\mu(l_1 + m) \approx m(2l_1^\mu)$ identically to eqs. (B.7) and (B.8) for the soft on-shell loop momentum $l_1^2 = m^2$. While near the three gluon vertex, we have three terms as seen in eq. (B.33). The $p_{2,\alpha}$ in the $g_{\beta\mu}p_{2,\alpha}$ term contracts with γ^α to give \not{p}_2 which would result in an additional factor of mass from the equation of motion, and can be ignored. Next, the $g_{\mu\alpha}p_{2,\beta}$ term contracts with $\gamma^\alpha l_1^\mu$ to give l_1 . This part of the numerator in eq. (B.33), along with the trace from eq. (B.19) gives

$$\begin{aligned}
n_3 &= (8m^2)l_1(p_{2,\beta})\gamma_\sigma [m^2g^{\beta\sigma} + p_1^\sigma p_2^\beta - p_2^\sigma p_1^\beta + g^{\sigma\beta}(p_2p_1)], \\
n_3 &= (8m^2)l_1 [m^2\not{p}_2 + \not{p}_1 p_2^2 - \not{p}_2(p_2p_1) + \not{p}_2(p_2p_1)], \\
n_3 &= (8m^2)l_1 [m^2\not{p}_2 + m^2\not{p}_1],
\end{aligned} \tag{B.34}$$

which is proportional to m^4 and cannot contribute to $n = 1$ coefficient. Only $g_{\alpha\beta}(-2p_{2,\mu})$ remains; this has the correct structure as it contracts with $\gamma^\alpha(2l_1^\mu)$ to

give $\gamma_\beta(-4p_2l_1)$. The numerator now reads

$$N_{3.3g} \approx m^2(-4p_2l_1)\gamma_\beta\gamma_\sigma \text{tr} [\gamma^\sigma(m - \not{p}_1)(m - \not{p}_2)\gamma^\beta], \quad (\text{B.35})$$

which is identical to eq. (B.17) up to the factor of (p_2l_1) which replaces the standard (p_2p_1) factor as in this case, soft gluon is emitted by the soft quark line with momentum l_1 which acts as “external” momentum instead of p_1 . We omit rest of the details for the direct evaluation of the three-loop diagrams as the remaining numerators reduce to the two-loop numerator in one of the ways shown above. The additional integral over the soft gluon momentum and corresponding Sudakov parameters can be performed straightforwardly, and do not provide any new insight. Only the diagrams in which the soft gluon is emitted by one of the soft quark lines or both emitted and absorbed by the on-shell external quark lines pose an additional challenge, similar to that of fig. 2.3(a) and (b); and can be evaluated similarly, see section 2.3.2 or [12] for reference.

Appendix C

Evaluation of Higgs production FF

Complete technical details of the calculations of the Higgs production FF from chapter 4 are provided in this appendix. Here we also go over how the symbolic diagrams are generated with the help of the algorithm QGRAF [16–19], followed by the evaluation of the trace with the help of FORM [20] for the example of the one-loop single soft quark exchange diagram fig. 4.2(a). Before we do so, let us derive the projector for this process.

A generic diagram for di-gluon to Higgs production is shown in fig. C.1; the details of the loop are not relevant at the moment. As shown in the figure, gluons have incoming momenta p_1 and p_2 , and the Higgs boson is outgoing with momentum $q = (p_1 + p_2)$. The most general form amplitude for such a process can have is

$$\mathcal{F}^{\mu\nu} \propto \Gamma^{\mu\nu} = F_{ggH}(q^2) [Ag^{\mu\nu}(p_2p_1) + Bp_1^\mu p_2^\nu + Cp_1^\nu p_2^\mu], \quad (\text{C.1})$$

where F_{ggH} denotes the FF, $\Gamma^{\mu\nu}$ is the vertex function obtained from the relevant Feynman diagram. The constants A, B and C can be obtained with help of the Ward identity, $p_{1,\mu}\Gamma^{\mu\nu} = p_{2,\nu}\Gamma^{\mu\nu} = 0$.

$$p_{1,\mu}\Gamma^{\mu\nu} = F_{ggH}(q^2) [Ap_1^\nu(p_2p_1) + 0 + Cp_1^\nu(p_2p_1)] = 0 \Rightarrow A = -C, \quad (\text{C.2})$$

where we have used on-shell condition $p_1^2 = 0$. Similarly, the second Ward identity with $p_{2,\nu}$ gives $A = -B$. We can now choose $A = 1 = -B = -C$, and write down the form projector must have

$$P_{\mu\nu} \propto [g_{\mu\nu}(p_2p_1) - p_{1,\mu}p_{2,\nu} - p_{1,\nu}p_{2,\mu}]. \quad (\text{C.3})$$

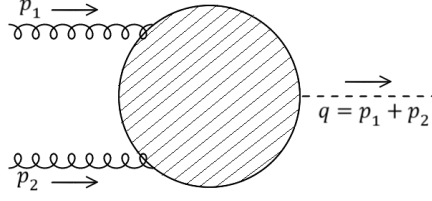


Figure C.1: Generic diagram for Higgs production via massive particle loop mediated gluon fusion. This diagram can also describe the Higgs boson to two photon decay.

Multiplying the above equation on both sides of eq. (C.1),

$$\begin{aligned}
 [g_{\mu\nu}(p_2 p_1) - p_{1,\mu} p_{2,\nu} - p_{1,\nu} p_{2,\mu}] \Gamma_{ggH}^{\mu\nu} &= \\
 F_{ggH}(q^2) [g_{\mu\nu}(p_2 p_1) - p_{1,\mu} p_{2,\nu} - p_{1,\nu} p_{2,\mu}] [g^{\mu\nu}(p_2 p_1) - p_1^\mu p_2^\nu - p_1^\nu p_2^\mu] \\
 [g_{\mu\nu}(p_2 p_1) - p_{1,\mu} p_{2,\nu} - p_{1,\nu} p_{2,\mu}] \Gamma_{ggH}^{\mu\nu} &= F_{ggH}(q^2) [(d-2)(p_2 p_1)^2] \\
 F_{ggH}(q^2) &= \frac{4}{(d-2)q^4} [g_{\mu\nu}(p_2 p_1) - p_{1,\mu} p_{2,\nu} - p_{1,\nu} p_{2,\mu}] \Gamma_{ggH}^{\mu\nu}, \quad (C.4)
 \end{aligned}$$

where we have used $q^2 = (p_1 + p_2)^2 = 2p_2 p_1$ in the final step. With that, we can now write down the final form of the projector as

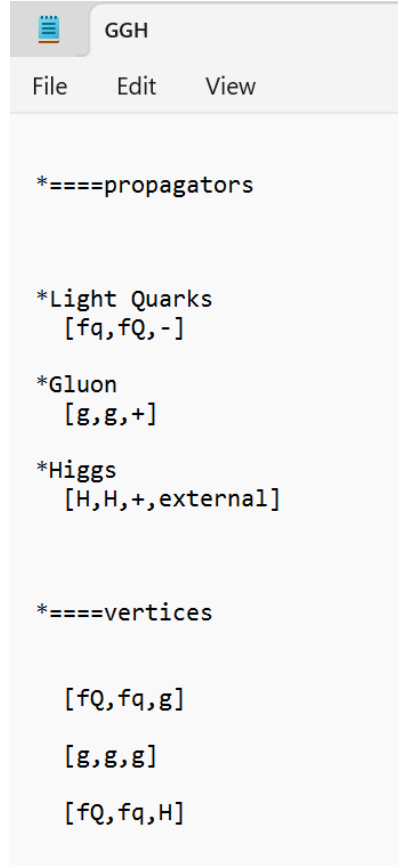
$$P_{\mu\nu} = \frac{4}{(d-2)} \frac{1}{q^4} [g_{\mu\nu}(p_2 p_1) - p_{1,\mu} p_{2,\nu} - p_{1,\nu} p_{2,\mu}]. \quad (C.5)$$

C.1 Factorizable contribution with single soft quark exchange

C.1.1 Diagram generation with QGRAF

The algorithm QGRAF is a tool that generates symbolic Feynman diagrams [17, 18]. The input that is written in the qgraf.dat file can be run on the Ubuntu terminal which has QGRAF binaries installed. For a detailed look at all the available options and ways to generate the diagrams within any field theory, please refer to the QGRAF documentation [16]. The two important aspects required in the input are the model file and the style file. The style file determines how the output is shown and the model file contains the details of the theory; i.e., the particles, and their interactions. For brevity, the style file is excluded from our discussion as it can be very easily customized to convenience, and the specific details are not relevant to our calculations and can be easily found in the documentation [16].

The model file shown in fig. C.3 is used in our calculation for the di-gluon to Higgs



```

GGH
File Edit View

*====propagators

*Light Quarks
[fq,fQ,-]

*Gluon
[g,g,+]

*Higgs
[H,H,+,external]

*====vertices

[fQ,fq,g]

[g,g,g]

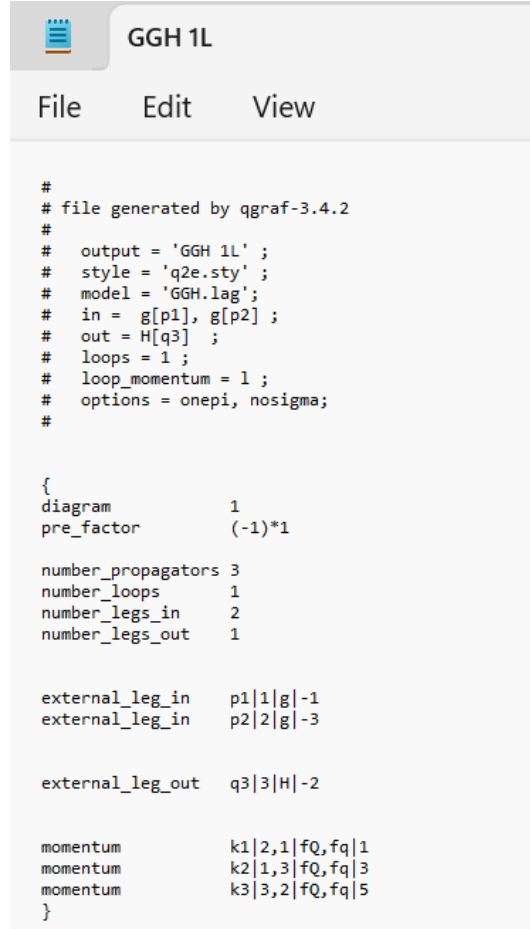
[fQ,fq,H]

```

Figure C.2: The QGRAF model file that was used to generate all the Higgs production diagrams. It defines a simplified QCD theory involving quark, antiquark, gluon, Higgs boson, and their possible interaction vertices.

production process. The lines starting with the `*` sign are comments and ignored by the compilers. The section labelled “propagators” is used to let the compiler know about all the particles in the theory. For this case, it includes a quark (`fq`) with antiquark (`fQ`) as its anti-particle; and gluon and Higgs boson, both of which are their own antiparticles. The signs declare the commutation rules followed by these particles with the negative (positive) sign for the fermions (bosons). The word “external” lets the compiler know that only the diagrams with the Higgs boson appearing as an external particle are of interest, and diagrams with internal Higgs lines are not generated. The next section labelled “vertices” is used to define all the possible or relevant vertices for the theory and the calculation. As expected for simplified QCD, there are the quark-antiquark-gluon and quark-antiquark-Higgs vertices. Other than that, there is the purely non-Abelian three gluon self-interaction vertex.

The partial output generated by QGRAF at one-loop is shown in fig. C.3. The first half of the picture with the lines starting with the `#` sign, is the input from the `qgraf.dat` file and is commented. The output is stored in a file named “GGH 1L”, which can be read via any standard text editor; with the style described in



```

GGH 1L
File Edit View

#
# file generated by qgraf-3.4.2
#
# output = 'GGH 1L' ;
# style = 'q2e.sty' ;
# model = 'GGH.lag';
# in = g[p1], g[p2] ;
# out = H[q3] ;
# loops = 1 ;
# loop_momentum = 1 ;
# options = onepi, nosigma;
#

{
  diagram          1
  pre_factor       (-1)*1

  number_propagators 3
  number_loops      1
  number_legs_in    2
  number_legs_out   1

  external_leg_in   p1|1|g|-1
  external_leg_in   p2|2|g|-3

  external_leg_out  q3|3|H|-2

  momentum          k1|2,1|fQ,fq|1
  momentum          k2|1,3|fQ,fq|3
  momentum          k3|3,2|fQ,fq|5
}

```

Figure C.3: Partial QGRAF output showing the symbolic version of fig. 4.2(a), and the initial code to generate all potential 1-loop diagrams for the theory defined by the model shown in fig. C.2.

“q2e.sty” file, and the model described in “GGH.lag” file shown in fig. C.2. The next lines define the incoming and outgoing particles, their momenta for the process of interest, and the number of loops we’re interested in with the loop momentum. The options “onepi” and “nosigma” restricts the number of diagrams generated to one particle irreducible only, and diagrams with no self-energies insertions respectively. As mentioned in section 4.1, there were a total of 2 diagrams generated at one-loop with these restrictions. The graphical representation of the symbolic diagram shown in fig. C.3 is given by fig. C.4 and is of course the same as fig. 4.2(a).

C.1.2 Trace evaluation in FORM

Now that fig. 4.2(a) has been produced by QGRAF, let us look at the FORM code used to evaluate the numerator to get this diagram’s contribution to the FF. By

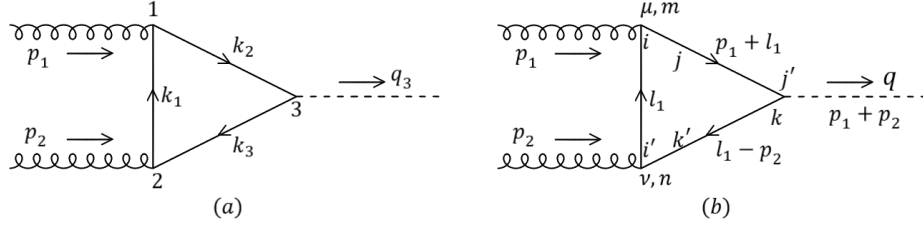


Figure C.4: Graphical representation of the symbolic Feynman diagram generated by QGRAF corresponding to fig. 4.2(a) in (a) the form of the symbolic output of fig. C.3, and (b) the momentum configuration used for the calculation. The Greek letters represent the vector indices, while color indices are denoted by the Latin letters “i”, “j” and “k”.

looking at the momentum flow shown in fig. C.4(b), we can write

$$i\mathcal{M}^{\mu\nu,mn} = - \int \frac{d^4 l_1}{(2\pi)^4} \frac{N_{C.4b}^{\mu\nu,mn}}{D_{C.4b}}, \quad (\text{C.6})$$

with

$$D_{C.4b} = (l_1^2 - m^2)\{(p_1 + l_1)^2 - m^2\}\{(l_1 - p_2)^2 - m^2\}, \quad (\text{C.7})$$

and

$$N_{C.4b}^{\mu\nu,mn} = \text{tr} \left[i(\not{p}_1 + \not{l}_1 + m)\delta_{jj'}(ig_s\gamma^\mu T_{ji}^m) \right. \\ \left. i(\not{l}_1 + m)\delta_{ii'}(ig_s\gamma^\nu T_{i'k'}^n)i(\not{l}_1 - \not{p}_2 + m)\delta_{kk'}\delta_{kj'} \right], \quad (\text{C.8})$$

where we can separate the trace over spacetime indices and generating matrices i.e., color indices. For the color we get,

$$c_{C.4b} = \text{tr} \left[\delta_{jj'}(T_{ji}^m)\delta_{ii'}(T_{i'k'}^n)\delta_{kk'}\delta_{kj'} \right], \\ c_{C.4b} = \text{tr} \left[T_{ji}^m T_{ij}^n \right], \\ c_{C.4b} = T_F \delta^{mn}. \quad (\text{C.9})$$

The Kronecker deltas for the colored propagators will be left implicit for the rest of the calculations. For the spacetime indices, the calculations can be performed manually but it can get overwhelming quickly as the number of loops increases. Alternatively, we can utilize an algorithm like FORM; fig. C.5 shows the FORM code for fig. C.4(b), which was run in the Ubuntu terminal with the FORM binaries installed. The output of FORM for the numerator before and after the projection can be seen in fig. C.6, from which we can write

$$N_{C.4b}^{\mu\nu} \propto (4m) \left[-p_1^\mu p_2^\nu + 2p_1^\mu l_1^\nu + p_1^\nu p_2^\mu - 2l_1^\mu p_2^\nu + 4l_1^\mu l_1^\nu - g^{\mu\nu}(p_2 p_1) \right] \quad (\text{C.10})$$



```

* calculating 1-loop Gluon gluon Higgs Amplitude
#-;
off statistics;
#define LOOP "1"
#define DIANUMBER "1"
S d, e;
dimension d;

* pi are incoming external, and li are loop momenta
Vector p1,p2,l1;

* non commuting fermion functions FTn inside fermion trace 'n'
F FT1, FT2;

* commuting glue prop and functions
CF Dg Den;

* Scalars, commas between the variables are optional
S ex L m ep;

* Indices
Index mu, nu, mu1, mu2;

* * * * *

local loop1 = ( FT1(L,p1+l1,L) * FT1(mu) * FT1(L,l1,L) * FT1(nu) * FT1(L,l1-p2,L) );
local pro = ( d_(mu,nu)*(p2.p1) - p1(nu) * p2(mu) - p1(mu) * p2(nu) ) * loop1 ;

***** Plugin in explicit Feynman-Rules, multiple i values for when there are multiple closed loops
#do i = 1,2
* gamma^mu in projector and/or vertices
id FT`i'(mu?)= g_(`i',mu);

* combined slash p
id FT`i'(p1?)= g_(`i',p1);

* (q1slash+m)/q1^2 propagator
id FT`i'(L,p1?,L) = (g_(`i',p1)+gi_(`i')*m)*Den(p1,m);

* g_{mu1,mu2}/q1^2 gluon prop in Feynman-gauge
id Dg(mu1?,mu2?,p1?)=d_(mu1,mu2)*Den(p1);
id FT`i'(ex)=1; * external particles
#enddo

***** Run the code up to this point *****
.sort

***** perform the trace *****

tracen 1; * replace 1 with 'i' and run a loop over 'i' for multiple traces

id p1.p1=0; * on-shell external gluon lines
id p2.p2=0;

id l1.l1 = m^2; * on-shell soft quark line

id d = 4 - 2*ep;

* If (count(l1,1) = 1 ) discard; * Ignores any terms linear in l1, Commented
If (count(ep,1) >= 1 ) discard; * Only keeps the terms proportional to ep^0

* Factors all Den functions (representing denominators of the propagators), and various powers of m
b Den m;

* Shows each term on new line in the output
print +s;

.end * End of the code

```

Figure C.5: Sample FORM code for fig. C.4(b) to reduce the numerator with the help of the projector from eq. (C.5) to get the Higgs FF.

```

Terminal - sneh9992@sneh9992-VirtualBox: /Win-home/Schools/UofA/Form/GGH
File Edit View Terminal Tabs Help
tform GGH_S.frm
TFORM 4.2 (Feb 17 2020) 64-bits 0 workers Run: Mon Mar 6 16:58:28 2023
* calculating 1-loop Gluon gluon Higgs Amplitude

#-;

loop1 =

+ Den(l1,m)*Den(p1 + l1,m)*Den( - p2 + l1,m)*m * (
- 4*p1(mu)*p2(nu)
+ 8*p1(mu)*l1(nu)
+ 4*p1(nu)*p2(mu)
- 8*p2(nu)*l1(mu)
+ 16*l1(mu)*l1(nu)
- 4*d_(mu,nu)*p1.p2
);

pro =

+ Den(l1,m)*Den(p1 + l1,m)*Den( - p2 + l1,m)*m * (
- 8*p1.p2^2
- 32*p1.l1*p2.l1
)

+ Den(l1,m)*Den(p1 + l1,m)*Den( - p2 + l1,m)*m^3 * (
+ 16*p1.p2
);

0.00 sec + 0.00 sec: 0.00 sec out of 0.00 sec
    
```

Figure C.6: Output of the sample FORM code shown in fig. C.5. The result labelled “loop1” is the trace over the closed quark loop in fig. C.4(b). The variable “pro” gives the product of the projector and the 1-loop result.

and

$$N_{C.4b}^{\mu\nu} P_{\mu\nu} \propto (8m) [2m^2(p_2 p_1) - \{(p_2 p_1)^2 + 4(p_2 l_1)(p_1 l_1)\}]. \quad (\text{C.11})$$

Before moving further, as a cross-check, we reproduce the result of eqs. (C.10) and (C.11) for the numerator starting from eq. (C.8) using the simple Dirac algebra. Since eq. (C.9) already accounts for the trace over the color indices, only the trace over the spacetime indices remains, which we now tackle.

$$N_{C.4b}^{\mu\nu} = (ig_s^2) \text{tr} [(\not{p}_1 + \not{l}_1 + m)\gamma^\mu(\not{l}_1 + m)\gamma^\nu(\not{l}_1 - \not{p}_2 + m)],$$

$$\begin{aligned}
 N_{C.4b}^{\mu\nu} = & (4i g_s^2 m) [\{p_1^\mu l_1^\nu - g^{\mu\nu}(p_1 l_1) + p_1^\nu l_1^\mu\} + \{p_1^\mu l_1^\nu + g^{\mu\nu}(p_1 l_1) - p_1^\nu l_1^\mu\} + \\
 & \{-p_1^\mu p_2^\nu - g^{\mu\nu}(p_2 p_1) + p_1^\nu p_2^\mu\} + \{l_1^\mu l_1^\nu - g^{\mu\nu} l_1^2 + l_1^\nu l_1^\mu\} + \\
 & \{l_1^\mu l_1^\nu + g^{\mu\nu} l_1^2 - l_1^\nu l_1^\mu\} + \{-l_1^\mu p_2^\nu - g^{\mu\nu}(p_2 l_1) + l_1^\nu p_2^\mu\} + \\
 & \{l_1^\mu l_1^\nu - g^{\mu\nu} l_1^2 + l_1^\nu l_1^\mu\} + \{-l_1^\mu p_2^\nu + g^{\mu\nu}(p_2 l_1) - l_1^\nu p_2^\mu\} + m^2 g^{\mu\nu}],
 \end{aligned}$$

$$N_{C.4b}^{\mu\nu} = (4i g_s^2 m) [2p_1^\mu l_1^\nu + p_1^\nu p_2^\mu - p_1^\mu p_2^\nu + 4l_1^\mu l_1^\nu - 2l_1^\mu p_2^\nu + g^{\mu\nu} \{m^2 - l_1^2 - p_2 p_1\}], \quad (\text{C.12})$$

is identical to the output of FORM eq. (C.10) up to the factor of (ig_s^2) , in the soft on-shell quark momentum limit of $l_1^2 = m^2$. Next, we multiply the projector from eq. (C.5) to further reduce the numerator for convenience.

$$N_{C.4b}^{\mu\nu} P_{\mu\nu} = eq. (\text{C.12}) \times eq. (\text{C.5}),$$

$$\begin{aligned} N_{C.4b}^{\mu\nu} P_{\mu\nu} &= \frac{16ig_s^2 m}{(d-2)q^4} [2(p_2 p_1)(p_1 l_1) + (p_2 p_1)^2 - (p_2 p_1)^2 + 4l_1^2(p_2 p_1) - 2(p_2 l_1)(p_2 p_1) \\ &\quad + d(p_2 p_1)\{m^2 - l_1^2 - p_2 p_1\} - (p_2 p_1)^2 - 4(p_1 l_1)(p_2 l_1) - (p_2 p_1)\{m^2 - l_1^2 - p_2 p_1\} \\ &\quad - 2(p_2 p_1)(p_1 l_1) + (p_2 p_1)^2 - 4(p_1 l_1)(p_2 l_1) + 2(p_2 p_1)(p_2 l_1) - (p_2 p_1)\{m^2 - l_1^2 - p_2 p_1\}], \\ N_{C.4b}^{\mu\nu} P_{\mu\nu} &= \frac{16ig_s^2 m}{(d-2)q^4} [4l_1^2(p_2 p_1) + (d-2)(p_2 p_1)\{m^2 - l_1^2 - p_2 p_1\} - 8(p_1 l_1)(p_2 l_1)], \\ N_{C.4b}^{\mu\nu} P_{\mu\nu} &= \frac{16ig_s^2 m}{q^4} [2m^2(p_2 p_1) - (p_2 p_1)^2 - 4(p_1 l_1)(p_2 l_1)], \end{aligned} \quad (\text{C.13})$$

where in the last line $l_1^2 = m^2$ and $d \rightarrow 4$ are applied; eqs. (C.11) and (C.13) are equivalent up to a factor of 2 as the projector is not properly normalized in the FORM code. Putting all these factors back together, the amplitude reduces to

$$[\mathcal{M}_{ggH}^q]_{C.4b} = - \int \frac{d^4 l_1}{(2\pi)^4} \frac{N_{C.4b}^{\mu\nu} P_{\mu\nu}}{D_{C.4b}}. \quad (\text{C.14})$$

Only the integration over the Sudakov parameter remains, to which we turn our attention.

C.1.3 Sudakov method for large double-logarithms

To perform the integral using the Sudakov's method [1, 21], we introduce the standard Sudakov parameterization for the loop momentum $l_1 = u_1 p_1 + v_1 p_2 + l_{1\perp}$. For transverse direction with $\rho_1 = -l_{1\perp}^2$, the integration measure can be decomposed as

$$d^4 l_1 = d^2 l_{1\parallel} d^2 l_{1\perp} \rightarrow \pi |p_2 p_1| du_1 dv_1 d\rho_1 \quad (\text{C.15})$$

[1, 21]. Each term in the denominator can be further simplified in accordance with the Sudakov parameters when the soft quark momentum goes on-shell. As per Cauchy's residue theorem the soft quark propagator $(l_1^2 - m^2)$ can be replaced by the Dirac

delta function [72],

$$l_1^2 - m^2 \approx [-2i\pi\delta(l_{1\perp}^2 + 2(p_2p_1)u_1v_1 - m^2)]^{-1} = [-2i\pi\delta(q^2u_1v_1 - \rho_1 - m^2)]^{-1}. \quad (\text{C.16})$$

Similarly, the eikonal approximation for remaining propagators is

$$(p_1 + l_1)^2 - m^2 \approx 2p_1l_1 = 2v_1(p_2p_1) = q^2v_1, \quad (\text{C.17})$$

$$(l_1 - p_2)^2 - m^2 \approx -2p_2l_1 = -2u_1(p_2p_1) = -q^2u_1. \quad (\text{C.18})$$

The validity of these approximations require $|u_1|, |v_1| < 1$ and $u_1v_1 > \rho$. The positive and negative Sudakov parameter contributions are symmetric, so the total integral is written in terms of the positive parameters. From eqs. (C.17) and (C.18) it is clear that the $(p_1l_1)(p_2l_1)$ term can be ignored as it cancels both the eikonal propagators and the integral will not be singular enough to generate the logarithms. Thus, the numerator further reduces to

$$N_{C.4b}^{\mu\nu}P_{\mu\nu} = \frac{64i\pi\alpha_s m}{q^4}(m^2q^2 - q^4/4),$$

$$N_{C.4b}^{\mu\nu}P_{\mu\nu} = -(16i\pi\alpha_s m)(1 - 4\rho), \quad (\text{C.19})$$

with $\rho = m^2/q^2 = m^2/(2p_2p_1)$. Only the integral

$$I_{C.4b} = \int \frac{d^4l_1}{(l_1^2 - m^2)\{(p_1 + l_1)^2 - m^2\}\{(l_1 - p_2)^2 - m^2\}} \quad (\text{C.20})$$

remains. Applying the soft and eikonal approximations, the integral reduces to

$$I_{C.4b} = \int du_1 dv_1 d\rho_1 |p_2p_1| \pi \frac{[-2i\pi\delta(q^2u_1v_1 - \rho_1 - m^2)]}{(q^2v_1)(-q^2u_1)}$$

$$I_{C.4b} = \frac{2i\pi^2|p_2p_1|}{q^4} \int_\rho^1 \frac{dv_1}{v_1} \int_{\rho/v_1}^1 \frac{du_1}{u_1}$$

$$I_{C.4b} = \frac{i\pi^2}{q^2} \ln^2 \rho \int_0^1 d\eta_1 \int_0^{1-\eta_1} d\xi_1 \quad (\text{C.21})$$

where in the last line we have introduced the normalized logarithmic variables $\eta_1 = \ln v_1 / \ln \rho$ and $\xi_1 = \ln u_1 / \ln \rho$. Plugging eq. (C.21) back into eq. (C.14) to obtain the amplitude gives

$$[\mathcal{M}_{ggH}^q]_{C.4b} \approx -\frac{-(16i\pi\alpha_s m)(1 - 4\rho)}{16\pi^4} T_{Fyq} \frac{i\pi^2}{q^2} \ln^2 \rho \int_0^1 d\eta_1 \int_0^{1-\eta_1} d\xi_1$$

$$[\mathcal{M}_{ggH}^q]_{C.4b} = -T_F \frac{\alpha_s y_q m (1-4\rho)}{\pi q^2} \ln^2 \rho \quad (\text{C.22})$$

From this, we can simply read off the Higgs production FF at one-loop for single soft quark exchange to be

$$\left[M_{ggH}^{q,1L} \right]_{1q} = (1-4\rho) \ln^2 \rho. \quad (\text{C.23})$$

The corresponding $n = 0$ and $n = 1$ coefficients are given by eqs. (4.13) and (4.14) respectively.

C.1.4 Single quark exchange effective diagram

The effective diagram with additional leading gluon exchange at two-loops is shown in fig. 4.2(b). The FF for this diagram is again dependent on the trace over the closed quark loop,

$$N_{4.2b}^{\mu\nu,mn} = \text{tr} \left[(\not{p}_1 + \not{l}_1 + \not{l}_2 + m) \gamma^\alpha T_{ij}^a (\not{p}_1 + \not{l}_1 + m) \gamma^\mu T_{jk}^m (\not{l}_1 + m) \gamma^\nu T_{kf}^n (\not{l}_1 - \not{p}_2 + m) \gamma_\alpha T_{fi}^a (\not{l}_1 + \not{l}_2 - \not{p}_2 + m) \right], \quad (\text{C.24})$$

with l_1 and l_2 as soft quark and gluon momentum respectively. We can separate the trace over the generators to get,

$$\begin{aligned} c_{4.2b} &= \text{tr} [T^a T^m T^n T^a] = \text{tr} [T^a T^a T^m T^n] \\ c_{4.2b} &= C_F \text{tr} [T^m T^n] \\ c_{4.2b} &= T_F C_F \delta^{mn}. \end{aligned} \quad (\text{C.25})$$

The factor of C_F above must be modified to $(C_F - C_A)$ due to the eikonal color charge non-conservation and the presence of the effective coupling in fig. 4.2(b). The remaining trace over the spacetime indices after being projected to the FF reduces to $\sim m(1-4\rho)$ when all the same approximations as the one-loop diagram are applied. Finally, the integration over the loop momenta is,

$$I_{4.2b} = \int \frac{d^4 l_1}{(l_1^2 - m^2) \{(p_1 + l_1)^2 - m^2\} \{(p_2 - l_1)^2 - m^2\}} \times \frac{d^4 l_2}{l_2^2 \{(p_1 + l_1 + l_2)^2 - m^2\} \{(p_2 - l_1 - l_2)^2 - m^2\}}. \quad (\text{C.26})$$

The soft and eikonal approximations involving just the momentum l_1 are identical to eqs. (C.16) to (C.18). For the soft gluon momentum l_2 ,

$$l_2^2 = \left[-2i\pi\delta(u_2 v_2 (2p_2 p_1) + l_{2\perp}^2) \right]^{-1}, \quad (\text{C.27})$$

$$(p_1 + l_1 + l_2)^2 - m^2 \approx 2p_2p_1(v_1 + v_2), \quad (\text{C.28})$$

$$(p_2 - l_1 - l_2)^2 - m^2 \approx -2p_2p_1(u_1 + u_2). \quad (\text{C.29})$$

The integral over l_2 is double-logarithmic when $u_1 < u_2$, and $v_1 < v_2$. Then eq. (C.26) reduces to,

$$\begin{aligned} I_{4.2b} &= -\frac{\pi^4}{(2p_2p_1)^2} \int_\rho^1 \frac{dv_1}{v_1} \int_{\rho/v_1}^1 \frac{du_1}{u_1} \int_{v_1}^1 \frac{dv_2}{v_2} \int_{u_1}^1 \frac{du_2}{u_2}, \\ I_{4.2b} &= -\frac{\pi^4}{(2p_2p_1)^2} \ln^4 \rho \int_0^1 d\eta_1 \int_0^{1-\eta_1} d\xi_1 \int_0^{\eta_1} d\eta_2 \int_0^{\xi_1} d\xi_2, \\ I_{4.2b} &= -\frac{\pi^4}{(2p_2p_1)^2} \ln^4 \rho \int_0^1 d\eta_1 \int_0^{1-\eta_1} d\xi_1 (\xi_1 \eta_1). \end{aligned} \quad (\text{C.30})$$

Putting all these factors together for the Higgs production FF of the effective diagram,

$$\begin{aligned} [M_{ggH}^q]_{4.2b} &= -\frac{\alpha_s}{\pi} (1 - 4\rho) (C_F - C_A) \ln^4 \rho \int_0^1 d\eta_1 \int_0^{1-\eta_1} d\xi_1 (\xi_1 \eta_1), \\ [M_{ggH}^q]_{4.2b} &= (1 - 4\rho) \ln^2 \rho \left[2 \int_0^1 d\eta_1 \int_0^{1-\eta_1} d\xi_1 (2z\xi_1\eta_1) \right]. \end{aligned} \quad (\text{C.31})$$

After exponentiating the integrand of eq. (C.31), we get the all-order result,

$$M_{ggH}^{(0)} = \ln^2 \rho g(z), \quad (\text{C.32})$$

and

$$\left[M_{ggH}^{(1)} \right]_{1q} = -4 \ln^2 \rho g(z), \quad (\text{C.33})$$

with $g(z)$ defined in eqs. (2.75) and (2.76). The asymptotic form of $g(z)$ is given by eqs. (2.81) and (2.83) for large values of z .

C.2 Contribution from triple soft quark exchange

C.2.1 The 3-loop diagrams

Recall from section 4.2 that of the four diagrams in consideration, only fig. 4.3(a) has contribution to $\mathcal{O}(m^3)$ coefficient $M_{ggH}^{(1)}$ of the FF. The numerator for this diagram is proportional to two traces,

$$\begin{aligned} N_{4.3a}^{\mu\nu, mn} &= \text{tr} \left[(\not{p}_2 + \not{l}_1 + \not{l}_2 + \not{l}_3 + m) \gamma_\rho T_{ji}^r (\not{l}_3 + m) \gamma_\alpha T_{ij}^a (\not{l}_1 + \not{l}_2 + \not{l}_3 - \not{p}_1 + m) \right] \\ &\quad \text{tr} \left[\gamma^\rho T_{kf}^r (\not{p}_2 + \not{l}_1 + m) \gamma^\nu T_{fd}^n (\not{l}_1 + m) \gamma^\mu T_{dh}^m (\not{l}_1 - \not{p}_1 + m) \gamma^\alpha T_{hk}^a (-\not{l}_2 + m) \right]. \end{aligned} \quad (\text{C.34})$$

Let us first separate the color factor,

$$\begin{aligned}
c_{4.3a} &= \text{tr} [T_{ji}^r T_{ij}^a] \text{tr} [T_{kf}^r T_{fd}^n T_{dh}^m T_{hk}^a], \\
c_{4.3a} &= T_F \delta^{ra} \text{tr} [T_{kf}^r T_{fd}^n T_{dh}^m T_{hk}^a], \\
c_{4.3a} &= T_F \text{tr} [T_{hk}^a T_{kf}^a T_{fd}^n T_{dh}^m], \\
c_{4.3a} &= T_F \text{tr} [C_F T_{hd}^n T_{dh}^m], \\
c_{4.3a} &= T_F^2 C_F \delta^{mn}, \tag{C.35}
\end{aligned}$$

where we have used the cyclic property of the traces in the second line. Letting the soft quark momenta go on-shell $l_i^2 = m^2$, and only keeping the terms that are either independent or quadratic in the loop momenta, the spacetime part of the eq. (C.34) reduces to

$$\begin{aligned}
N_{4.3a}^{\mu\nu} &\approx 8m^3 [(q^2 - 12m^2) (2p_1^\mu p_2^\nu - 2p_1^\nu p_2^\mu + g^{\mu\nu} q^2)] \\
&\quad + 64m^3 [q^2 (l_1^\mu l_2^\nu + l_1^\nu l_2^\mu - l_1^\mu l_1^\nu) + 12l_1^\mu l_1^\nu]. \tag{C.36}
\end{aligned}$$

Since we are only interested in $\mathcal{O}(m^3)$, most of the terms above can be ignored as they are either higher order or would cancel the eikonal factors in the denominator. Applying the projector to eq. (C.36) gives

$$N_{4.3a}^{\mu\nu} P_{\mu\nu} \approx 16q^2 m^3. \tag{C.37}$$

Again we only have the integral over the loop momenta left,

$$\begin{aligned}
I_{4.3a} &= \int \frac{d^4 l_1}{(l_1^2 - m^2) \{(l_1 - p_1)^2 - m^2\} \{(p_2 + l_1)^2 - m^2\}} \frac{d^4 l_2}{(l_2^2 - m^2) (l_1 + l_2 - p_1)^2} \times \\
&\quad \frac{1}{(p_2 + l_1 + l_2)^2} \frac{d^4 l_3}{(l_3^2 - m^2) \{(l_1 + l_2 + l_3 - p_1)^2 - m^2\} \{(p_2 + l_1 + l_2 + l_3)^2 - m^2\}}. \tag{C.38}
\end{aligned}$$

The soft and eikonal approximations not involving the momentum l_3 are identical to the one and two-loop cases of eqs. (C.16) to (C.18), (C.28) and (C.29); similarly the remaining approximations involving l_3 are,

$$l_i^2 - m^2 = [2\pi i \delta(2u_i v_i p_2 p_1 - m^2 - \rho_i)]^{-1} \tag{C.39}$$

$$(l_1 + l_1 + l_3 - p_1)^2 - m^2 \approx -2p_2 p_1 (v_1 + v_2 + v_3), \tag{C.40}$$

$$(p_2 + l_1 + l_2 + l_3)^2 - m^2 \approx 2p_2 p_1 (u_1 + u_2 + u_3). \tag{C.41}$$

The integrals produce the double-logarithms when $u_1 < u_2 < u_3$, and $v_1 < v_2 < v_3$ with the additional constraint $u_1 v_1 > \rho$. Triple integral of eq. (C.38) then reduces to,

$$I_{4.3a} \approx -\frac{i\pi^6}{(2p_2 p_1)^3} \int_{\rho}^1 \frac{dv_1}{v_1} \int_{\rho/v_1}^1 \frac{du_1}{u_1} \int_{v_1}^1 \frac{dv_2}{v_2} \int_{u_1}^1 \frac{du_2}{u_2} \int_{v_2}^1 \frac{dv_3}{v_3} \int_{u_2}^1 \frac{du_3}{u_3},$$

$$I_{4.3a} = -\frac{i\pi^6}{(2p_2 p_1)^3} \ln^6 \rho \int_0^1 d\eta_1 \int_0^{1-\eta_1} d\xi_1 \int_0^{\eta_1} d\eta_2 \int_0^{\xi_1} d\xi_2 \int_0^{\eta_2} d\eta_3 \int_0^{\xi_2} d\xi_3, \quad (\text{C.42})$$

$$I_{4.3a} = -\frac{i\pi^6}{720 q^6} \ln^6 \rho. \quad (\text{C.43})$$

Putting the factors from eqs. (C.35), (C.37) and (C.43) together, along with a factor of 4 for symmetric diagrams, to obtain the contribution to $M_{ggH}^{(1)}$ coefficient of the asymptotic expansion of the Higgs production FF gives,

$$\left[M_{ggH}^{(1)} \right]_{4.3a} = \frac{x^2 T_F C_F}{45} \ln^2 \rho. \quad (\text{C.44})$$

We shift our attention to the remaining diagrams of fig. 4.3. The numerators of these diagrams are:

$$N_{4.3b}^{\mu\nu} = \text{tr} \left[(\not{p}_2 + \not{l}_1 + \not{l}_2 + \not{l}_3 + m) \gamma_{\rho} (\not{l}_3 + m) \gamma_{\alpha} (\not{l}_1 + \not{l}_2 + \not{l}_3 - \not{p}_1 + m) \right] \\ \text{tr} \left[\gamma^{\rho} (\not{l}_1 + m) \gamma^{\mu} (\not{l}_1 - \not{p}_1 + m) \gamma^{\alpha} (-\not{l}_2 + m) \gamma^{\nu} (-\not{p}_2 - \not{l}_2 + m) \right],$$

$$N_{4.3b}^{\mu\nu} \approx 32m^5 (6p_1^{\mu} p_2^{\nu} + 2p_1^{\nu} p_2^{\mu} - g^{\mu\nu} q^2) \\ + 8m [q^4 (l_1^{\nu} l_2^{\mu} - l_1^{\mu} l_2^{\nu}) + 8m^2 q^2 (2l_1^{\mu} l_2^{\nu} + l_3^{\mu} l_3^{\nu}) - 96m^4 l_1^{\mu} l_2^{\nu}]; \quad (\text{C.45})$$

$$N_{4.3c}^{\mu\nu} = \text{tr} \left[(\not{p}_2 + \not{l}_1 + \not{l}_2 + \not{l}_3 + m) \gamma_{\rho} (\not{l}_2 + m) \gamma^{\alpha} (\not{p}_1 - \not{l}_1 + m) \right] \\ \gamma^{\mu} (-\not{l}_1 + m) \gamma^{\nu} (-\not{l}_1 - \not{p}_2 + m) \gamma^{\rho} (\not{l}_3 + m) \gamma_{\alpha} (\not{l}_1 + \not{l}_2 + \not{l}_3 - \not{p}_1 + m),$$

$$N_{4.3c}^{\mu\nu} \approx 48m^5 (2p_1^{\mu} p_2^{\nu} - 2p_1^{\nu} p_2^{\mu} + g^{\mu\nu} q^2) - 8m (48m^4 l_1^{\mu} l_1^{\nu}) + \\ 8m [q^4 (l_2^{\nu} l_3^{\mu} - l_2^{\mu} l_3^{\nu}) - 2m^2 q^2 (3l_1^{\mu} l_2^{\nu} + 3l_1^{\nu} l_3^{\mu} + 3l_1^{\nu} l_2^{\mu} + 3l_1^{\mu} l_3^{\nu} - 4l_2^{\mu} l_3^{\nu} + 4l_2^{\nu} l_3^{\mu})]; \quad (\text{C.46})$$

and

$$N_{4.3d}^{\mu\nu} = \text{tr} \left[(\not{p}_2 + \not{l}_1 + \not{l}_2 + \not{l}_3 + m) \gamma_{\rho} (\not{l}_1 + m) \gamma^{\mu} (\not{l}_1 - \not{p}_1 + m) \right] \\ \gamma^{\alpha} (-\not{p}_1 + m) \gamma^{\nu} (-\not{l}_2 - \not{p}_2 + m) \gamma^{\rho} (\not{l}_3 + m) \gamma_{\alpha} (\not{l}_1 + \not{l}_2 + \not{l}_3 - \not{p}_1 + m),$$

$$N_{4.3d}^{\mu\nu} \approx 16m^5 (g^{\mu\nu}q^2 - 2p_1^\nu p_1^\mu - 6p_1^\mu p_2^\nu) + 8m (48m^4 l_1^\mu l_1^\nu) + 8m [q^4 (l_2^\mu l_3^\nu - l_2^\nu l_3^\mu) + 2m^2 q^2 (l_1^\mu l_1^\nu - 2l_1^\mu l_2^\nu + 3l_1^\mu l_3^\nu + 2l_1^\nu l_3^\mu - l_2^\mu l_2^\nu - 2l_2^\mu l_3^\nu + 5l_2^\nu l_3^\mu - 2l_3^\mu l_3^\nu)]. \quad (\text{C.47})$$

All the terms are already at the order of m^5 . Applying the projector verifies that $P_{\mu\nu}N_{4.3b}^{\mu\nu} = P_{\mu\nu}N_{4.3c}^{\mu\nu} = P_{\mu\nu}N_{4.3d}^{\mu\nu} = 0$ at $\mathcal{O}(m^3)$; and these diagrams start contributing at N3LP. Thus, eq. (C.44) gives the full contribution to $M_{ggH}^{(1)}$ from triple soft quark exchange diagrams at three-loops, as shown in eq. (4.17).

C.2.2 Effective diagrams

From the effective diagrams of the scalar FF and the single quark exchange Higgs production; it is straightforward to see that fig. 4.4 are the effective diagrams for triple soft quark exchange. We can simply focus on the integral over the soft gluon momentum l_4 as the integrals over the soft quark momenta are not affected and are still given by eqs. (C.16) to (C.18), (C.28), (C.29) and (C.39) to (C.42). For fig. 4.4, the contribution of the spacetime part of the numerator to the FF in the double-logarithmic region at $\mathcal{O}(m^3)$ reduces to

$$N_{4.3}^{\mu\nu}P_{\mu\nu} \approx \pm 32m^3 q^4; \quad (\text{C.48})$$

with positive answer for fig. 4.4(b), and negative for (a) and (c). Focusing on fig. 4.4(a), the color factor for which is given by

$$\begin{aligned} c_{4.4a} &= \text{tr} [T^r T^a] \text{tr} [T^r T^d T^n T^m T^d T^a] \\ c_{4.4a} &= T_F C_F \text{tr} [T^a T^n T^m T^a] \\ c_{4.4a} &= T_F C_F^2 \text{tr} [T^n T^m] \\ c_{4.4a} &= T_F^2 C_F^2, \end{aligned} \quad (\text{C.49})$$

with reduced color factor of C_F , which must be modified to $(C_F - C_A)$. Integral over l_4 is

$$\int \frac{d^4 l_4}{l_4^2 \{(l_1 + l_4 + p_2)^2 - m^2\} \{(l_1 + l_4 - p_1)^2 - m^2\}}. \quad (\text{C.50})$$

The residue of soft gluon propagator can be taken identically to eq. (C.27), for all three effective diagrams. Relevant eikonal approximations for fig. 4.4(a) with standard Sukadov parameterization for l_4 are

$$(l_1 + l_4 + p_2)^2 - m^2 \approx 2p_2 p_1 (u_1 + u_4), \quad (\text{C.51})$$

$$(l_1 + l_4 - p_1)^2 - m^2 \approx 2p_2 p_1 (v_1 + v_4); \quad (\text{C.52})$$

which are double-logarithmic when $v_1 < v_4 < 1$, and $u_1 < u_4 < 1$. Integral in eq. (C.50) then reduces to,

$$2 \int_{v_1}^1 \frac{dv_4}{v_4} \int_{u_1}^1 \frac{du_4}{u_4} = 2 \ln^2 \rho \int_0^{\eta_1} d\eta_4 \int_0^{\xi_1} d\xi_4 = (2\eta_1 \xi_1) \ln^2 \rho. \quad (\text{C.53})$$

Combining these factors with the modified color gives

$$\begin{aligned} \left[M_{ggH}^{(1)} \right]_{4.4a} &= 16x^2 T_F C_F \ln^2 \rho \int_0^1 d\eta_1 \int_0^{1-\eta_1} d\xi_1 \int_0^{\eta_1} d\eta_2 \int_0^{\xi_1} d\xi_2 \\ &\quad \int_0^{\eta_2} d\eta_3 \int_0^{\xi_2} d\xi_3 (2z\eta_1 \xi_1). \end{aligned} \quad (\text{C.54})$$

Next, for fig. 4.4(b) the color factor is,

$$\begin{aligned} c_{4.4b} &= \text{tr} [T^d T^g] \text{tr} [T^b T^n T^m T^a] f^{arg} f^{brd} \\ c_{4.4b} &= T_F \text{tr} [T^b T^n T^m T^a] f^{arg} f^{brg} \\ c_{4.4b} &= T_F C_A \text{tr} [T^a T^n T^m T^a] \\ c_{4.4b} &= T_F^2 C_F C_A. \end{aligned} \quad (\text{C.55})$$

Eikonal color charge non-conservation implies that the reduced color factor C_A must be modified to $(C_A - C_F)$. Soft gluon momentum integral is

$$\int \frac{d^4 l_4}{l_4^2 (l_1 + l_2 + l_4 + p_2)^2 (l_1 + l_2 + l_4 - p_1)^2}. \quad (\text{C.56})$$

Eikonal approximations for gluon propagators on the edges are

$$(l_1 + l_2 + l_4 + p_2)^2 \approx 2p_2 p_1 (u_1 + u_2 + u_4), \quad (\text{C.57})$$

$$(l_1 + l_2 + l_4 - p_1)^2 \approx 2p_2 p_1 (v_1 + v_2 + v_4); \quad (\text{C.58})$$

which are double-logarithmic when $v_1 < v_2 < v_4 < 1$, and $u_1 < u_2 < u_4 < 1$. Integral in eq. (C.56) then reduces to,

$$2 \int_{v_2}^1 \frac{dv_4}{v_4} \int_{u_2}^1 \frac{du_4}{u_4} = 2 \ln^2 \rho \int_0^{\eta_2} d\eta_4 \int_0^{\xi_2} d\xi_4 = (2\eta_2 \xi_2) \ln^2 \rho. \quad (\text{C.59})$$

Combining these factors with the modified color gives

$$\left[M_{ggH}^{(1)} \right]_{4.4a} = 16x^2 T_F C_F \ln^2 \rho \int_0^1 d\eta_1 \int_0^{1-\eta_1} d\xi_1 \int_0^{\eta_1} d\eta_2 \int_0^{\xi_1} d\xi_2 \int_0^{\eta_2} d\eta_3 \int_0^{\xi_2} d\xi_3 (-2z\eta_2\xi_2). \quad (\text{C.60})$$

Lastly for fig. 4.3(c),

$$\begin{aligned} c_{4.4c} &= \text{tr} [T^d T^a T^r T^d] \text{tr} [T^r T^n T^m T^a] \\ c_{4.4c} &= C_F \text{tr} [T^a T^r] \text{tr} [T^r T^n T^m T^a] \\ c_{4.4c} &= T_F C_F \text{tr} [T^a T^n T^m T^a] \\ c_{4.4c} &= T_F^2 C_F^2, \end{aligned} \quad (\text{C.61})$$

which has reduced color factor C_F changed to $(C_F - C_A)$. Integral over l_4

$$\int \frac{d^4 l_4}{l_4^2 \{(l_1 + l_2 + l_3 + l_4 + p_2)^2 - m^2\} \{(l_1 + l_2 + l_3 + l_4 - p_1)^2 - m^2\}}, \quad (\text{C.62})$$

with eikonal approximations given by

$$(l_1 + l_2 + l_3 + l_4 + p_2)^2 - m^2 \approx 2p_2 p_1 (u_1 + u_2 + u_3 + u_4), \quad (\text{C.63})$$

$$(l_1 + l_2 + l_3 + l_4 - p_1)^2 - m^2 \approx 2p_2 p_1 (v_1 + v_2 + v_3 + v_4), \quad (\text{C.64})$$

is double-logarithmic when $v_1 < v_2 < v_3 < v_4 < 1$ and $u_1 < u_2 < u_3 < u_4 < 1$. Integral in eq. (C.62) then reduces to,

$$2 \int_{v_3}^1 \frac{dv_4}{v_4} \int_{u_3}^1 \frac{du_4}{u_4} = 2 \ln^2 \rho \int_0^{\eta_3} d\eta_4 \int_0^{\xi_3} d\xi_4 = (2\eta_3 \xi_3) \ln^2 \rho. \quad (\text{C.65})$$

The contribution of this last diagram is

$$\left[M_{ggH}^{(1)} \right]_{4.4c} = 16x^2 T_F C_F \ln^2 \rho \int_0^1 d\eta_1 \int_0^{1-\eta_1} d\xi_1 \int_0^{\eta_1} d\eta_2 \int_0^{\xi_1} d\xi_2 \int_0^{\eta_2} d\eta_3 \int_0^{\xi_2} d\xi_3 (2z\eta_3\xi_3). \quad (\text{C.66})$$

Exponentiating the answers of eqs. (C.54), (C.60) and (C.66) after summing them, gives the all-order result for triple soft quark exchange diagrams

$$\left[M_{ggH}^{(1)} \right]_{3q} = 16x^2 T_F C_F \ln^2 \rho \int_0^1 d\eta_1 \int_0^{1-\eta_1} d\xi_1 \int_0^{\eta_1} d\eta_2 \int_0^{\xi_1} d\xi_2 \int_0^{\eta_2} d\eta_3 \int_0^{\xi_2} d\xi_3 \left(e^{2z\eta_3\xi_3} e^{-2z\eta_2\xi_2} e^{2z\eta_1\xi_1} \right), \quad (\text{C.67})$$

which when normalized to the three-loop result of eq. (4.17) reduces to the final form of eqs. (4.19) and (4.20). While we have not analytically computed the large- z asymptotic for the function $h(z)$, coefficients of Taylor expansion, $h(z) = 1 + \sum_{n=1}^{\infty} h_n z^n$, are given in table 4.1. From the asymptotic form of the functions $g(z)$ and $f(z)$ given in eqs. (2.81), (2.83), (3.20) and (3.29), we can say that

$$h(z \rightarrow \infty) \propto \mathcal{O}(1/z^7), \quad (\text{C.68})$$

and

$$h(-z \rightarrow \infty) \propto \mathcal{O}(1/z^3). \quad (\text{C.69})$$

C.3 Non-factorizable contribution with single soft quark exchange

Diagrams in consideration in this section at two and three-loops are given in figs. 4.5 and 4.6. Starting with fig. 4.5(a), the two-loop diagram, the numerator is

$$N_{4.5a}^{\mu\nu} = \text{tr} \left[(l_1 + \not{p}_1 + m) \gamma^\mu (l_1 + m) \gamma^\alpha (l_2 + m) \gamma^\nu (l_2 - \not{p}_2 + m) \gamma_\alpha (l_1 - \not{p}_2 + m) \right]. \quad (\text{C.70})$$

Standard and modified Sudakov parameterization for l_1 and l_2 are $l_1 = u_1 p_1 + v_1 p_2 + l_{1\perp}$ and $l_2 = u_2 l_1 + v_2 p_2 + l_{2\perp}$. The denominator for this diagram is

$$D_{4.5a} = \{(p_1 + l_1)^2 - m^2\} (l_1^2 - m^2) (l_2^2 - m^2) \{(l_2 - p_2)^2 - m^2\} \{(l_1 - p_2)^2 - m^2\} (l_1 - l_2)^2. \quad (\text{C.71})$$

Propagators can be approximated as

$$l_1^2 - m^2 = \left[-2i\pi\delta(2u_1 v_1 p_2 p_1 + l_{1\perp}^2 - m^2) \right]^{-1}, \quad (\text{C.72})$$

$$l_2^2 - m^2 = \left[-2i\pi\delta(2u_2 v_2 p_2 l_1 + l_{2\perp}^2 - m^2) \right]^{-1} = \left[-2i\pi\delta(2u_2 v_2 u_1 p_2 p_1 + l_{2\perp}^2 - m^2) \right]^{-1}, \quad (\text{C.73})$$

$$(l_1 - l_2)^2 \approx -2l_1 l_2 \approx -v_2 (2p_2 l_1), \quad (\text{C.74})$$

$$(p_1 + l_1)^2 - m^2 \approx 2p_1 l_1 \approx v_1 (2p_2 p_1), \quad (\text{C.75})$$

$$(l_2 - p_2)^2 - m^2 \approx -2p_2l_2 \approx -u_2(2p_2l_1) \approx -u_2u_1(2p_2p_1), \quad (\text{C.76})$$

$$(l_1 - p_2)^2 - m^2 \approx -2p_2l_1 \approx -u_1(2p_2p_1). \quad (\text{C.77})$$

As mentioned in section 4.3, the numerator must be proportional to p_2l_1 to cancel one of the eikonal factors coming from eqs. (C.74) and (C.76). After projecting the numerator to the FF, eq. (C.70) reduces to

$$N_{4.5a}^{\mu\nu} P_{\mu\nu} \approx 16p_2l_2 + 16\rho(p_2p_1 - 2p_2l_2). \quad (\text{C.78})$$

Since the Dirac chain of the numerator clearly cannot provide the required factor, the contribution of this diagram in the large double-logarithmic region of the high-energy approximation vanishes. Let us quickly evaluate the color factor as well:

$$\begin{aligned} c_{4.5a} &= \text{tr} [T^m T^a T^n T^a] = T_{ji}^m T_{hk}^n T_{ih}^a T_{kj}^a \\ c_{4.5a} &= \frac{T_{ji}^m T_{hk}^n}{2} \left(\delta_{ij} \delta_{hk} - \frac{1}{N_c} \delta_{ih} \delta_{kj} \right) \\ c_{4.5a} &= \frac{1}{2} \left(T_{jj}^m T_{kk}^n - \frac{1}{N_c} T_{jh}^m T_{hj}^n \right) \\ c_{4.5a} &= -\frac{1}{2N_c} \text{tr} [T^m T^n] \\ c_{4.5a} &= T_F (C_F - C_A/2) \delta^{mn}; \end{aligned} \quad (\text{C.79})$$

where we have used the tracelessness of the generators.

Let us inspect the three-loop diagrams of fig. 4.6 in which there is an additional soft gluon exchange on the two-loop topology of fig. 4.5(a). For fig. 4.6(a), we denote the additional soft gluon momentum by k'_1 with Sudakov parameterization $k'_1 = r'_1 p_1 + w'_1 p_2 + k'_{1\perp}$. The numerator for this diagram

$$\begin{aligned} N_{4.6a}^{\mu\nu} &= \text{tr} [(\not{p}_1 + \not{l}_1 - \not{k}'_1 + m) \gamma^\rho (\not{p}_1 + \not{l}_1 + m) \gamma^\mu (\not{l}_1 + m) \gamma^\alpha (\not{l}_2 + m) \gamma^\nu \\ &\quad (\not{l}_2 - \not{p}_2 + m) \gamma_\rho (\not{l}_2 - \not{k}'_1 - \not{p}_2 + m) \gamma_\alpha (\not{l}_1 - \not{k}'_1 - \not{p}_2 + m)], \end{aligned} \quad (\text{C.80})$$

reduces to

$$N_{4.6a}^{\mu\nu} P_{\mu\nu} \approx -32m^3(p_2l_1 + p_2p_1), \quad (\text{C.81})$$

upon projection in the double-logarithmic approximation. The color factor for this diagram is

$$\begin{aligned} c_{4.6a} &= \text{tr} [T^r T^m T^a T^n T^r T^a] = T_{ji}^m T_{fe}^n T_{cj}^r T_{ed}^r T_{dc}^a T_{if}^a \\ c_{4.6a} &= \frac{T_{ji}^m T_{fe}^n}{4} \left(\delta_{cd} \delta_{je} - \frac{1}{N_c} \delta_{cj} \delta_{ed} \right) \left(\delta_{ci} \delta_{fd} - \frac{1}{N_c} \delta_{if} \delta_{cd} \right) \end{aligned}$$

$$c_{4.6a} = \frac{T_{ji}^m T_{fe}^n}{4N_c^2} (\delta_{je} \delta_{if} - N_c \delta_{ij} \delta_{ef})$$

$$c_{4.6a} = T_F (C_F - C_A/2)^2 \delta^{mn}; \quad (\text{C.82})$$

corresponding to the reduced factor $c_{4.6a} = (C_F - C_A/2)$. For the denominator

$$D_{4.6a} = \{(p_1 + l_1 - k'_1)^2 - m^2\} \{(p_1 + l_1)^2 - m^2\} (l_1^2 - m^2) (l_2^2 - m^2) (l_1 - l_2)^2$$

$$\{(l_2 - p_2)^2 - m^2\} \{(l_2 - k'_1 - p_2)^2 - m^2\} \{(l_1 - k'_1 - p_2)^2 - m^2\} k_1'^2, \quad (\text{C.83})$$

eikonal approximations of eqs. (C.72) to (C.76) still apply; for the remainder we have

$$(l_1 - k'_1 - p_2)^2 - m^2 \approx -2p_2(l_1 - k'_1) \approx (r'_1 - u_1)(2p_2 p_1) \approx -u_1(2p_2 p_1), \quad (\text{C.84})$$

$$(p_1 + l_1 - k'_1)^2 - m^2 \approx 2p_1(l_1 - k'_1) \approx (2p_1 p_2)(v_1 - w'_1) \approx -w'_1(2p_2 p_1), \quad (\text{C.85})$$

$$(l_2 - k'_1 - p_2)^2 - m^2 \approx 2p_2(k'_1 - l_2) \approx (2p_1 p_2)(r'_1 - u_1 u_2) \approx r'_1(2p_2 p_1). \quad (\text{C.86})$$

The integral over l_1 is double-logarithmic when $|u_1|, |v_1| < 1$ with additional constraint $u_1 v_1 > \rho$. Similarly, integral over l_2 is double-logarithmic when $|u_2|, |v_2| < 1$ with the constraint $u_2 v_2 u_1 > \rho$. Lastly, k'_1 integral requires $u_1 > r'_1 > u_1 u_2$, and $1 > w'_1 > v_1$. The integral can be reduced as

$$I_{4.6a} = \int d^4 l_1 d^4 l_2 d^4 k'_1 \frac{N_{4.6a}^{\mu\nu} P_{\mu\nu}}{D_{4.6a}}$$

$$I_{4.6a} \approx \frac{-16im^3 \pi^6}{q^4} \int_\rho^1 \frac{dv_1}{v_1} \int_{\rho/v_1}^1 \frac{du_1}{u_1} \int_{\rho/u_1}^1 \frac{dv_2}{v_2} \int_{\rho/(u_1 v_2)}^1 \frac{du_2}{u_2} \int_{v_1}^1 \frac{dw'_1}{w'_1} \int_{u_1 u_2}^{u_1} \frac{dr'_1}{r'_1}$$

$$I_{4.6a} \approx \frac{-16im^3 \pi^6}{q^4} \ln^6 \rho \int_0^1 d\eta_1 \int_0^{1-\eta_1} d\xi_1 \int_0^{1-\xi_1} d\eta_2 \int_0^{1-\xi_1-\eta_2} d\xi_2 \int_0^{\eta_1} d\eta_3 \int_{\xi_1}^{\xi_1+\xi_2} d\xi_3$$

$$I_{4.6a} = \frac{-8im^3 \pi^6}{q^4} \ln^6 \rho \int_0^1 d\eta_1 \int_0^{1-\eta_1} d\xi_1 \int_0^{1-\xi_1} d\eta_2 \int_0^{1-\xi_1-\eta_2} d\xi_2 (2\eta_1 \xi_2)$$

$$I_{4.6a} = \frac{-2im^3 \pi^6}{9q^4} \ln^6 \rho, \quad (\text{C.87})$$

where we have introduced similar normalized logarithmic variable over r'_1 and w'_1 as that of u_3 and v_3 ; and can see that double-logarithmic integral just over k'_1 reduces to $(2\eta_1 \xi_2)$. Putting all the factors together, the contribution of fig. 4.6(a) to the Higgs production FF at NNLP can be written as

$$\left[M_{ggH}^{(1)} \right]_{4.6a} = -\frac{x^2}{18} \ln^2 \rho (C_F - C_A/2)^2. \quad (\text{C.88})$$

Next, for fig. 4.6(b), we first focus only on the integral over the soft gluon

momentum denoted by k_1 in fig. 4.6(b). With Sudakov parameterization $k_1 = r_1 p_1 + w_1 p_2 + k_{1\perp}$, this integral is double-logarithmic for $1 > w_1 > v_1$, and $1 > r_1 > u_1$. Then the integral over k_1 reduces to

$$2 \int_{v_1}^1 \frac{dw_1}{w_1} \int_{u_1}^1 \frac{dr_1}{r_1} = 2 \ln^2 \rho \int_0^{\eta_1} d\eta_3 \int_0^{\xi_1} d\xi_3 = (2\eta_1 \xi_1) \ln^2 \rho. \quad (\text{C.89})$$

The full denominator for this diagram is

$$D_{4.6b} = \{(p_1 + l_1 - k_1)^2 - m^2\} \{(p_1 + l_1)^2 - m^2\} (l_1^2 - m^2) (l_2^2 - m^2) \\ \{(l_2 - p_2)^2 - m^2\} \{(l_1 - p_2)^2 - m^2\} \{(l_1 - k_1 - p_2)^2 - m^2\} (l_1 - l_2)^2 k_1^2. \quad (\text{C.90})$$

Integrals over l_1 in the double-logarithmic region still require a factor of $p_2 l_1$ in the numerator, which for the planar diagram is generated in two different ways. Since the double-logarithmic region over k_1 required $k_1 > l_1$, the lower eikonal quark propagator in the light-cone coordinates can be expanded as

$$S(l_1 - k_1 - p_2) \sim \frac{l_1 - \not{k}_1 - \not{p}_2 + m}{(l_1 - k_1 - p_2)^2 - m^2} \\ \approx \frac{-\gamma^- p_2^+}{2p_2^+ k_1^- (1 - l_1^-/k_1^-)} \\ \approx -\frac{\gamma^-}{2k_1^-} \left(1 + \frac{l_1^-}{k_1^-}\right). \quad (\text{C.91})$$

Similarly, for the upper eikonal quark propagator, we have

$$S(p_1 - k_1 + l_1) \approx \frac{\not{p}_1 - \not{k}_1 + \not{l}_1 + m}{(p_1 - k_1 + l_1)^2 - m^2} \\ \approx \frac{\gamma^+ (p_1 - k_1 + l_1)^-}{-2p_1^- k_1^+} \\ \approx -\frac{\gamma^+}{2k_1^+} \left(1 + \frac{l_1^- - k_1^-}{p_1^-}\right). \quad (\text{C.92})$$

Due to the cyclic property of the traces, we can rearrange the propagators such that eqs. (C.91) and (C.92) are directly multiplied; resulting in

$$S(l_1 - k_1 - p_2) S(p_1 - k_1 + l_1) \sim \frac{\gamma^-}{k_1^-} \left(1 + \frac{l_1^-}{k_1^-}\right) \frac{\gamma^+}{k_1^+} \left(1 + \frac{l_1^- - k_1^-}{p_1^-}\right) \\ \approx \frac{\gamma^-}{k_1^-} \left(1 + \frac{l_1^-}{k_1^-} + \frac{l_1^-}{p_1^-} - \frac{k_1^-}{p_1^-} + \frac{l_1^- l_1^-}{k_1^- p_1^-} - \frac{l_1^-}{p_1^-}\right) \frac{\gamma^+}{k_1^+}$$

$$\approx \frac{\gamma^-}{k_1^-} \left(1 + \frac{l_1^-}{k_1^-} - \frac{k_1^-}{p_1^-} + \frac{l_1^-}{k_1^-} \frac{l_1^-}{p_1^-} \right) \frac{\gamma^+}{k_1^+}. \quad (\text{C.93})$$

Since the relevant term l_1^-/p_1^- gets cancelled in the above equation, the three-loop planar diagram of fig. 4.6(b) does not contribute to FF. This cancellation was not present for the case of nonplanar diagram fig. 4.6(a) as for the propagator $S(l_1 - k'_1 - p_2)$, the condition $r'_1 < u_1$ implies that $k'_1 < l_1$; this propagator in the light-cone coordinates reduces to

$$S(l_1 - k'_1 - p_2) \sim \frac{l_1 - k'_1 - p_2 + m}{(l_1 - k'_1 - p_2)^2 - m^2} \approx \frac{-p_2^+ \gamma^-}{2p_2^+ l_1^-} = -\frac{\gamma^-}{2l_1^-}. \quad (\text{C.94})$$

The required factor of l_1^- for cancellation in $1/(p_2 l_1) \approx 1/(p_2^+ l_1^-)$ comes from the propagator $S(p_1 + l_1 - k'_1)$ as real (virtual) gluons have transversal (lightcone) polarization; and the double-logarithmic condition, $w'_1 > v_1$ implies $k'_1 > l_1$; the propagator reduces to

$$S(p_1 + l_1 - k'_1) \sim \frac{\not{p}_1 + \not{l}_1 - \not{k}'_1 + m}{(p_1 + l_1 - k'_1)^2 - m^2} \approx \frac{(p_1 + l_1 - k'_1)^- \gamma^+}{2p_1^- k_1'^+} = \frac{\gamma^+}{2k_1'^+} \left(1 + \frac{l_1^- - k_1'^-}{p_1^-} \right). \quad (\text{C.95})$$

Bringing the focus back to the planar diagram, the color factor for which is

$$\begin{aligned} c_{4.6b} &= \text{tr} [T^r T^m T^a T^n T^a T^r] = T_{ji}^m T_{fe}^n T_{cj}^r T_{dc}^r T_{ed}^a T_{if}^a \\ c_{4.6b} &= \frac{T_{ji}^m T_{fe}^n}{4} \left(\delta_{cc} \delta_{jd} - \frac{1}{N_c} \delta_{cj} \delta_{cd} \right) \left(\delta_{di} \delta_{fe} - \frac{1}{N_c} \delta_{if} \delta_{ed} \right) \\ c_{4.6b} &= \frac{T_{ji}^m T_{fe}^n}{4} \left(\frac{N_c^2 - 1}{N_c} \delta_{ji} \delta_{ef} - \frac{N_c^2 - 1}{N_c^2} \delta_{if} \delta_{ej} \right) \\ c_{4.6b} &= \frac{(2C_F - C_A)C_F}{2} (T_{jf}^m T_{fj}^n - N_c T_{jj}^m T_{ff}^n) \\ c_{4.6b} &= T_F C_F (C_A/2 - C_F) \delta^{mn}, \end{aligned} \quad (\text{C.96})$$

with $c_{4.6b} = C_F$ as the reduced factor.

Let us now demonstrate how after adding the non-Abelian diagrams fig. 4.6(c) and (d) the Sudakov double-logarithmic corrections factors out into the external gluon lines leaving the $(C_F - C_A)$ structure of the non-Sudakov double-logarithms dictated by the eikonal color non-conservation. The color factor for fig. 4.6(c) reads

$$\begin{aligned} c_{4.6c} &= f^{nrs} \text{tr} [T^r T^m T^a T^s T^a] = f^{nrs} T_{ji}^m T_{fd}^s T_{cj}^r T_{dc}^a T_{if}^a \\ c_{4.6c} &= \frac{f^{nrs}}{2} \left(T_{ij}^r T_{ji}^m T_{ff}^s - \frac{1}{N_c} T_{id}^s T_{dj}^r T_{ji}^m \right) \end{aligned}$$

$$\begin{aligned}
 c_{4.6c} &= \frac{(2C_F - C_A)}{4} f^{nrs} [T^s, T^r]_{ij} T_{ji}^m \\
 c_{4.6c} &= (C_F - C_A/2) \frac{(-i)}{2} f^{nrs} f^{ers} T_{ij}^e T_{ji}^m \\
 c_{4.6c} &= (C_F - C_A/2) \frac{(-i)}{2} C_A \delta^{ne} T_F \delta^{me} \\
 c_{4.6c} &= -iT_F (C_F - C_A/2) \frac{C_A}{2} \delta^{mn}; \tag{C.97}
 \end{aligned}$$

giving the reduced factor of $c_{4.5c} = C_A/2$. The denominator for this diagram is

$$\begin{aligned}
 D_{4.6c} &= \{(p_1 + l_1 - k_1)^2 - m^2\} \{(p_1 + l_1)^2 - m^2\} (l_1^2 - m^2) (l_2^2 - m^2) \\
 &\quad \{(l_2 - k_1 - p_2)^2 - m^2\} \{(l_1 - k_1 - p_2)^2 - m^2\} (l_1 - l_2)^2 (p_2 + k_1)^2 k_1^2. \tag{C.98}
 \end{aligned}$$

To see the eikonal factorization, we relabel the soft gluon momentum to k_1 in fig. 4.6(a) and add it to fig. 4.6(b), and (c) with common color factor $C_A/2$. Note that since $c_{4.6b} = C_F$, fig. 4.6(b) must be added manually with the required color. Similarly, the color of fig. 4.6(a) should be modified from $(C_F - C_A/2)$ to $(C_F - C_A)$. The sum

$$\frac{C_A}{2} \left(\frac{1}{D_{4.6a}} + \frac{1}{D_{4.6b}} + \frac{1}{D_{4.6c}} \right), \tag{C.99}$$

after excluding the common factors, is proportional to

$$\begin{aligned}
 &\frac{1}{\{(p_2 - l_2)^2 - m^2\} \{(p_2 + k_1 - l_2)^2 - m^2\}} + \frac{1}{\{(p_2 - l_2)^2 - m^2\} \{(p_2 - l_1)^2 - m^2\}} \\
 &\quad + \frac{1}{(p_2 + k_1)^2 \{(p_2 + k_1 - l_2)^2 - m^2\}} \\
 &\approx \frac{1}{(p_2 + k_1 - l_2)^2 - m^2} \left[\frac{1}{2p_2 k_1} + \frac{1}{-2p_2 l_2} \right] + \frac{1}{\{(p_2 - l_2)^2 - m^2\} \{(p_2 - l_1)^2 - m^2\}} \\
 &\approx \frac{1}{2p_2 (k_1 - l_2)} \left[\frac{2p_2 (k_1 - l_2)}{(2p_2 k_1)(-2p_2 l_2)} \right] + \frac{1}{(-2p_2 l_2)(-2p_2 l_1)} \\
 &\approx \frac{1}{(-2p_2 l_2)} \left[\frac{2p_2 (k_1 - l_1)}{(2p_2 k_1)(-2p_2 l_1)} \right]. \tag{C.100}
 \end{aligned}$$

Plugging this back into eq. (C.99) with the remaining factors in the eikonal approximation, we obtain

$$\begin{aligned}
 \frac{C_A}{2} \left(\frac{1}{D_{4.6a}} + \frac{1}{D_{4.6b}} + \frac{1}{D_{4.6c}} \right) &\approx \left(\frac{C_A}{2} \right) \frac{1}{(l_1^2 - m^2)(l_2^2 - m^2)k_1^2} \\
 &\quad \frac{1}{(-2l_1 l_2)} \frac{1}{(2p_1 l_1)} \frac{1}{\{2p_1(l_1 - k_1)\}} \frac{1}{\{(2p_2(k_1 - l_1)\}} \times \frac{2p_2(k_1 - l_1)}{(-2p_2 l_2)(2p_2 k_1)(-2p_2 l_1)}
 \end{aligned}$$

$$\approx \left(\frac{C_A}{2} \right) \frac{1}{(l_1^2 - m^2)(l_2^2 - m^2)k_1^2} \frac{1}{(-2l_1l_2)} \frac{1}{(2p_1l_1)} \frac{1}{\{2p_1(l_1 - k_1)\}} \frac{1}{(-2p_2l_2)(2p_2k_1)(-2p_2l_1)}. \quad (\text{C.101})$$

This has resulted in factorization of the soft emission on the lower line.

Let us now tackle fig. 4.6(d). The color factor given by $c_{4.6d} = f^{mrs}T^rT^aT^nT^aT^s$ is similar to the color factor of fig. 4.6(c), and identically reduces to eq. (C.97) with $c_{4.5d} = C_A/2$. Denominator is

$$D_{4.6d} = \{(p_1 + l_1 - k_1)^2 - m^2\}(l_1^2 - m^2)(l_2^2 - m^2)\{(l_2 - p_2)^2 - m^2\} \{(l_1 - p_2)^2 - m^2\}\{(l_1 - k_1 - p_2)^2 - m^2\}(l_1 - l_2)^2(p_1 - k_1)^2k_1^2. \quad (\text{C.102})$$

Eikonal factorization happens when fig. 4.6(b) and (d) are added with the common color factor of $(-C_A/2)$; cancelling the manual addition of fig. 4.6(b) for the factorization of fig. 4.6(c). The minus sign for fig. 4.6(d) is a result of the loop momentum insertion from the expansion of the lower eikonal line. The sum

$$\begin{aligned} & -\frac{C_A}{2} \left(\frac{1}{D_{4.6b}} + \frac{1}{D_{4.6d}} \right) \propto \frac{1}{(p_1 + l_1)^2 - m^2} + \frac{1}{(p_1 - k_1)^2} \\ & \propto \frac{1}{(2p_1l_1)} + \frac{1}{(-2p_1k_1)} \\ & \approx \left(-\frac{C_A}{2} \right) \frac{1}{(l_1^2 - m^2)(l_2^2 - m^2)k_1^2} \frac{1}{(-2p_2l_2)} \frac{1}{(-2p_2l_1)} \frac{1}{\{2p_2(k_1 - l_1)\}} \frac{1}{(-2l_1l_2)} \\ & \qquad \qquad \qquad \frac{1}{\{2p_1(l_1 - k_1)\}} \times \left[\frac{2p_1(l_1 - k_1)}{(2p_1l_1)(-2p_1k_1)} \right] \\ & \approx \left(-\frac{C_A}{2} \right) \frac{1}{(l_1^2 - m^2)(l_2^2 - m^2)k_1^2} \frac{1}{(-2p_2l_2)} \frac{1}{(-2p_2l_1)} \frac{1}{\{2p_2(k_1 - l_1)\}} \frac{1}{(-2l_1l_2)} \frac{1}{(2p_1l_1)} \frac{1}{(-2p_1k_1)}, \quad (\text{C.103}) \end{aligned}$$

leads to factorization of the soft gluon on the upper line.

The factorization requires the final missing piece fig. C.7; adding this diagram with eqs. (C.101) and (C.103) in the eikonal approximation leads to complete factorization of the soft gluon. Total contribution at three-loops reduces to the effective diagram fig. 4.5(b), same as fig. 4.6(a) with an effective soft exchange. The final contribution

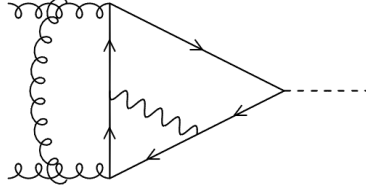


Figure C.7: The final diagram required for the eikonal factorization of the soft gluon for the 3-loop diagrams fig. 4.6(c) and (d). The wavy line represents the exchange of eikonal gluon between the soft and eikonal quark lines.

to the FF by three-loop non-factorizable diagrams is

$$\left[M_{ggH}^{(1),3L} \right]_{NF} = -\frac{(C_A - C_F)(C_A - 2C_F)x^2}{9} \ln^2 \rho; \quad (\text{C.104})$$

which is the same as eq. (4.26), and accounts for the symmetric diagrams.